

**CIVIL ENGINEERING STUDIES**  
Illinois Center for Transportation Series No. 16-018  
UILU-ENG-2016-2018  
ISSN: 0197-9191

# **BRIDGE DECKS: MITIGATION OF CRACKING AND INCREASED DURABILITY**

Prepared By  
**Ardavan Ardeshirilajimi**  
**Di Wu**

**Piyush Chaunsali**  
**Paramita Mondal**

University of Illinois at Urbana-Champaign

**Ying Tung Chen**  
**Mohammad Mahfuzur Rahman**  
**Ahmed Ibrahim**  
**Will Lindquist**  
**Riyadh Hindi**  
Saint Louis University

Research Report No. FHWA-ICT-16-016

A report of the findings of  
**ICT PROJECT R27-139**  
**Bridge Decks: Mitigation of Shrinkage Cracking (Phase 2 Study)**

---

**Illinois Center for Transportation**

**June 2016**

**ILLINOIS CENTER FOR  
TRANSPORTATION**





**TECHNICAL REPORT DOCUMENTATION PAGE**

<b>1. Report No.</b> FHWA-ICT-16-016		<b>2. Government Accession No.</b>		<b>3. Recipient's Catalog No.</b>	
<b>4. Title and Subtitle</b> Bridge Decks: Mitigation of Cracking and Increased Durability				<b>5. Report Date</b> June 2016	
				<b>6. Performing Organization Code</b>	
<b>7. Author(s)</b> Ardavan Ardeshirilajimi, Di Wu, Piyush Chaunsali, Paramita Mondal, Ying Tung Chen, Mohammad Mahfuzur Rahman, Ahmed Ibrahim, Will Lindquist, and Riyadh Hindi				<b>8. Performing Organization Report No.</b> ICT-16-018 UILU-ENG-2016-2018	
<b>9. Performing Organization Name and Address</b> Illinois Center for Transportation Department of Civil and Environmental Engineering University of Illinois at Urbana-Champaign 205 North Mathews Avenue, MC-250 Urbana, IL 61801				<b>10. Work Unit No.</b>	
				<b>11. Contract or Grant No.</b> R27-139 (Phase 2)	
<b>12. Sponsoring Agency Name and Address</b> Illinois Department of Transportation (SPR) Bureau of Material and Physical Research 126 East Ash Street Springfield, IL 62704				<b>13. Type of Report and Period Covered</b> July 1, 2013, through June 30, 2016	
				<b>14. Sponsoring Agency Code</b> FHWA	
<b>15. Supplementary Notes</b> Conducted in cooperation with the U.S. Department of Transportation, Federal Highway Administration.					
<b>16. Abstract</b> The application of pre-soaked lightweight aggregates (LWA) as an internal curing agent in concrete to reduce the cracking due to drying shrinkage is thoroughly studied in this report. It is determined that although LWA can significantly reduce autogenous shrinkage, its effect on drying shrinkage is minimal and in some cases it can even increase the drying shrinkage. Moreover, the combined effects of LWA and expansive cement (Type K) and LWA and shrinkage-reducing admixtures (SRAs) on drying shrinkage is also studied. It is shown that addition of Type K cement or SRA to mixtures containing LWA can significantly reduce drying shrinkage and make the mixture more volumetrically stable.					
<b>17. Key Words</b> lightweight aggregates, expansive cement, shrinkage cracking			<b>18. Distribution Statement</b> No restrictions. This document is available through the National Technical Information Service, Springfield, VA 22161.		
<b>19. Security Classif. (of this report)</b> Unclassified		<b>20. Security Classif. (of this page)</b> Unclassified		<b>21. No. of Pages</b> 77 + appendices	<b>22. Price</b>



## **ACKNOWLEDGMENT, DISCLAIMER, MANUFACTURERS' NAMES**

This publication is based on the results of ICT-R27-139, **Bridge Decks: Mitigation of Shrinkage Cracking (Phase II Study)**. ICT-R27-139 was conducted in cooperation with the Illinois Center for Transportation; the Illinois Department of Transportation; and the U.S. Department of Transportation, Federal Highway Administration.

Members of the Technical Review panel were the following:

- James Krstulovich, TRP Chair, Illinois Department of Transportation
- Julie Beran, Illinois Department of Transportation
- Dan Brydl, Federal Highway Administration
- Mike Copp, Illinois Department of Transportation
- Darrin Davis, Illinois Department of Transportation
- David Greifzu, Illinois Department of Transportation
- Gary Kowalski, Illinois Department of Transportation
- Matt Mueller, Illinois Department of Transportation
- Brian Pfeifer, Federal Highway Administration
- Randy Riley, Illinois Chapter, American Concrete Pavement Association
- Darrell Tiesman, Illinois Department of Transportation
- Dan Tobias, Illinois Department of Transportation
- Melinda Winkelman, Illinois Department of Transportation
- Steve Worsfold, Illinois Department of Transportation

The contents of this report reflect the view of the authors, who are responsible for the facts and the accuracy of the data presented herein. The contents do not necessarily reflect the official views or policies of the Illinois Center for Transportation, the Illinois Department of Transportation, or the Federal Highway Administration. This report does not constitute a standard, specification, or regulation.

Trademark or manufacturers' names appear in this report only because they are considered essential to the object of this document and do not constitute an endorsement of product by the Federal Highway Administration, the Illinois Department of Transportation, or the Illinois Center for Transportation.

## EXECUTIVE SUMMARY

Concrete bridge decks are highly susceptible to cracking caused by drying shrinkage due to their large surface-to-volume ratios, which result in a high rate of moisture loss from the exposed surface. This study examined the effectiveness of pre-soaked lightweight aggregates (LWA) on shrinkage mitigation. Furthermore, the combined effects of shrinkage-compensating cements and shrinkage-reducing admixtures (SRA) with LWA on shrinkage behavior were also explored.

LWA can provide an extra moisture reservoir for concrete and cure the mixture from within. It can therefore alleviate self-desiccation (or internal drying) that occurs as a result of cement hydration. Hence, autogenous shrinkage can be greatly reduced when LWA is added to a mixture. Shrinkage-compensating cements can develop compressive stresses in the concrete due to their expansive nature that can later counteract tensile stresses induced by drying shrinkage. SRAs can decrease the capillary stresses and drying shrinkage by reducing surface tension of pore solution in the mixture. All of these methods for reducing shrinkage cracking were tried separately and in combination with each other to develop specifications for the Illinois Department of Transportation (IDOT).

It was found that LWA can be highly effective in reducing autogenous deformation. However, its effect on drying shrinkage was minimal, and in some cases, it even increased drying shrinkage of mortar (obtained in accordance with ASTM C596) and concrete mixtures (obtained in accordance with ASTM C157). By using different exposure conditions to control the rate of evaporation of moisture from the mixtures to the surrounding environment, it was observed that when internal curing is incorporated in a severe drying condition, it can increase the drying shrinkage. In a milder drying condition, however, LWA can be slightly effective in reducing drying shrinkage. Moreover, it was shown that conventional external curing methods (such as wet or sealed curing) can increase the effectiveness of LWA in reducing drying shrinkage.

When LWA was added to the mixtures with Type K cement, a calcium sulfoaluminate (CSA)-based shrinkage-compensating cement, a considerable increase in early-age expansion was observed. It is believed that internal curing can promote hydration of Type K cement, which results in higher expansion. Moreover, it was shown that a decrease in modulus, as a result of the addition of LWA, can also be a cause of the increased expansion. Even in an unsealed condition, the net shrinkage can be greatly reduced by adding LWA to mixtures containing Type K cement. The dosage of LWA was shown to have a considerable effect on the strength of mixtures with CSA cement. It was shown that replacing 11.6% of fine aggregate with LWA can increase 7-day and 28-day compressive strength of the mixture. However, higher dosages can result in a decrease in compressive strength, which is believed to be due to the highly porous nature of LWA and its low intrinsic strength. Moreover, the addition of SRA was found to be another method for reducing drying shrinkage. It was shown that mixtures with both SRA and LWA show superior performance in terms of autogenous and drying shrinkage.

Large-scale lab tests to monitor strains within a scaled prototypical bridge bay were run concurrently with the small-scale materials tests. Though the small-scale materials tests showed the effectiveness of LWA and SRA in mitigating shrinkage, it was important to verify whether the same trends would be

observed at the laboratory scale before these shrinkage mitigation methods are implemented widely by IDOT.

In Phase I of the research project, a control mix using a typical IDOT concrete bridge deck mix design and a mix containing a partial replacement of portland cement with Type K cement were evaluated by comparing strain and temperature data measured through the deck and supporting girders for a period of 6 months. The results showed that the Type K cement has higher expansion than the control mix at early ages, but the rate of shrinkage is similar to that of the control mix; that is, the addition of Type K cement essentially adjusted the shrinkage curve to start at the point of maximum expansion, at which point the concrete shrank at a similar rate to that of the control.

For Phase II (the current phase) of the project, two more mix designs were evaluated, one containing a partial replacement of sand with LWA and another incorporating a SRA; the results were compared with the control and Type K data from Phase I. When the total shrinkage following the initial expansion was compared, the deck containing Type K cement had the largest total shrinkage, which was comparable to the control. The deck containing SRA had the least total shrinkage over time. In addition, as the LWA concrete deck shrinks following the curing period, it does so at a slower rate compared with both the control and Type K decks. Based on the strain and visual observation, no cracks formed in the LWA and SRA decks.

In addition to the experimental decks, a bridge deck near Peoria, Illinois, was constructed with concrete containing Type K cement and monitored and compared with the experimental results. When the average longitudinal strain from the Type K Peoria deck was compared with the Type K experimental deck, the trend was similar; however, the Peoria Type K experienced a smaller expansion during the first 7 days. This may be due to more restraint in the actual bridge deck compared with the experimental deck or due to differences in the mix designs, particularly with respect to the use of Class C fly ash in the actual bridge deck.

Finite element models of the scaled experimental decks as well as the Peoria bridge were created and compared with the measured strain data. By applying a uniform temperature load, the shrinkage of concrete can be closely simulated in both experimental and actual bridge decks, and in the future, the strain caused by drying shrinkage can be found by subtracting the strain caused by actual temperatures using the finite element model.

# CONTENTS

<b>CHAPTER 1: INTRODUCTION</b> .....	<b>1</b>
<b>CHAPTER 2: LITERATURE REVIEW</b> .....	<b>3</b>
<b>2.1 INTERNAL CURING MOTIVATION</b> .....	<b>3</b>
<b>2.2 MIXTURE PROPORTIONING WITH INTERNAL CURING</b> .....	<b>3</b>
<b>2.3 CHARACTERIZATION OF LWA FOR INTERNAL CURING</b> .....	<b>4</b>
<b>2.4 SPATIAL DISTRIBUTION OF LWA FOR INTERNAL CURING</b> .....	<b>4</b>
<b>2.5 EFFECT OF INTERNAL CURING ON SHRINKAGE OF MORTAR AND CONCRETE MIXTURES</b> .....	<b>5</b>
2.5.1 Effect of Internal Curing on Plastic Shrinkage .....	5
2.5.2 Effect of Internal Curing on Autogenous Shrinkage .....	5
2.5.3 Effect of Internal Curing on Drying Shrinkage.....	5
<b>2.6 EFFECT OF INTERNAL CURING ON MECHANICAL PROPERTIES</b> .....	<b>6</b>
2.6.1 Effect of Internal Curing on Compressive Strength.....	6
2.6.2 Tensile Strength .....	6
2.6.3 Elastic Modulus .....	7
<b>CHAPTER 3: EFFECTS OF LWA ON DEFORMATION PROPERTIES OF MORTAR AND CONCRETE MIXTURES</b> .....	<b>8</b>
<b>3.1 COMPARISON OF THE EFFECTIVENESS OF THREE TYPES OF LWA ON SHRINKAGE MITIGATION OF MORTAR MIXTURES</b> .....	<b>8</b>
3.1.1 Characteristics of Different LWAs .....	8
3.1.2 Effects of Different Types of LWAs on Autogenous Shrinkage .....	10
3.1.3 Effects of Different Types of LWAs on Drying Shrinkage .....	10
3.1.4 Summary .....	11
<b>3.2 EFFECTIVENESS OF LWA ON MITIGATION OF AUTOGENOUS SHRINKAGE IN MORTAR MIXTURES</b> .....	<b>12</b>
3.2.1 Effects of Dosage of LWA and W/C on Autogenous Shrinkage of Mortar Mixtures.....	12
3.2.2 Effects of Soaking Time of LWA on Autogenous Shrinkage of Mortar Mixtures .....	13
3.2.3 Summary .....	14
<b>3.3 EFFECTIVENESS OF LWA ON MITIGATION OF DRYING SHRINKAGE IN MORTAR MIXTURES</b> .....	<b>14</b>
3.3.1 Effectiveness of LWA in Reducing Drying Shrinkage of Mortar Mixtures When No Curing Is Applied.....	15
3.3.2 Effectiveness of LWA in Reducing Drying Shrinkage of Mortar Mixtures When Wet or Sealed Curing Is Applied.....	17
3.3.3 Summary .....	19
<b>3.4 EFFECTIVENESS OF LWA ON MITIGATION OF DRYING SHRINKAGE OF CONCRETE MIXTURES</b> .....	<b>19</b>
3.4.1 Effectiveness of LWA in Reducing Autogenous Shrinkage of Concrete .....	19
3.4.2 Effectiveness of LWA in Reducing Drying Shrinkage of Concrete .....	20
3.4.3 Summary .....	21

<b>CHAPTER 4: EFFECTS OF COMBINING INTERNAL CURING WITH USE OF EXPANSIVE ADDITIVE SUCH AS TYPE K CEMENT ON SHRINKAGE OF MORTAR AND CONCRETE.....</b>	<b>22</b>
<b>4.1 EFFECTS OF INTERNAL CURING ON DEFORMATION OF OPC-CSA MORTAR SPECIMENS.....</b>	<b>22</b>
4.1.1 Sealed Curing Condition .....	22
4.1.2 Unsealed Curing Conditions .....	23
<b>4.2 EFFECT OF INTERNAL CURING ON DEFORMATION OF OPC-CSA CONCRETE SPECIMENS.....</b>	<b>24</b>
<b>4.3 EFFECT OF INTERNAL CURING ON MICROSTRUCTURE OF OPC-CSA BLENDS .....</b>	<b>25</b>
<b>4.4 EFFECT OF MODULUS ON DEFORMATION OF OPC-CSA MORTAR SPECIMENS .....</b>	<b>27</b>
<b>4.5 SUMMARY .....</b>	<b>30</b>
<b>CHAPTER 5: EFFECTS OF COMBINING INTERNAL CURING WITH USE OF SHRINKAGE-REDUCING ADMIXTURES ON SHRINKAGE OF MORTAR AND CONCRETE .....</b>	<b>31</b>
<b>5.1 EFFECTS OF SRA ON AUTOGENOUS DEFORMATION OF MORTAR AND CONCRETE MIXTURES WITH INTERNAL CURING .....</b>	<b>31</b>
<b>5.2 EFFECTS OF SRA ON DRYING SHRINKAGE OF MORTAR AND CONCRETE MIXTURES WITH INTERNAL CURING .....</b>	<b>33</b>
<b>5.3 SUMMARY.....</b>	<b>35</b>
<b>CHAPTER 6: BRIDGE DECK MODELS .....</b>	<b>36</b>
<b>6.1 BRIDGE BAY DESIGN .....</b>	<b>36</b>
6.1.1 Strain and Temperature Gage Locations.....	37
<b>6.2 MIX DESIGN.....</b>	<b>39</b>
<b>6.3 CONCRETE TEST RESULTS .....</b>	<b>40</b>
<b>6.4 STRAIN AND TEMPERATURE VARIATION IN THE BRIDGE DECKS .....</b>	<b>41</b>
6.4.1 LWA Concrete Deck.....	41
6.4.2 SRA Concrete Deck .....	45
<b>CHAPTER 7: PEORIA TYPE K BRIDGE INSTRUMENTATION.....</b>	<b>50</b>
<b>7.1 OVERVIEW OF THE BRIDGE .....</b>	<b>50</b>
7.1.1 Structure of the Bridge.....	51
7.1.2 Concrete Mix Design .....	52
<b>7.2 INSTRUMENTATION SETUP .....</b>	<b>52</b>
7.2.2 Vibrating Wire Strain Gage.....	55
<b>7.3 STRAIN AND TEMPERATURE VARIATION IN THE BRIDGE DECKS .....</b>	<b>57</b>
7.3.1 Foil Strain Gage Readings .....	57
7.3.2 Vibrating Wire Strain Gage Readings .....	59
7.3.3 Temperature Readings .....	61
<b>7.4 SUMMARY.....</b>	<b>62</b>
<b>CHAPTER 8: FINITE ELEMENT ANALYSIS .....</b>	<b>63</b>
<b>8.1 ABAQUS EXPERIMENTAL BAY MODEL .....</b>	<b>63</b>
<b>8.2 RESULTS FOR ABAQUS EXPERIMENTAL BAY.....</b>	<b>65</b>
<b>8.3 RESULTS FOR ABAQUS PEORIA TYPE K BRIDGE MODEL .....</b>	<b>66</b>
<b>8.4 ABAQUS PEORIA TYPE K BRIDGE RESULTS .....</b>	<b>68</b>

<b>CHAPTER 9: CONCLUSIONS.....</b>	<b>40</b>
<b>REFERENCES .....</b>	<b>75</b>
<b>APPENDIX A: MATERIALS AND METHODS.....</b>	<b>78</b>
<b>A.1 MATERIALS .....</b>	<b>78</b>
A.1.1 Raw Materials .....	78
A.1.2 Mixture Proportions.....	78
<b>A.2 TEST METHODS .....</b>	<b>80</b>
A.2.1 Mixing Procedure .....	80
A.2.2 Restrained Expansion of Type K Concrete .....	80
A.2.3 Unrestrained (Free) Deformation of Mortar Mixtures .....	81
A.2.4 Compressive Strength .....	82
A.2.5 Drying Shrinkage of Mortar and Plain Concrete .....	82
A.2.6 Measurement of Capillary Porosity and Evaporable Water Content .....	82
<b>APPENDIX B: LARGE-SCALE TESTING RESULTS.....</b>	<b>84</b>
<b>B.1 LARGE-SCALE TESTING RESULT: LWA.....</b>	<b>84</b>
<b>B.2 LARGE-SCALE TESTING RESULT: SRA.....</b>	<b>88</b>

## CHAPTER 1: INTRODUCTION

Shrinkage cracking is a predominant deterioration mechanism greatly affecting the durability and service life of concrete structures. Besides plastic shrinkage which occurs in the first few hours, autogenous and drying shrinkage are the major shrinkage mechanisms threatening the integrity of a concrete structure. Autogenous shrinkage is caused by the self-desiccation (or internal drying) that occurs when cement hydrates. Autogenous shrinkage generally increases with a decrease in the water-to-cement (w/c) ratio. On the other hand, drying shrinkage is a result of external moisture loss due to exposure to an unsaturated environment. Therefore, concrete bridge decks are highly susceptible to drying shrinkage cracking due to their high surface-to-volume ratio, which results in a high rate of evaporation of moisture from the exposed surface. The formation of these cracks allows deicing chemicals and other harmful materials to penetrate into the concrete which can increase the potential for corrosion of the embedded steel bars. Allowing water to penetrate into the concrete can also increase the possibility of freeze-thaw deterioration.

The NCHRP 380 report (Krauss and Rogalla 1996) included a survey sent to all departments of transportation (DOTs) in the United States to evaluate the extent of the problem of bridge deck cracking. More than 60% of the agencies acknowledged transverse cracking due to shrinkage to be problematic. Moreover, it was also reported that half of the bridges in the United States develop cracking at early ages. Throughout the state of Illinois, transverse cracks at fairly regular intervals at both the positive and negative moment regions of bridge decks are commonly observed.

Recently, Hopper et al. (2015) performed a comprehensive literature review of the factors affecting early-age cracking of bridge decks. Below is a summary of their findings and recommendations to help reduce shrinkage cracking in bridge decks:

- Effect of concrete material properties: Type of cement (use of cements with lower heat of hydration, lower early-age strength, and coarser particle size is recommended), type of aggregate (use of aggregates with high resistance to cracking, low shrinkage, high modulus of elasticity, and low absorption capacity is recommended), supplementary cementitious materials (use of fly ash and avoiding the use of ground granulated blast-furnace slag and silica fume are recommended), chemical admixtures (use of shrinkage-reducing admixtures and avoiding the use of set-modifying admixtures are recommended), and fiber reinforcement (use of microfibers is recommended).
- Effect of mixture proportions: Cement paste content (lower cement paste content is recommended) and water to cementitious materials ratio (water to cementitious materials in the range of 0.40 to 0.48 is recommended).
- Effect of concrete's fresh and hardened properties: Slump (concretes with higher slump are more susceptible to cracking), compressive strength (mixtures that were designed to have an unnecessarily high strength are more prone to cracking), and modulus of elasticity (concretes with higher modulus of elasticity are more prone to cracking).

- Effect of construction methods: Site ambient temperature (a minimum range of 40°F to 45°F and a maximum range of 80°F to 90°F is recommended) and construction procedure (insufficient vibration and improper curing can increase susceptibility to cracking).
- Effect of structural design factors: Bridge deck design (use of concrete girders, maximizing girder spacing, increasing the thickness of the bridge deck and the top cover, and reducing the reinforcement bar size and spacing are recommended).

The great extent to which shrinkage cracking occurs in bridge decks demands an improvement in bridge deck designs in order to reduce the potential to cracking. The most feasible and economical way to address this problem is by approaching it from the materials side (i.e., reducing the shrinkage susceptibility of concrete by manipulating mixture proportion and design). Understanding the effectiveness of these methods in mitigating shrinkage is the primary objective of this phase of the project.

The following are the most significant conclusions of the first phase of this project, which focused on the use of shrinkage-compensating cements and SRAs to mitigate cracking in bridge decks (Chaunsali et al. 2013):

- The use of Type K and Type G in plain concrete effectively compensated for drying shrinkage.
- The use of supplementary cementitious materials influenced the extent of expansion in Type K and Type G concrete and subsequently affected the net shrinkage.
- 28-day compressive strengths of Type K and Type G concretes were found to be similar or higher than those of plain concrete mixtures.
- The effectiveness of SRAs in reducing shrinkage cracking was verified.
- The strain monitoring of the bridge deck model with and without Type K highlighted the reduction in tensile strain on the order of 40 to 50 microstrains at early ages.

The second phase of the project focused on the use of pre-soaked LWA as an internal curing agent and its effect on autogenous and drying shrinkage of mortar and concrete mixtures. Moreover, because there is limited research on the combined effect of LWA and shrinkage-compensating cements, as well as LWA and SRA, the potential for combining these shrinkage mitigation strategies was also studied. In addition to small-scale materials testing, large-scale laboratory models and finite element modeling were used to fully understand the potential of these shrinkage mitigation strategies before widely applying the technologies in the field.

## CHAPTER 2: LITERATURE REVIEW

This chapter provides a comprehensive review of previous studies on the subject of internal curing using pre-soaked lightweight aggregates (LWA). Internal curing is commonly defined as supply of water through reservoirs of porous aggregates to promote hydration or replace moisture loss due to evaporation or self-desiccation. LWA is the most widespread aggregate used for internal curing.

For a comprehensive literature review on the use of expansive cements to mitigate concrete shrinkage and a summary of investigations by other DOTs, please refer to the final report of the first phase of this project (Chaunsali et al. 2013).

### 2.1 INTERNAL CURING MOTIVATION

Traditional external curing techniques include ponding, fogging, misting, and using wet burlap. However, for high-performance concretes or generally for concretes with low water-to-cement (w/c) ratios, capillary porosity becomes isolated during the first few days of hydration (Aitcin 2003). Thus, the external water can penetrate only a few millimeters into the concrete, whereas the interior of the concrete undergoes severe self-desiccation (Bentz 2002). In contrast, internal curing is capable of distributing water more equally across the cross section of the concrete (Castro et al. 2011).

Hence, the goal of internal curing is to provide sufficient amounts of water with a proper spatial distribution in order to maximize the hydration of cementitious components and to minimize the autogenous stresses and strains. Therefore, internal curing could potentially increase strength, reduce porosity and permeability, and mitigate shrinkage cracking (Bentz and Weiss 2011).

### 2.2 MIXTURE PROPORTIONING WITH INTERNAL CURING

When cement hydrates, its total volume decreases. This phenomenon is referred to as chemical shrinkage (Powers 1935). If no extra water is provided to the mixture—in a sealed system, for example—cement paste will self-desiccate (i.e., vapor-filled pores will be formed within the hydrating paste structure, which can lead to a reduction in internal relative humidity).

Accordingly, assuming no water loss to the surrounding environment, the amount of required internal curing water can be determined by considering the amount of water demand of the hydrating phases. In other words, the volume of the internal curing water should be equal to the volume of the voids created by chemical shrinkage. The following equation is provided by Castro et al. (2011) for obtaining the required mass of dry LWA:

$$M_{LWA} = \frac{C_f \times CS \times \alpha_{max}}{S \times \phi_{LWA24h} \times \psi}$$

where  $C_f$  (kg/m<sup>3</sup>) is the cement content of the mixture,  $CS$  (g of water/g of cement) is the chemical shrinkage of the binder at 100% reaction,  $\alpha_{max}$  (0 to 1) is the maximum degree of hydration,  $S$  is the saturation degree based on the 24-hour absorption,  $\phi_{LWA24h}$  (g of water/g of dry LWA) is the 24-hour absorption, and  $\psi$  (0 to 1) is the fraction of water released from the LWA at high relative humidity. In

a pure portland cement system, for a w/c ratio of 0.36 or higher, the maximum expected degree of hydration is 1. For a lower w/c ratio, however, the degree of hydration can be estimated by  $(w/c)/0.36$  (Bentz et al. 2005). Chemical shrinkage could be obtained experimentally in accordance with ASTM C1608-12 or theoretically in accordance with the method proposed by Bentz et al. (2005). Saturation degree, absorption, and desorption of LWA will be discussed in detail in the next section.

### **2.3 CHARACTERIZATION OF LWA FOR INTERNAL CURING**

X-ray absorption studies indicate that during drying, water will preferentially move from coarser pores to finer pores (Bentz et al. 2001). Thus, for LWA to function efficiently as an internal curing reservoir, the water-filled pores in LWA must be larger than those in the surrounding paste matrix so that water can be released to the hydrating cement when needed.

The ability of LWA to release water can be quantified by measuring its absorption and desorption properties. ASTM C1761/C1761M-13b provides standard methods of measuring absorption and desorption properties of LWA. This standard suggests using the paper towel method for determining absorption capacity. It should be noted that absorption of LWA is a time-dependent property (i.e., the absorption is increased as the period of submersion in water is increased). Most commonly, 24-hour absorption is used. Castro et al. (2011) presented time-dependent absorption values for several different types of LWA that are commonly used throughout the United States. Their results indicate a wide range of 24-hour absorption, ranging from 6.0% to 30.5%. It should be noted that the amount of LWA required for internal curing is inversely proportional to its absorption capacity. Thus, a higher level of absorption is preferred for internal curing.

For LWA to be suitable for internal curing, its absorbed water should be released readily at high relative humidities. The saturated salt solutions method is recommended in ASTM C1761/C1761M-13b for determining the desorption properties of LWA at different relative humidities. Several studies show that approximately 90% of the 24-hour absorbed water is readily released at high relative humidities of more than 93% for most types of LWA that are commonly used in the United States (Bentz et al. 2005; Radlinska et al. 2008; Castro et al. 2011). Any type of LWA that is unable to release most of its absorbed water at a high level of relative humidity (i.e., 93%) is believed to be undesirable for internal curing purposes (Castro et al. 2011).

### **2.4 SPATIAL DISTRIBUTION OF LWA FOR INTERNAL CURING**

Another important aspect in determining the efficiency of LWA is the distance that the absorbed water can travel from the reservoirs into the cement paste that determines the fraction of the cement paste that can be protected by internal curing. Studies estimate that the water from LWA can travel between 1.8 and 3 mm into the cement paste matrix at early ages (Trtik 2011; Henkensiefken 2011). Moreover, it is reported that as the permeability of the cement paste decreases during curing, the water transport will be limited to between 100 and 200  $\mu\text{m}$  (Bentz 1999). It is also shown that much of the water within the LWA is released during the first 24 hours of hydration (Bentz et al. 2006). More specifically, the majority of water movement from the LWA to the paste occurs between 7 and 11 hours, which corresponds to the rapid rate of hydration and the development of pore pressure (Trtik et al. 2011).

Using a hard-core/soft-shell microstructural model, Henkensiefken et al. (2009a) modeled 16 different mixtures with aggregates of varying sizes and showed that, assuming the same travel distance for water, finer aggregates could protect larger fraction of paste than coarse aggregates. Using a fine-graded LWA will result in a maximum distance of 2 mm between the paste matrix and LWA surface, which results in an efficient mitigation of self-desiccation.

## **2.5 EFFECT OF INTERNAL CURING ON SHRINKAGE OF MORTAR AND CONCRETE MIXTURES**

### **2.5.1 Effect of Internal Curing on Plastic Shrinkage**

Because the supply of additional water from LWA reduces the magnitude of the capillary stresses that are developed during drying, replacement of normal-weight sand with LWA can provide a significant reduction of plastic shrinkage cracking. If a sufficient volume of LWA is used, plastic shrinkage cracking could even be entirely eliminated (Henkensiefken et al. 2010). It has also been reported that concrete mixtures in the field with internal curing show less plastic shrinkage than conventional concrete mixtures without internal curing (Villarreal 2008).

### **2.5.2 Effect of Internal Curing on Autogenous Shrinkage**

It has been shown in the literature that at lower dosages of LWA (replacing less than 11% of fine aggregate with LWA), the autogenous shrinkage of LWA mortar mixtures is similar to that of plain mortar mixtures. However, using higher dosages of LWA could make the mixture nearly volumetrically stable (Henkensiefken et al. 2009b). Another noteworthy finding in the literature is that no considerable improvement was observed when using LWA dosages higher than what is required by the mixture to eliminate self-desiccation in sealed systems (Henkensiefken et al. 2009b). In accordance with ASTM C158 (commonly known as the ring test), Henkensiefken (2009b) demonstrated that a reduction in autogenous shrinkage (as a result of incorporating LWA) resulted in a delay in onset of cracking. At low dosages of LWA, cracks occur at early ages, similar to plain mortar mixtures. However, as the dosage of LWA is increased, the onset of cracking is greatly extended (Henkensiefken et al. 2009b). It is reported that replacing around 24% of fine aggregate with LWA can eliminate shrinkage cracking due to autogenous shrinkage entirely (Henkensiefken et al. 2009b).

Bentz (2007) observed that incorporating internal curing through LWA could provide a significant reduction of autogenous shrinkage in blended cement mortars (with silica fume [SF], fly ash [FA] and slag), while for mortar mixtures with SF, higher dosages of LWA were required to effectively mitigate autogenous shrinkage. Golias et al. (2012) reported that when the same amount of internal curing water is added to the mixture at the time of mixing, by using a higher amount of oven-dried LWA (as opposed to pre-soaked LWA) nearly identical autogenous shrinkage improvement could be achieved.

### **2.5.3 Effect of Internal Curing on Drying Shrinkage**

Henkensiefken et al. (2009b) showed that low dosages of LWA prove to be ineffective in mitigating drying shrinkage caused by the combined effects of external and internal drying. However, when the dosage is increased beyond a critical level, the shrinkage could be mitigated and when even higher dosages are used, mixtures show a significant expansion at early ages. Radlinska et al. (2008)

observed that replacing a percentage of fine aggregates (natural sand) with LWA could reduce the early-age shrinkage in unsealed systems. However, it was also indicated that when internal relative humidity reaches equilibrium with ambient relative humidity, the ultimate drying shrinkage of mixtures with LWA is comparable with that of the plain mixtures.

With accordance to ASTM C1581, Henkensiefken et al. (2009b) reported that mortar mixtures with low dosages of LWA crack at an early age in unsealed systems. However, as the dosage is increased to a sufficient level, the onset of cracking is greatly extended or in some cases cracking is completely eliminated.

## **2.6 EFFECT OF INTERNAL CURING ON MECHANICAL PROPERTIES**

Compared with natural sand, LWA has much weaker mechanical properties (specifically a lower intrinsic strength), which arise from its highly porous nature. Therefore, a decrease in strength, known as the strength ceiling, is anticipated when LWA is added to the mixture (Moreno et al. 2014; Videla 2000). However, it is also commonly believed that internal curing can result in a denser microstructure by promoting cement hydration. Therefore, whether LWA can provide better mechanical properties to a mortar or concrete mixture greatly depends on whether the increased hydration caused by internal curing can compensate for the low intrinsic strength of LWA.

### **2.6.1 Effect of Internal Curing on Compressive Strength**

Golias et al. (2013) reported that in wet and moist curing conditions, there is no considerable increase in strength associated with incorporating LWA, while under sealed and drying conditions, incorporation of LWA results in higher compressive strength—and the improvement is more significant at later ages. Bentz (2007) observed a 10% increase in the compressive strength of blended cement mortars (with SF, FA, and slag) at later ages. Wasserman and Bentur (1996) indicated that for LWAs of similar intrinsic strength, the LWA with higher absorption will result in higher-strength concrete because of its denser interfacial transition zone. Moreover, it was reported that an LWA with pozzolanic reactivity can further increase the compressive strength.

In contrast, Zhutovsky et al. (2004) observed that concrete made with LWA has slightly lower strength, whether with or without silica fume. Zhutovsky and Kovler (2012) observed that as a result of incorporating internal curing, compressive strength was unaffected at a w/c ratio of 0.33 and was reduced by 10% and 4% at w/c ratios of 0.25 and 0.21, respectively.

### **2.6.2 Tensile Strength**

Shin et al. (2010) reported that the splitting tensile strength of LWA mortars decreases with an increase in dosage of LWA. Golias et al. (2012) observed that at a low w/c ratio of 0.3, the splitting tensile strength of internally cured samples is lower than that of a plain mixture and that the percent reduction decreases progressively with an increase in age. However, at a high w/c ratio of 0.5, the splitting tensile strength of the internally cured samples was higher than that of plain mixtures.

### **2.6.3 Elastic Modulus**

Golias et al. (2012) observed that under any tested curing conditions (wet, moist, sealed, and drying), the plain mixtures show a higher elastic modulus than the internally cured samples. Shin et al. (2010) also reported that the elastic modulus decreases with an increase in the dosage of LWA.

## **CHAPTER 3: EFFECTS OF LWA ON DEFORMATION PROPERTIES OF MORTAR AND CONCRETE MIXTURES**

This chapter presents a detailed study on the effects of LWA on deformation properties (shrinkage, and early-age expansion) of mortar and concrete mixtures. Three types of LWA are discussed in terms of their efficiency of reducing shrinkage. In addition, the effects of dosage of LWA, w/c ratio, and soaking period of LWA on autogenous and drying shrinkage of mortar mixtures is explored. Finally, a discussion of the shrinkage behavior of concrete mixtures with LWA is presented. It should be noted that throughout this report the dosage of LWA refers to the replacement percentage of fine aggregate (sand) with LWA.

### **3.1 COMPARISON OF THE EFFECTIVENESS OF THREE TYPES OF LWA ON SHRINKAGE MITIGATION OF MORTAR MIXTURES**

The objective of this section is to compare three types of LWA and determine the most crucial properties of an LWA that influence its effectiveness in shrinkage mitigation under sealed and unsealed conditions. Hence, deformation of mortar specimens with three types of LWA under sealed and unsealed conditions is presented and discussed. Two of the LWAs used in this study were manufactured expanded blast-furnace slag, designated LWA-A and LWA-B. The third, designated LWA-C, is manufactured rotary-kilned expanded shale.

#### **3.1.1 Characteristics of Different LWAs**

The specific gravities of LWA-A, LWA-B, and LWA-C in a saturated surface dry (SSD) condition were 1.88, 2.15, and 1.69, respectively. The results for the sieve analysis, absorption, and desorption isotherms of these LWAs are shown in Figures 1, 2, and 3, respectively. As shown in the figures, the gradation of LWA-B and LWA-C is similar, and LWA-A is coarser—but all of them could be regarded as fine aggregates. Moreover, the absorption capacity of LWA-C is close to that of LWA-A and is higher than that of LWA-B. Finally, the desorption capacity of both LWA-B and LWA-C is higher than that of LWA-A.

Four different mixtures were prepared for each w/c of 0.34 and 0.44: a plain mixture with 0% LWA and three mixtures with 38%, 54%, and 35% replacement percentages of fine aggregate with pre-soaked LWA-A, LWA-B and LWA-C, respectively. It should be noted that pre-soaked LWAs were prepared by adding water (an amount equal to 24-hour absorption) to oven-dried, air-cooled LWAs and allowing at least 1 day for the LWAs to absorb all the water before using them in a mixture. This process was followed because it can ensure consistency in the saturation degree of LWAs among different batches. Moreover, the dosages of LWA-A, LWA-B, and LWA-C described above were calculated to provide the same amount of water for internal curing. The mixture proportions are shown in Table A.2 in Appendix A.

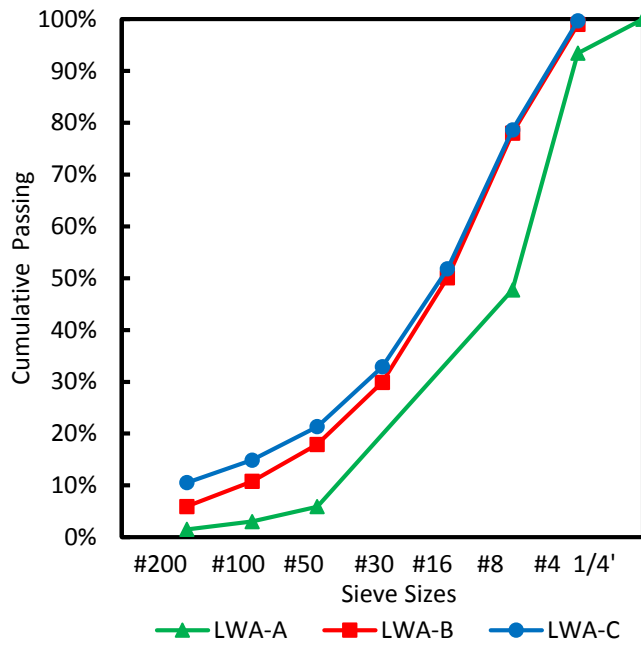


Figure 1. Sieve analysis of three types of LWA.

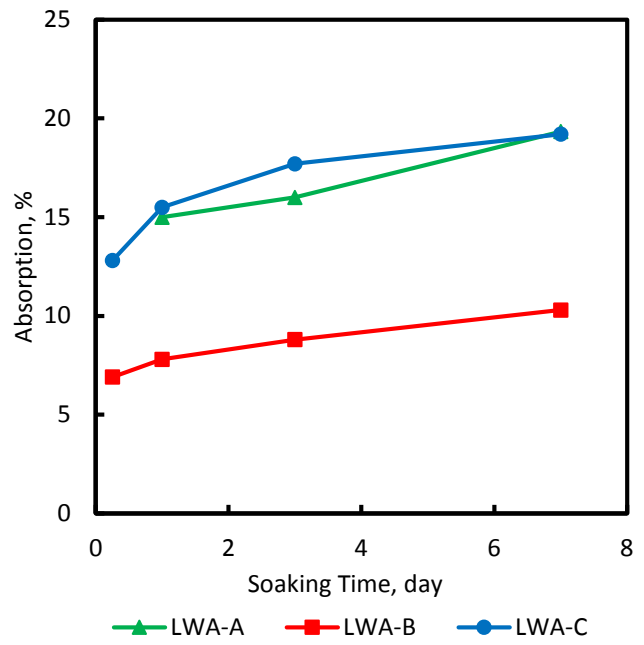


Figure 2. Absorption isotherms of three types of LWA.

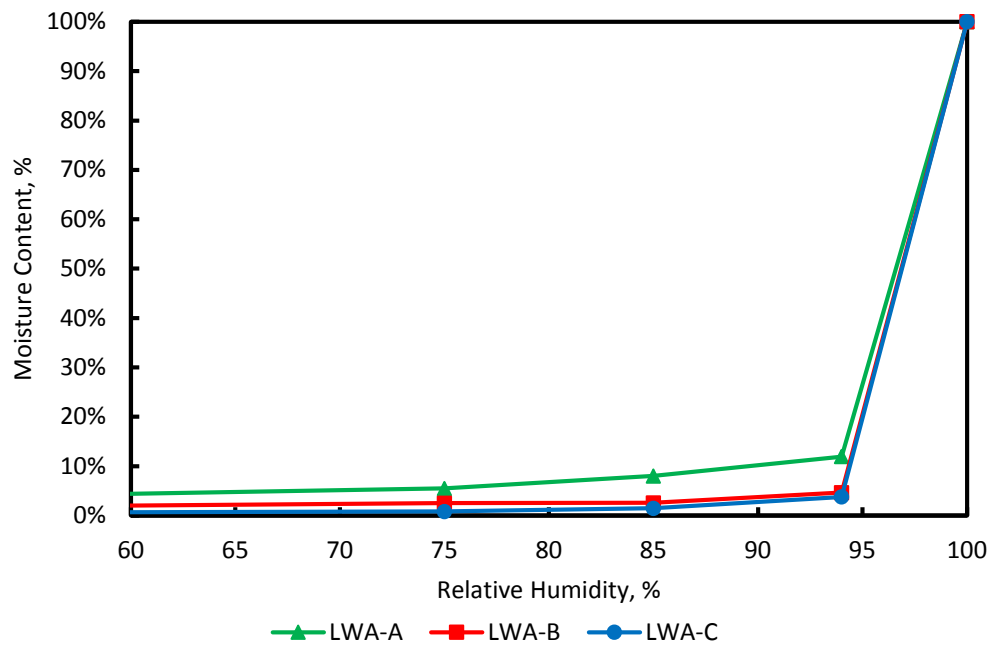


Figure 3. Desorption isotherms of three types of LWA.

### 3.1.2 Effects of Different Types of LWAs on Autogenous Shrinkage

Mortar prisms for shrinkage measurement were prepared in accordance with ASTM C596 (see Section A.2.5 in Appendix A for a detailed explanation of the method). The autogenous shrinkage of sealed mortar prisms at 0.34 and 0.44 w/c ratio is presented in Figures 4 and 5, respectively. The data from the first 24 hours were obtained from corrugated tubes, as explained in Section A.2.3 of Appendix A. An expansion during the first 24 hours was seen for mixtures with LWA, and is fairly similar regardless of LWA type (LWA-A; LWA-B; LWA-C). It was reported by Brooks (2015) that this expansion at early age occurs as a result of absorption of water by cement gel and forcing the gel particles apart with a resultant swelling pressure. It can also be seen from Figures 4 and 5 that all three types of LWA improved the shrinkage behavior in the sealed condition. Additionally, the effectiveness of three types of LWAs on shrinkage mitigation was very similar. Therefore, a reasonable conclusion is that the reduction in autogenous shrinkage in the sealed condition is very similar when using different types of LWAs, assuming that the same amount of internal curing water is provided.

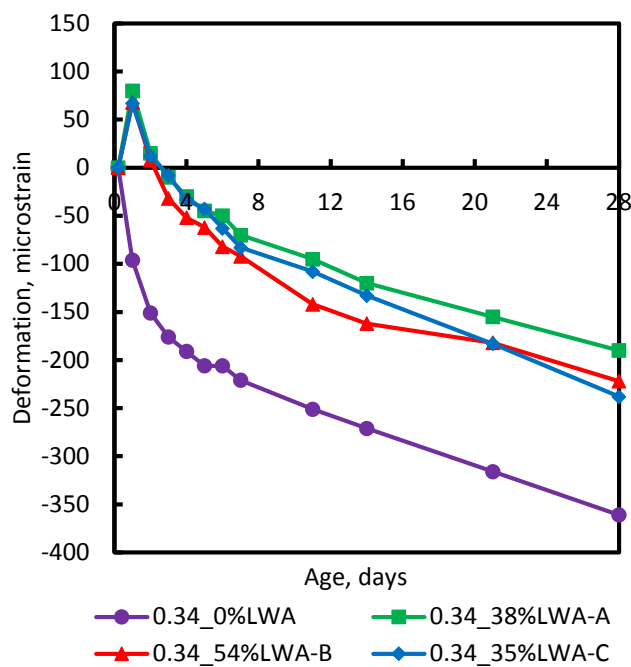


Figure 4. Autogenous (sealed) shrinkage of mortar specimens at 0.34 w/c ratio.

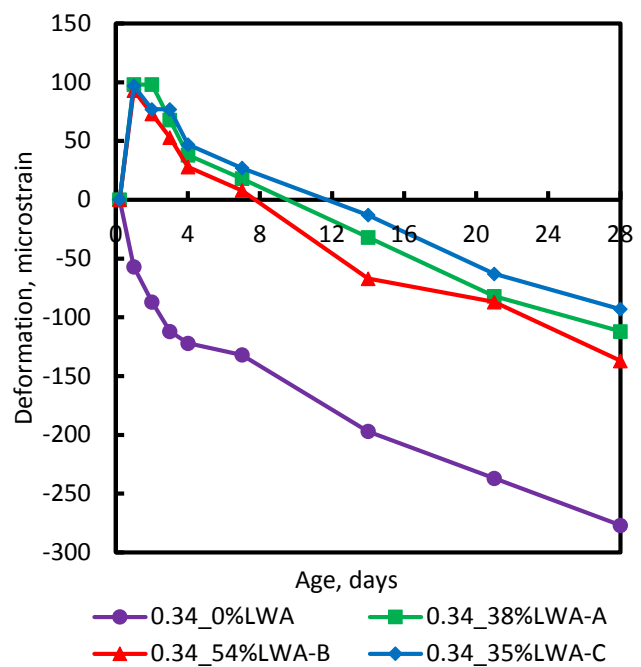
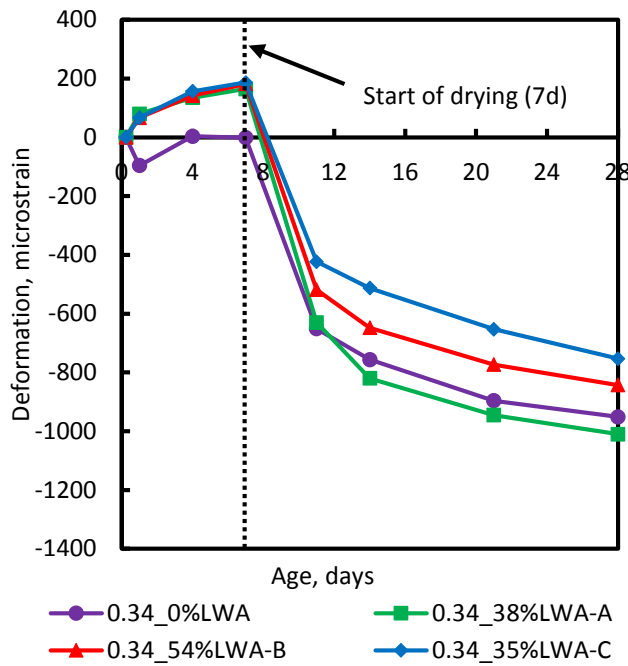


Figure 5. Autogenous (sealed) shrinkage of mortar specimens at 0.44 w/c ratio.

### 3.1.3 Effects of Different Types of LWAs on Drying Shrinkage

For measuring the effects of different types of LWAs on drying shrinkage, mortar prisms were demolded at day 1, cured in lime-saturated water for 6 days, and then exposed to drying at a constant temperature of 20 to 24°C (68 to 75°F) and relative humidity (50% ± 4%). The early-age expansion and subsequent drying shrinkage of unsealed mortar prisms at 0.34 and 0.44 w/c ratio are

presented in Figures 6 and 7, respectively. It should be noted that the deformations within the first 24 hours are from corrugated tube tests. It can be seen that all specimens with LWA expanded almost the same amount within the first 7 days, and the expansion was higher than that of the plain mixture. This early-age expansion is the primary source of difference in the net shrinkage of the control mixture and mortars with LWAs at 28 days. Moreover, it can be observed that the LWA-A shows similar shrinkage behavior as the control mixture. This is believed to be due to the coarser aggregate size of LWA-A compared with the other two LWAs. Providing the same amount of water through coarser LWA can reduce the “protected” paste volume; i.e. more paste is subjected to autogenous shrinkage since the volume of the provided water is distributed less uniformly. Another factor influencing the deformation behavior of mixtures with LWAs is believed to be the difference in the modulus of the specimens. As mentioned in Chapter 2, the addition of LWAs can result in a reduction in dynamic modulus of elasticity of concrete and mortar mixtures. It is hypothesized that a change in modulus can affect deformation properties (this hypothesis is examined in Section 4.4).



**Figure 6. Drying shrinkage (unsealed) of mortar specimens at 0.34 w/c ratio.**

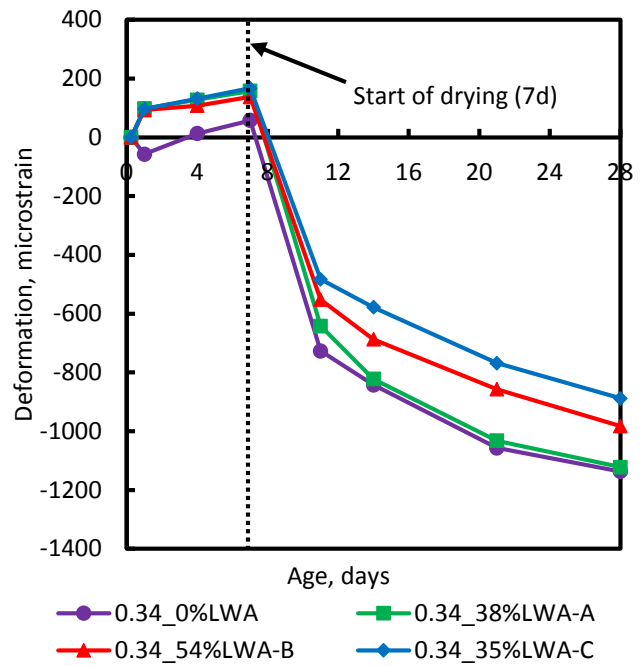


**Figure 7. Drying shrinkage (unsealed) of mortar specimens at 0.44 w/c ratio.**

### 3.1.4 Summary

It is important to remember that the type and source of LWAs can cause a difference in the effectiveness of mitigating autogenous and drying shrinkage as a result of different desorption characteristics, gradation, and modulus—even when the same amount of internal curing water is provided. However, the three types of LWA used in this study performed in a similar manner in sealed conditions and effectively reduced autogenous shrinkage. In contrast, incorporating internal curing

does not result in a considerable reduction in drying shrinkage. It should be noted that the LWA-C performed slightly better than the other two LWAs, especially in the unsealed curing condition, and hence was used for performing the rest of the experiments presented in this report.

### **3.2 EFFECTIVENESS OF LWA ON MITIGATION OF AUTOGENOUS SHRINKAGE IN MORTAR MIXTURES**

The objective of this part of the study was to investigate the effects of the dosage of pre-soaked LWA, w/c ratio, and soaking time of LWA on the shrinkage of mortar mixtures with LWA. Four mixtures for each w/c of 0.34 and 0.44 with 0%, 13%, 25%, and 38% LWA were prepared and cured under sealed or unsealed conditions. The mixture proportions are shown in Table A.3 in Appendix A. An extra mixture with LWA pre-soaked for a longer period of time (7 days) was also prepared and cured under sealed and unsealed conditions. It should be noted that the LWA discussed in this section of the report was the same as LWA-C described in the previous section.

#### **3.2.1 Effects of Dosage of LWA and W/C on Autogenous Shrinkage of Mortar Mixtures**

The measured autogenous shrinkage of mortar specimens with w/c ratios of 0.34 and 0.44 is presented in Figures 8 and 9, respectively. It can be seen that for both w/c ratios, the total shrinkage decreases as the dosage of the LWA increases. This is expected because higher dosages of LWA could provide higher amounts of extra water and thus could maintain a higher internal relative humidity. Additionally, the early-age expansion increases with the increase in LWA dosage.

Regarding the effects of w/c ratio on autogenous shrinkage, the results presented in Figures 8 and 9 can be compared for the same LWA dosage. It can be observed that for any LWA dosage, the specimens with a 0.44 w/c ratio showed less shrinkage than those with a 0.34 w/c ratio. This is because a higher w/c ratio could maintain the internal relative humidity at a higher level and for a longer period of time, which could mitigate self-desiccation and reduce autogenous shrinkage. However, another way to look at the data is that autogenous shrinkage can be effectively reduced by incorporating LWA without increasing the w/c ratio.

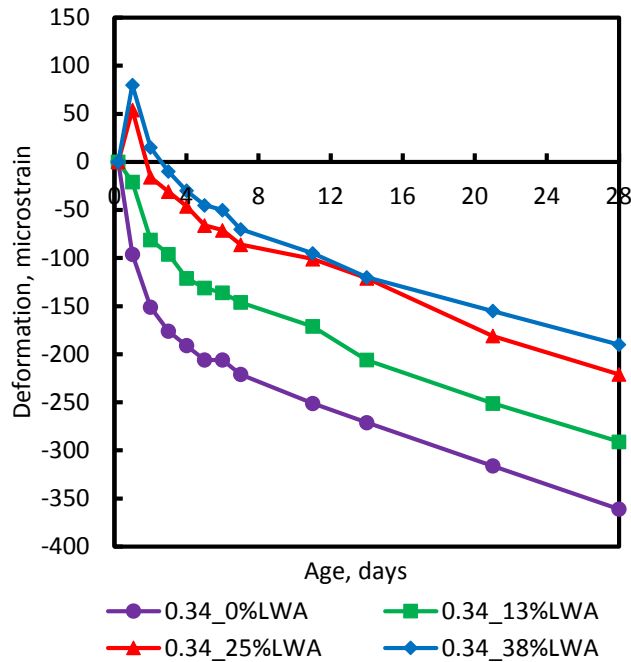


**Figure 8. Deformation results for sealed mortar specimens at 0.34 w/c.**

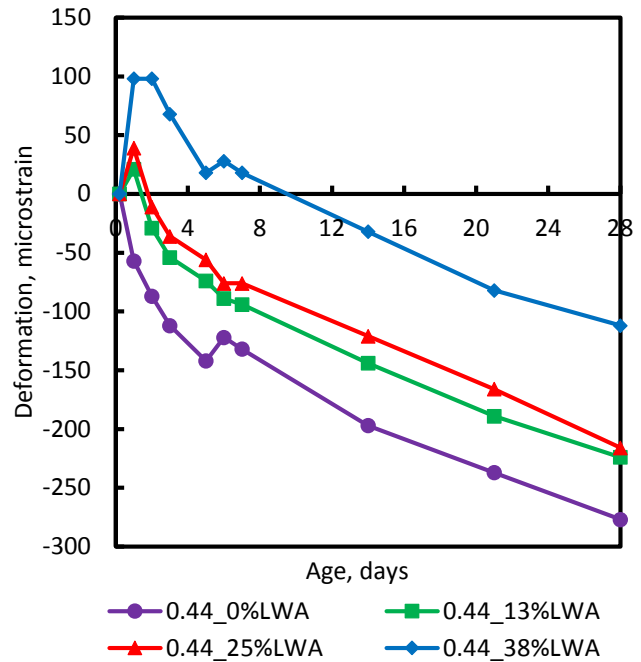


**Figure 9. Deformation results for sealed mortar specimens at 0.44 w/c.**

### 3.2.2 Effects of Soaking Time of LWA on Autogenous Shrinkage of Mortar Mixtures

This section summarizes the effects of soaking time of LWA (which correlates with the amount of water absorbed by the LWA, as shown in Figure 2) on autogenous shrinkage. For the experiments performed in this section, the pre-soaked LWA was prepared by mixing oven-dried, air-cooled LWA with an amount of water sufficient for a 7-day absorption and then allowing the specimen to absorb the added water for at least 7 days. Figure 10 provides the comparison of the deformation of 38% LWA replacement dosage soaked for 1 day and 7 days at 0.34 w/c. It can be seen that a longer soaking period increases the early-age expansion and results in a lower net shrinkage at 28 days. It is believed that this behavior is due to the extra water provided, which could further minimize self-desiccation and maintain the internal relative humidity at a higher value.

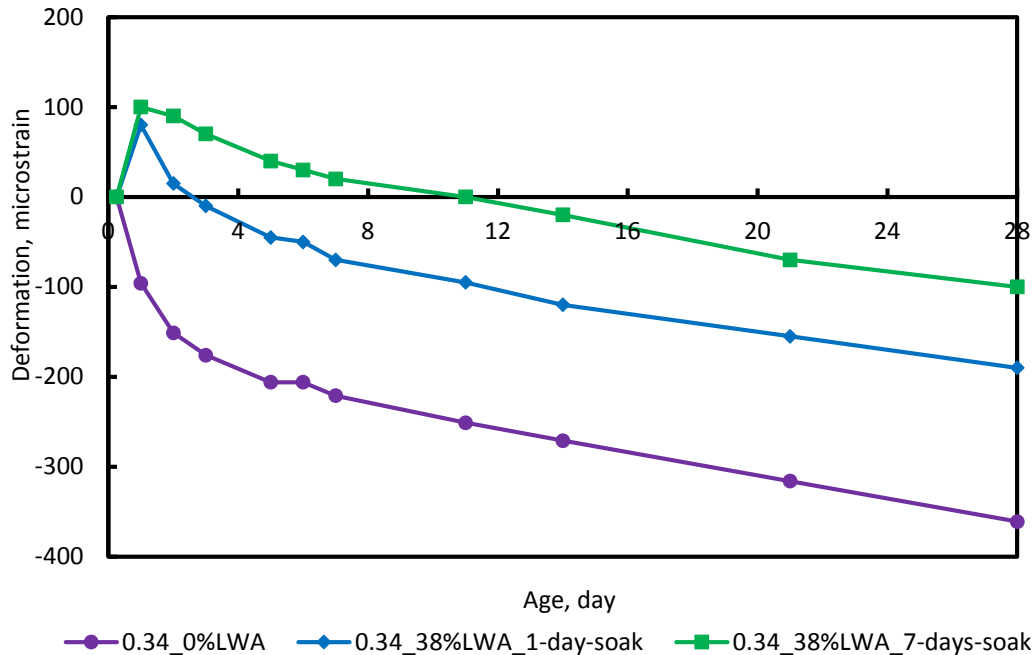


**Figure 10. Effect of soaking time on autogenous deformation of mortar specimens.**

### 3.2.3 Summary

Under sealed conditions, autogenous shrinkage decreases and early-age expansion increases as the dosage of the LWA is increased. Specimens with a higher w/c ratio showed less net shrinkage at 28 days. However, replacing a portion of the sand with LWA is an effective method of reducing autogenous shrinkage without increasing the w/c ratio. Finally, it was observed that a longer soaking time could improve the effectiveness of LWA in reducing autogenous shrinkage. This is a significant finding because it indicates that instead of increasing the dosage of LWA to better mitigate autogenous shrinkage, a lower dosage with a longer soaking time (7 days instead of 1 day) can be used. The results presented in this section demonstrate that autogenous shrinkage is inversely proportional to the amount of internal curing water provided (i.e., increasing the amount of internal curing water, whether by increasing the dosage of LWA or by increasing the initial moisture content of LWA through a longer soaking time, results in a decrease in autogenous shrinkage).

### 3.3 EFFECTIVENESS OF LWA ON MITIGATION OF DRYING SHRINKAGE IN MORTAR MIXTURES

As discussed in Section 3.1.3, LWA might not successfully mitigate drying shrinkage. This section provides the details and findings of a thorough study to better understand the effects of pre-soaked LWA on drying shrinkage of mortar specimens.

The severity of drying conditions was adjusted by exposing a different number of sides of the mortar prisms to the drying environment. The specimens with four sides unsealed represent a severe drying condition because moisture loss occurs from the entire surface. On the other hand, the specimens with two sides and with one side unsealed represent milder drying conditions. This method was used

to study the effects of the severity of drying conditions on the efficiency of LWA to reduce drying shrinkage. It should be noted that while applying the results of this work to real-world scenarios, the severity of drying conditions depends on the rate of evaporation of water from concrete to the surrounding environment. The factors influencing such rate include but are not limited to relative humidity, wind speed, and air temperature of the surrounding environment.

In this work, two different curing procedures (sealed curing and wet curing under lime-saturated water) were used, and the drying shrinkage results were compared to identify the most suitable curing method when LWA is used in a mixture.

For this part of the study, three mixes were prepared—one with an effective w/c ratio of 0.34 without any LWA, one with an effective w/c ratio of 0.34 with 38% of fine aggregate replaced with LWA, and a third mix with an effective w/c of 0.43 without any LWA. The 0.43 w/c mixture represents the equivalent total w/c ratio for the mix with LWA (considering the internal curing water). The mixture proportions are shown in Table A.4 in Appendix A. Table 1 is a complete listing of specimen designations used in this section.

**Table 1. Specimen Designations**

Specimen designation	No curing	6 days wet curing	6 days sealed curing	4 sides unsealed	2 sides unsealed	1 side unsealed
4UNC	×			×		
2UNC	×				×	
1UNC	×					×
4U6DW		×		×		
2U6DW		×			×	
1U6DW		×				×
4U6DS			×	×		
2U6DS			×		×	
1U6DS			×			×

### 3.3.1 Effectiveness of LWA in Reducing Drying Shrinkage of Mortar Mixtures When No Curing Is Applied

Figures 11, 12, and 13 show the drying shrinkage of mortar specimens when no curing is applied and when four sides, two sides, and one side of the mortar prisms were unsealed. Not applying curing basically means that the specimens are exposed to drying immediately after demolding at an age of 1 day. It can generally be seen in Figures 11, 12, and 13 that when the exposure condition is less severe (fewer number of sides unsealed), the drying shrinkage (for the same mixture) is lower as a result of a lower rate of moisture loss to the surrounding environment. When a severe drying condition is applied, the specimen with LWA behaves only slightly better than the 0.34\_0%LWA mix and also shows more shrinkage than the 0.43\_0%LWA mixture. However, in a mild drying condition (i.e., the specimen with one side unsealed), the mix with LWA shows lower shrinkage compared with the two other mixtures.

To better illustrate this behavior, Figures 14 and 15 show the drying shrinkage and mass loss of 0.34, 38% versus 0.43, 0% mortar specimens in different exposure conditions. These two mixtures have the same total w/c ratio (considering the internal curing water for 0.34, 38% mixture); however, the mass loss plot shows a different behavior based on exposure condition. In a severe drying condition, the mix with LWA shows a higher mass loss, but when a milder drying condition is implemented, the mix without LWA shows a higher mass loss.

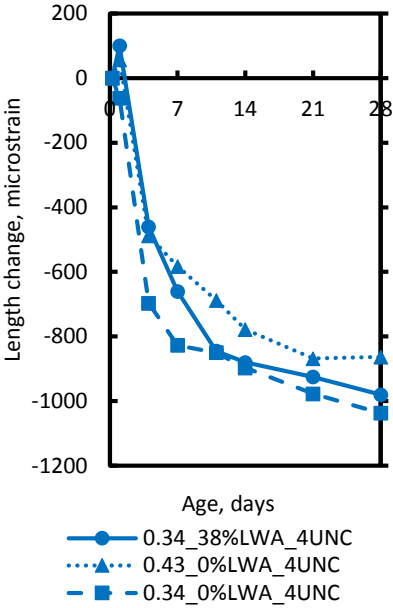


**Figure 11. Drying shrinkage of specimens with four sides unsealed; no curing.**

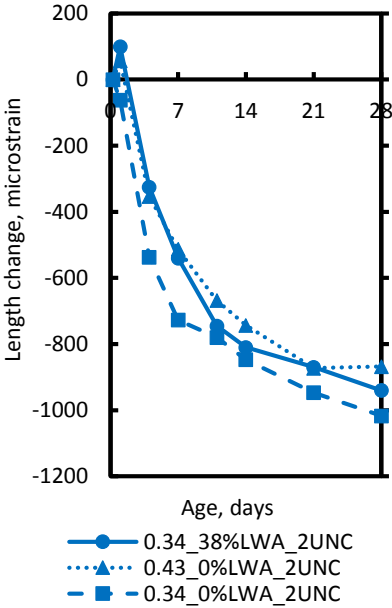


**Figure 12. Drying shrinkage of specimens with two sides unsealed; no curing.**

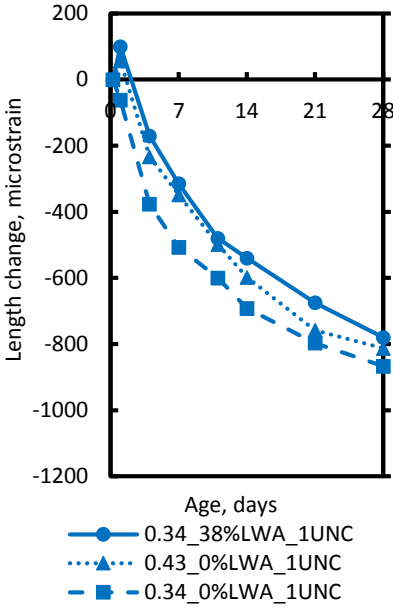


**Figure 13. Drying shrinkage of specimens with one side unsealed; no curing.**

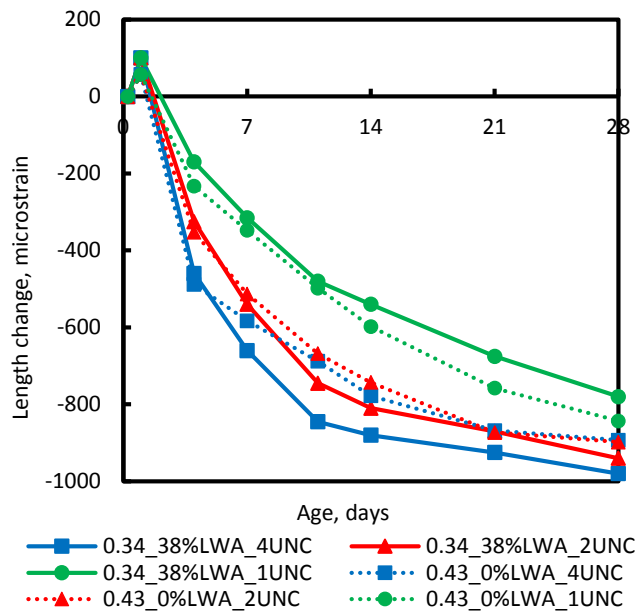


**Figure 14. Drying shrinkage of 0.34, 38% versus 0.43, 0% mortar specimens in different exposure conditions.**

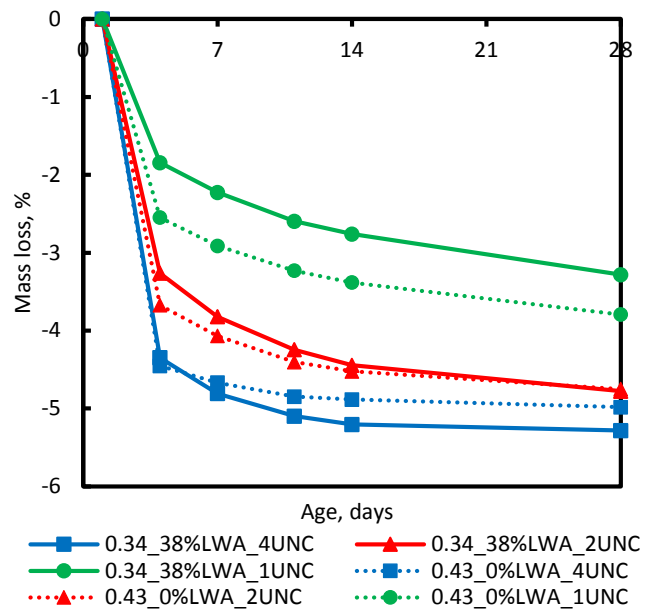


**Figure 15. Mass loss of 0.34, 38% versus 0.43, 0% mortar specimens in different exposure conditions.**

### 3.3.2 Effectiveness of LWA in Reducing Drying Shrinkage of Mortar Mixtures When Wet or Sealed Curing Is Applied

Figures 16, 17, and 18 present drying shrinkage of mortar prisms measured during various degrees of drying achieved through four sides, two sides, and one side being unsealed, after using different curing methods for the first 7 days. Both wet curing and sealed curing was performed on shrinkage prisms immediately after demolding at the age of 1 day. Wet-cured specimens were placed in lime-saturated water for 6 days and then were exposed to drying. Sealed-cured specimens were sealed on all sides, with aluminum tape, for 6 days and then were exposed to drying. It is clear from the figures that either of the two methods of curing, wet or sealed, is beneficial in reducing drying shrinkage of specimens with LWA compared with no curing. Even in a severe drying condition (4U), the LWA specimens show considerably lower shrinkage than the 0.34\_0%LWA and 0.43\_0%LWA mixtures did. Figure 19 presents a comparison between sealed and wet curing methods. It can be seen that wet curing is more advantageous than sealed curing in reducing the drying shrinkage, even when LWA is used to provide internal curing. This is primarily related to the increase in early-age expansion (during the first 7 days of aging) when wet curing is provided.

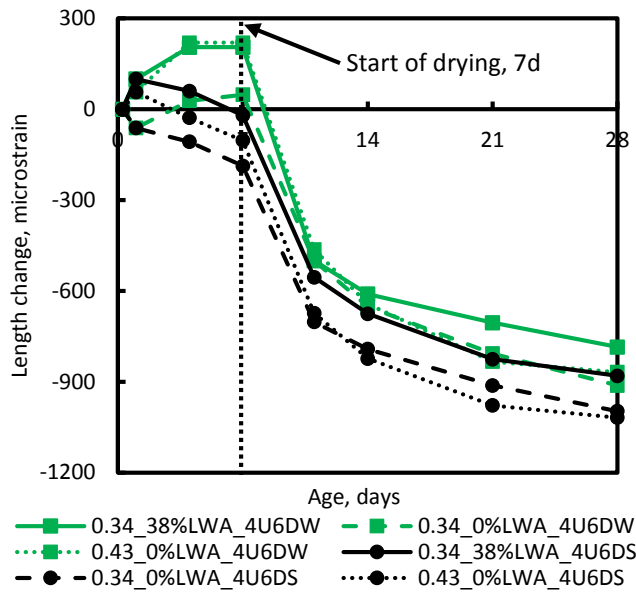


Figure 16. Drying shrinkage of specimens with four sides unsealed; no curing.

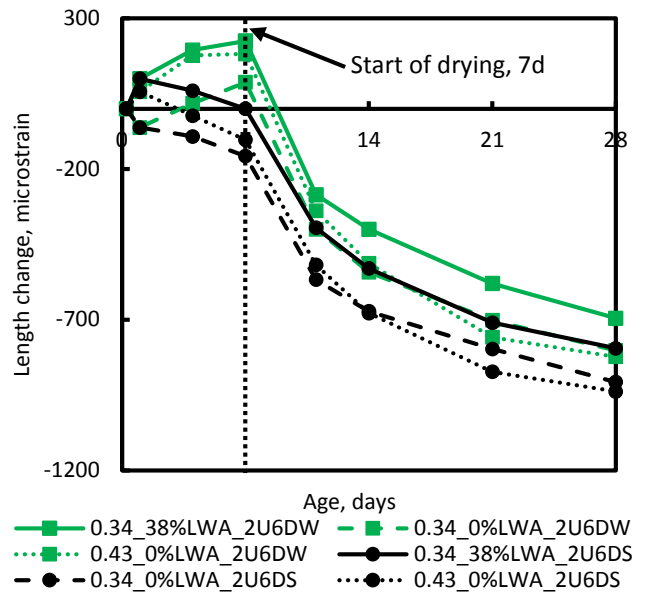


Figure 17. Drying shrinkage of specimens with two sides unsealed; no curing.

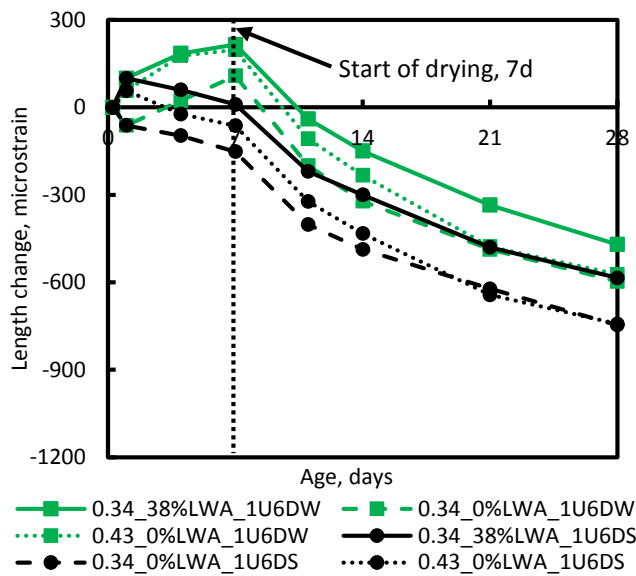


Figure 18. Drying shrinkage of specimens with one side unsealed; no curing .

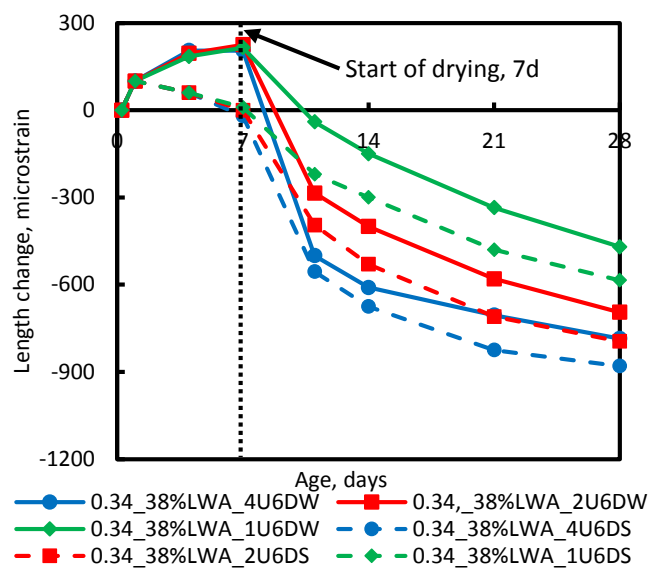


Figure 19. Drying shrinkage from wet and sealed curing under different exposure conditions.

### 3.3.3 Summary

This section presented a detailed discussion of the effect of pre-soaked LWA on drying shrinkage of mortar specimens. To change the rate of evaporation of moisture from the specimens and study its effect on drying shrinkage, different specimens with a different number of unsealed sides (one, two, and four) were prepared and exposed to the drying environment.

In a severe drying condition, when no curing method is applied, LWA is not beneficial in reducing drying shrinkage. However, in a milder drying condition, LWA can be favorable in reducing drying shrinkage. LWA can be effective in reducing drying shrinkage, even in a severe drying condition when either type of curing method (wet or sealed) is used. This finding shows the significance of conventional external curing, even in mixes in which internal curing is implemented. Moreover, wet curing is more beneficial than sealed curing mainly because of the increased early-age expansion caused by the absorption of water.

## 3.4 EFFECTIVENESS OF LWA ON MITIGATION OF DRYING SHRINKAGE OF CONCRETE MIXTURES

In this section, the effects of LWA on the deformation of concrete specimens under both sealed and unsealed conditions are presented and discussed. Similar to what was described in the previous sections, three mixtures were prepared: one with an effective w/c ratio of 0.39 without any LWA, one with an effective w/c ratio of 0.39 with 38% LWA in terms of replacement percentage of fine aggregate with LWA, and a third mix with an effective w/c of 0.55 without any LWA. The mix with 0.55 w/c ratio represents the equivalent total w/c ratio for the mix with LWA (considering the internal curing water). It should be noted that a control mixture with a w/c ratio of 0.39 was chosen for this evaluation because it represents the w/c ratio that IDOT generally uses for concrete bridge decks. Table A.5 in Appendix A presents a detailed mix design for the concrete mixtures.

As with the previous tests, the specimens were either sealed completely to measure autogenous shrinkage or were exposed to varying degrees of drying under different conditions—four sides unsealed (4U) and one side unsealed (1U)—to measure drying shrinkage. The effects of curing on drying shrinkage were also measured by curing one set of specimens in lime-saturated water and then exposing them to drying.

### 3.4.1 Effectiveness of LWA in Reducing Autogenous Shrinkage of Concrete

It can be seen in Figure 20 that the autogenous shrinkage of the concrete prisms is considerably smaller than that of the mortar prisms. This is expected because the presence of the coarse aggregates in concrete provides volume stability for the mixture and reduces length change. The concrete mixture was designed in a way to equate the total volume percentage of LWA in concrete and mortar mixtures, i.e. 38% replacement of fine aggregate with LWA in mortar mixtures and 76% replacement of fine aggregate with LWA in concrete mixtures both corresponds with 21% LWA in terms of total volume of the mixture. From Figure 20 it can also be seen that the addition of LWA greatly helps in reducing autogenous shrinkage. Even when the same amount of water (sum of the mixing water plus that provided by internal curing) is added to a mixture upfront (i.e., the 0.55\_0%LWA mixture), autogenous shrinkage increases as compared to the mix with LWA. It can

therefore be concluded that although increasing the total w/c ratio helps reduce autogenous shrinkage, and doing so by adding pre-soaked LWA is more beneficial than by increasing the w/c ratio.

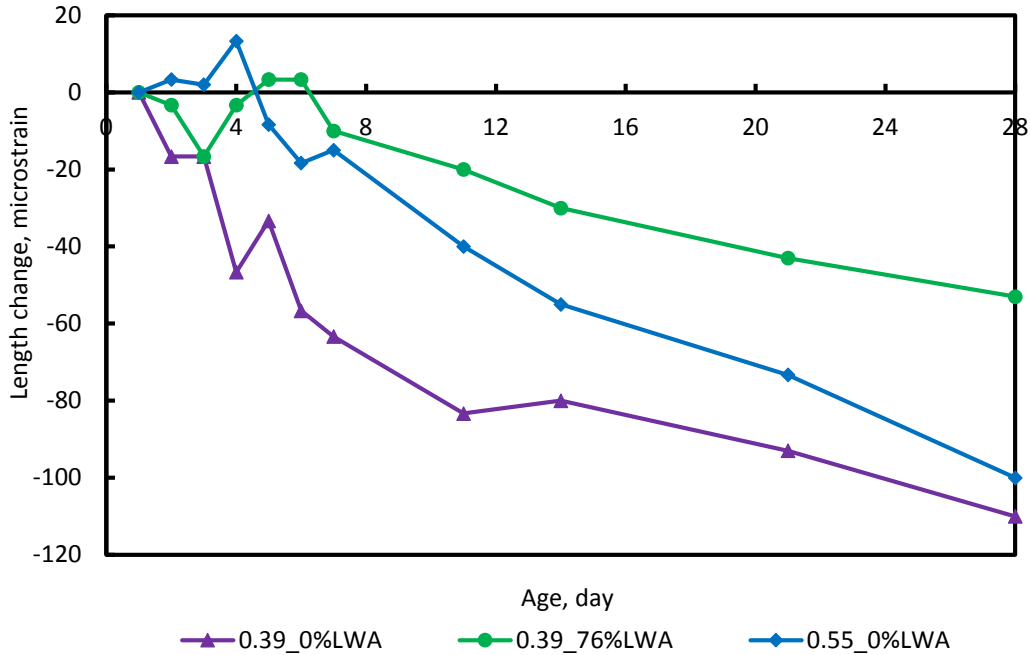


**Figure 20. Autogenous shrinkage of sealed concrete prisms.**

### 3.4.2 Effectiveness of LWA in Reducing Drying Shrinkage of Concrete

Figures 21 and 22 show the drying shrinkage of the four-side and one-side unsealed concrete specimens when no curing is applied. Figure 23 shows the early-age expansion and drying shrinkage of the four-side unsealed concrete specimens when wet curing is applied. The specimens in Figure 23 are cured for 6 days after demolding (which occurs 1 day after casting) and then exposed to drying. It can be seen that only when the specimens are subjected to drying with one-side unsealed does the mixture with LWA show lower shrinkage as compared to the control (i.e., the 0.39\_0%LWA mixture). In the other two cases (four-sides unsealed with no curing versus 6 days wet curing) the length deformation of the 0.39\_76%LWA mix is almost identical to that of the 0.39\_0%LWA. This again emphasizes the inability of LWA to counteract drying shrinkage in a severe drying condition. Moreover, it can be seen from Figure 23 that the mix with LWA expanded less than the other two mixes. It should be noted that higher early-age expansion results in a higher amount of built-up compressive stress in the mixture, which can later be used to counteract the tensile stresses caused by drying shrinkage.

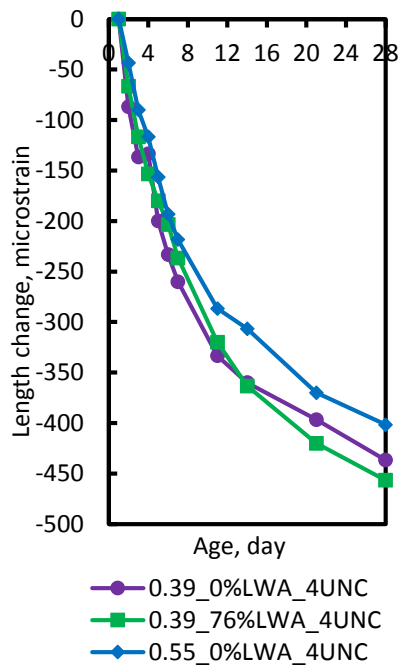


**Figure 21. Drying shrinkage of specimens with four sides unsealed; no curing.**

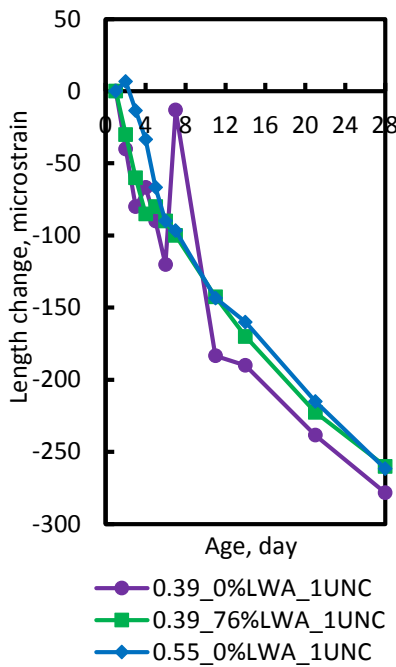


**Figure 22. Drying shrinkage of specimens with one side unsealed; no curing.**

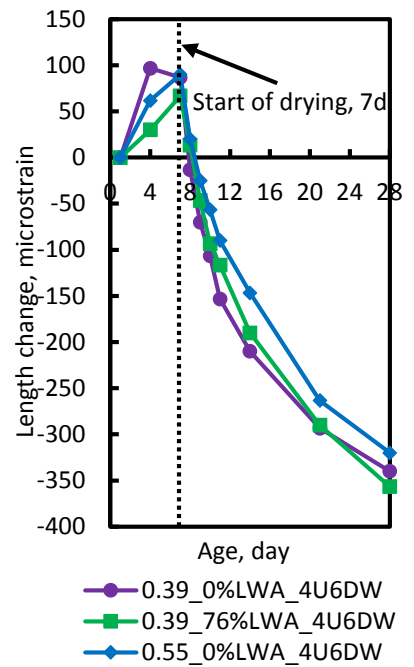


**Figure 23. Drying shrinkage of specimens with four sides unsealed; wet curing.**

### 3.4.3 Summary

From the analysis of the experimental results of concrete prisms with LWA under sealed and unsealed conditions, it was concluded that under sealed conditions, addition of LWA could dramatically reduce the autogenous shrinkage of concrete. However, under unsealed conditions, LWA decreased early-age expansion and did not affect the drying shrinkage of concrete later on.

## **CHAPTER 4: EFFECTS OF COMBINING INTERNAL CURING WITH USE OF EXPANSIVE ADDITIVE SUCH AS TYPE K CEMENT ON SHRINKAGE OF MORTAR AND CONCRETE**

Calcium sulfoaluminate (CSA)-based expansive cements such as Type K additives were developed for shrinkage compensation of concrete. The expansive nature of CSA-based cements can be used to enhance the resistance against shrinkage cracking by inducing compressive stress in concrete. Because of the higher water demand of CSA cement for achieving full hydration compared with ordinary portland cement (OPC), elevated water-to-cement (w/c) ratios for OPC-CSA cement blends are required for successful mitigation of shrinkage. This chapter examines the effects of using pre-soaked LWA on deformation properties of OPC-CSA mortar and concrete specimens as an alternative to increasing the w/c ratio. The motivation behind this idea is to promote CSA hydration and increase the early-age expansion of OPC-CSA blends by curing the concrete internally while avoiding the undesirable impacts of an increased w/c ratio on the microstructure of the mixture. The influence of LWA addition on autogenous and drying shrinkage of mixtures with 15% replacement of OPC with CSA cement was studied. In addition to evaluating early-age expansion and shrinkage properties, total capillary porosity and compressive strength measurements on the mixtures at different ages were performed.

### **4.1 EFFECTS OF INTERNAL CURING ON DEFORMATION OF OPC-CSA MORTAR SPECIMENS**

A control mortar specimen without CSA cement or LWA was prepared as a reference point. In all the other mixes, 15% of the OPC was replaced with CSA cement, and different dosages of LWA (in terms of percentage of fine aggregate replaced) were added. Mixture proportions for the mortar specimens are presented in Table A.6 in Appendix A. The number following “CSA” refers to the replacement percentage of OPC with CSA cement, and the number following “LWA” represents the replacement percentage of fine aggregate with LWA. An additional mixture with a 0.412 w/c ratio was also prepared. That mix had the same total w/c ratio as the 0.34\_15%CSA\_35%LWA mixture. Therefore, comparing 0.34\_15%CSA-35%LWA and 0.412\_15%CSA\_0%LWA will assist in determining the efficiency of internal curing as opposed to increasing the w/c ratio.

#### **4.1.1 Sealed Curing Condition**

The deformation results of sealed OPC-CSA mortar specimens are shown in Figure 24. Addition of CSA to the control mixture results in a considerable early-age expansion that results in a positive deformation at the age of 28 days for all the mixtures with CSA. The main cause of this early-age expansion is formation of ettringite crystals from the hydration of ye’elimite. As can be seen in Figure 24, this early-age expansion is amplified when LWA is added to the mixture. More precisely, a progressive increase in expansion is seen with an increase in the dosage of LWA. As mentioned previously in Chapter 2, LWA can increase the internal relative humidity (or, in other words, decrease the drop in internal relative humidity) of the mixture by releasing its absorbed water. Therefore, hydration is generally promoted in mixtures containing LWA particles. Moreover, it can be observed

that 0.412\_15%CSA\_0%LWA did not expand as much as 0.34\_15%CSA\_35%LWA. It should be noted that those two mixtures had the same total w/c ratio; however, in the 0.34\_15%CSA\_35%LWA mix, internal curing was incorporated, and its advantage over merely increasing the w/c ratio can be observed.

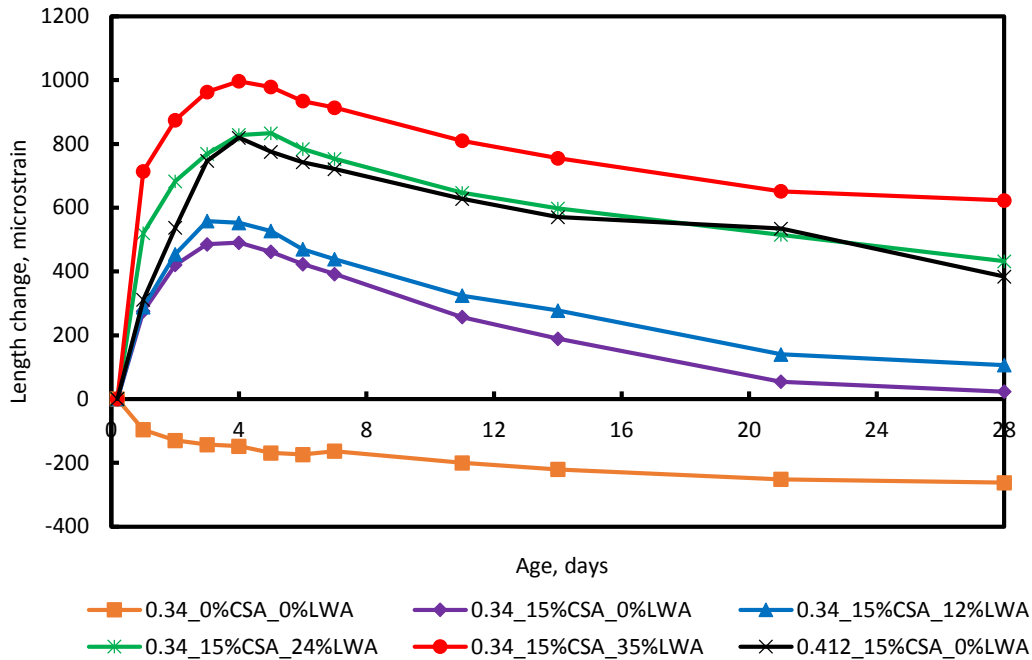


**Figure 24. Expansion and autogenous shrinkage of OPC-CSA mortar specimens in sealed condition.**

#### 4.1.2 Unsealed Curing Conditions

The early-age expansion and subsequent drying shrinkage of unsealed OPC-CSA mortar specimens are shown in Figure 25, while Figure 26 shows the mass change results of OPC-CSA mortar specimens in the unsealed curing condition. It should be noted that the data for the first 24 hours are the same as for sealed specimens, and both were collected using the corrugated tube protocol. Similar to the sealed specimens, an increase in early-age expansion can be observed when higher dosages of LWA are added to OPC-CSA mixtures. Here, the specimens are demolded at 1 day of age and then cured in lime-saturated water for 6 days. After that, the specimens were exposed to drying. Although during the first 7 days of aging, there was an excess of accessible water for the specimens to counteract self-desiccation, the specimens with LWA showed higher early-age expansion. This finding shows the advantage of using internal curing even in the presence of prolonged external curing. From Figure 25, it can also be observed that 0.412\_15%CSA\_0%LWA showed higher early-age expansion compared with 0.34\_15%CSA\_35%LWA. Therefore, internal curing is effective in promoting hydration of CSA cement and increasing early-age expansion; however, providing the extra water as mixing water can be more effective.

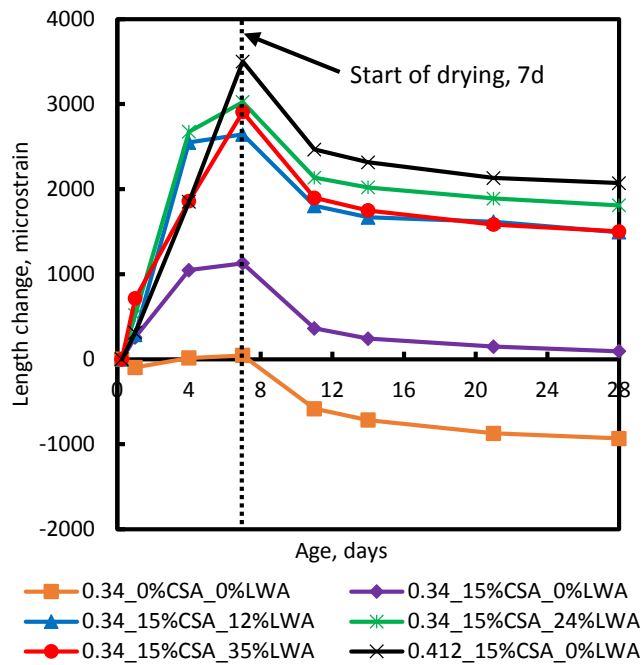


**Figure 25. Expansion and drying shrinkage results of OPC-CSA mortar specimens in unsealed curing condition.**

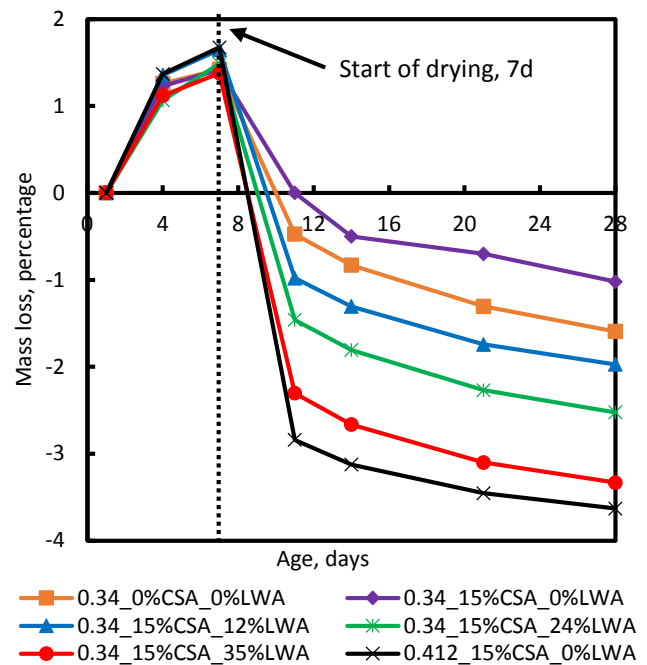


**Figure 26. Mass change results of OPC-CSA mortar specimens in unsealed curing condition.**

## 4.2 EFFECT OF INTERNAL CURING ON DEFORMATION OF OPC-CSA CONCRETE SPECIMENS

In order to study effects of LWA on deformation properties of OPC-CSA concrete mixtures, four mixtures were prepared. A low base w/c ratio of 0.34 for these mixtures were chosen. One control mixture with 0.34 w/c and without CSA nor LWA was prepared as the control mixture. For all the other mixtures 15% of OPC was replaced by CSA. A detailed mix proportion of the concrete mixtures is presented in Table A.7 in Appendix A. It can be seen that a mixture with 15% CSA, 0% LWA and with a w/c ratio of 0.49 was also prepared as the equivalent w/c ratio mixture for the mixture with 71% replacement of fine aggregate with LWA.

Figure 27 presents the deformation results of OPC-CSA concrete specimens in sealed curing condition with restraint. The method for preparing restraint concrete prisms is explained in detail in Section A.2.2 of Appendix A. The lower deformation of concrete compared with mortar specimens is expected because concrete possesses a higher volume stability due to presence of the coarse aggregate. Although the addition of restraint will limit the expansion behavior of CSA cement particles, the built-up compressive stress will later assist the mix in offsetting the tensile stress development due to autogenous shrinkage.

It can also be seen from Figure 27 that similar to mortar mixtures, addition of CSA to the mixture results in significant early-age expansion. Furthermore, increasing the total w/c of the mixture (either by adding pre-soaked LWA or by increasing the mixing w/c ratio) increases this early-age expansion.

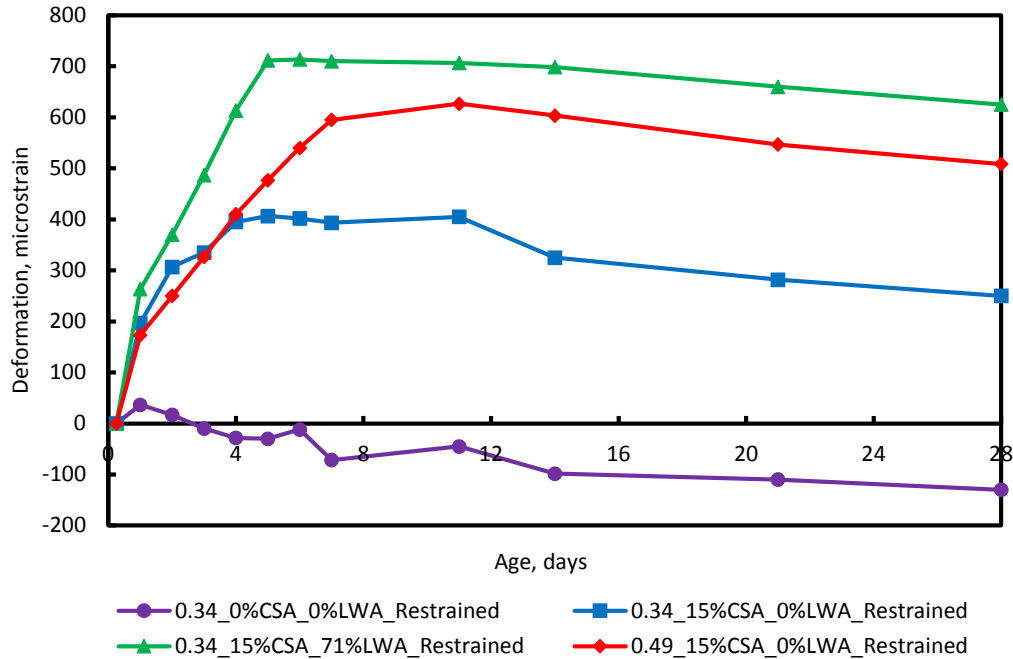
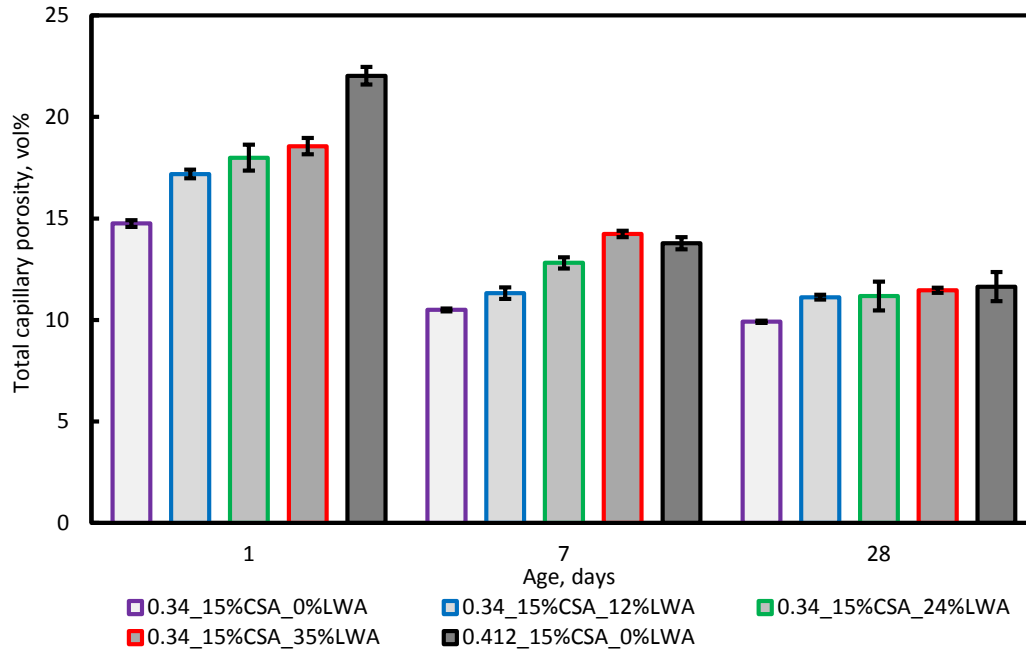


Figure 27. Expansion of OPC-CSA restraint concrete prisms in sealed curing condition.

### 4.3 EFFECT OF INTERNAL CURING ON MICROSTRUCTURE OF OPC-CSA BLENDS

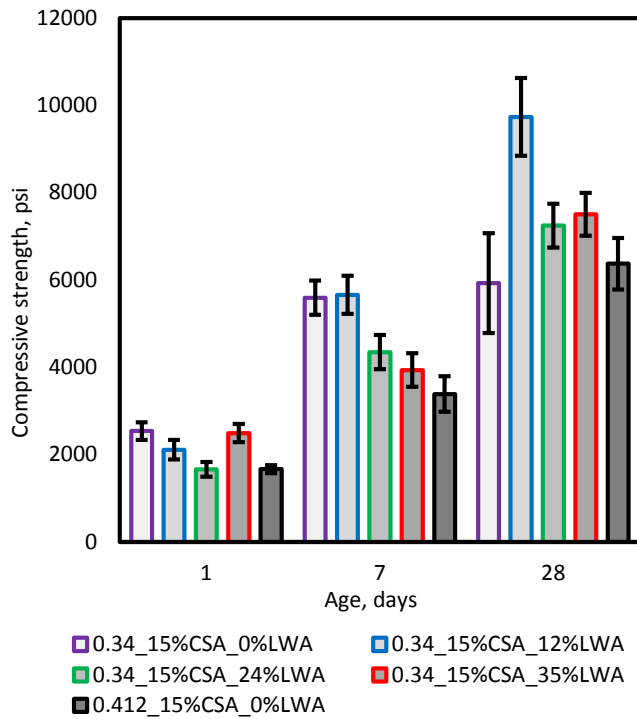
To further indicate the advantage of internal curing over increasing w/c ratio in OPC-CSA blends, total capillary porosity of the mixtures presented in Figure 24 was measured and is shown in Figure 28. As expected, the porosity of 0.412\_15%CSA\_0%LWA is higher than other mixes at day 1, right after demolding, which can be the reason behind the higher mass gain of this mixture during lime-saturated wet curing, as shown in Figure 26. Other values in Figure 28 (7 and 28 days) were measured while keeping the samples in a sealed condition. It can be seen that the trend alters after a period of sealed curing, which can be associated with the pores in LWA. It has been shown in the literature that the pores in LWA are relatively larger than the pores in cement paste (Henkensiefken et al. 2009b). Therefore, mixes with LWA hold a disadvantage in terms total porosity—assuming 15% porosity in LWA, with respect to the mix with 35% LWA, almost 3% of the total volume of the mixture is LWA’s pores. Therefore, it is not unexpected to see a lower total capillary porosity for 0.412\_15%CSA15\_0%LWA compared with 0.34\_15%CSA\_35%LWA at 7 days of age.



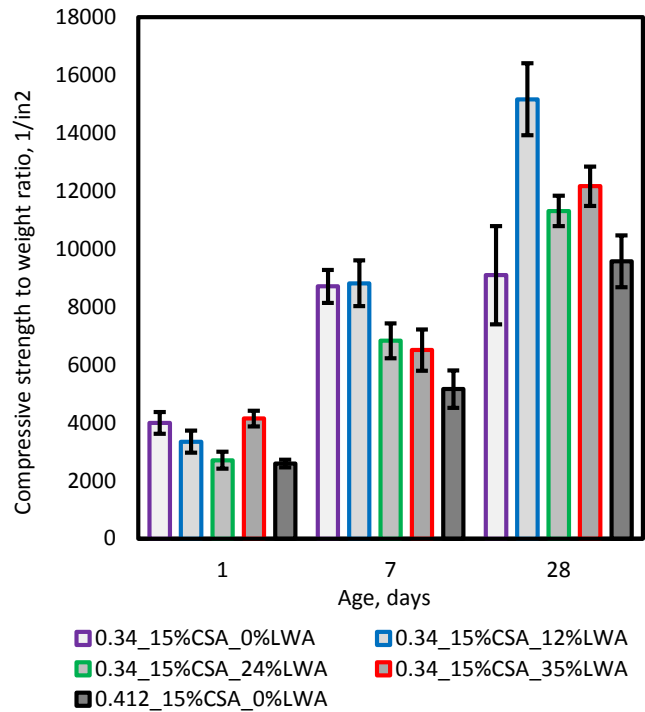
**Figure 28. Total capillary porosity results of OPC-CSA mortar specimens in the sealed curing condition.**

Figure 29 shows the compressive strength results of OPC-CSA mortar specimens in the wet curing condition. The values shown are the average of three 2x2x2-in cube specimens; the standard deviation of the values is shown as error bars on the plot. It should be noted that after demolding at the age of 1 day, the specimens were cured in a moist environment with 100% relative humidity. Compared with natural sand, LWA has weaker mechanical properties, which arise from its highly porous nature. Therefore, it is expected to observe a decrease in compressive strength when sand is replaced by LWA. Moreover, although the total w/c ratio of the 0.34\_15%CSA\_35%LWA and 0.412\_15%CSA\_0%LWA mixtures is the same, the one with LWA shows higher compressive strength. This again demonstrates the advantage of using internal curing instead of increasing the w/c ratio of the mixture.

Figure 30 shows the compressive strength to weight ratio of OPC-CSA mortar specimens. Replacing sand with LWA decreases the weight of the mixture because LWA has a lower specific gravity. Although the trend shown in Figure 30 is not much different than what is seen in Figure 29, the advantage of 0.34\_15%CSA\_35%LWA over 0.412\_15%CSA\_0%LWA is amplified. For instance, at day 1, 0.34\_15%CSA\_35%LWA showed a 49% higher compressive strength and a 60% higher compressive strength-to-weight ratio compared with the 0.412\_15%CSA\_0%LWA mix.



**Figure 29. Compressive strength results of OPC-CSA mortar specimens in a wet curing condition (1 Psi = 6.9 KPa).**



**Figure 30. Compressive strength-to-weight ratio of OPC-CSA mortar specimens in a wet curing condition.**

#### 4.4 EFFECT OF MODULUS ON DEFORMATION OF OPC-CSA MORTAR SPECIMENS

It has been shown so far that the driving force for the early-age expansion (ettringite formation) is increased when pre-soaked LWA is added to the mixtures with CSA cement. To further investigate this early-age expansion, the dynamic modulus of the samples was measured at different ages. The results are shown in Figure 31. A 22% decrease in dynamic modulus at an age of 7 days can be seen in the OPC-CSA sample when 35% LWA was added. Generally, if the driving force is comparable, a lower dynamic modulus will result in higher deformation. Therefore, it is expected that mixes with LWA will show higher deformation.

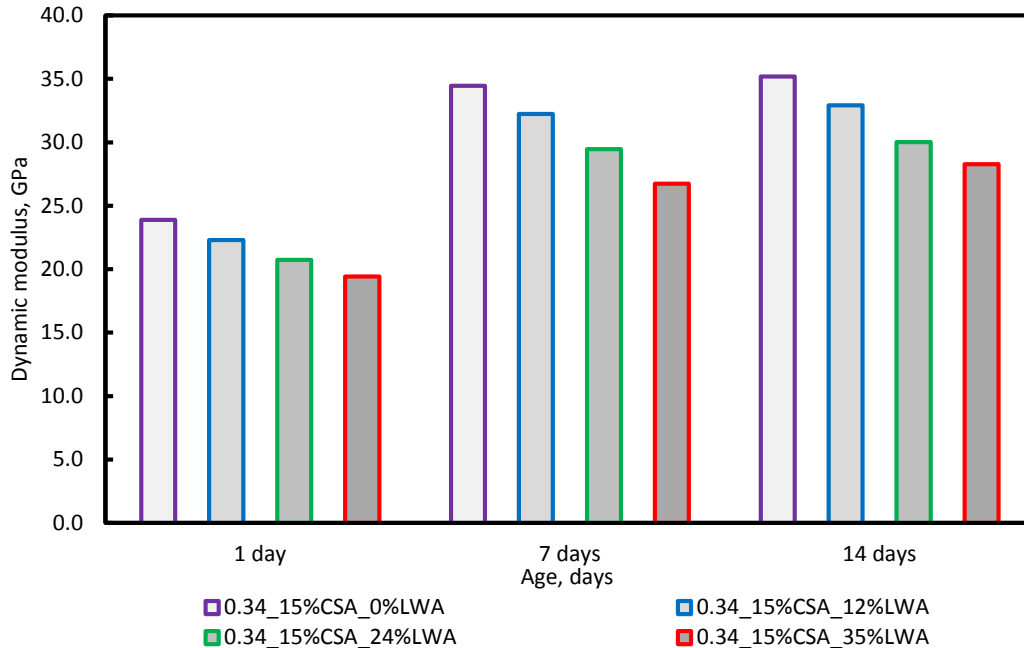


**Figure 31. Dynamic modulus of OPC-CSA mortar samples (1 GPa = 145 ksi).**

To further investigate the effect of modulus of deformation of mortar specimens, an inert inclusion was used to reduce the modulus of the 0.34\_15%CSA\_0%LWA mixture, and the effect of deformation was studied and compared with that of the 0.34\_15%CSA\_0%LWA plain mixture. Crumb rubber was used in this study as an inert material. It has been reported that the modulus of elasticity of concrete decreases significantly with addition of crumb rubber (or ground scrap tire rubber) to concrete (Eldin and Senouci 1993). To maintain consistent gradation, crumb rubber particles retained on a #8 sieve (passing a #4 sieve) were used. To keep the driving force for expansion similar, sand was replaced with crumb rubber in this mix.

After several attempts, it was concluded that replacing 18% of fine aggregate with crumb rubber results in a decrease in dynamic modulus that can be seen when 35% of fine aggregate is replaced with LWA (in the 0.34\_15%CSA\_35%LWA mixture). The dynamic modulus of this mix (designated as 0.34\_15%CSA\_18%R) is presented in Figure 32. Modulus results for 0.34\_15%CSA\_35%LWA are also presented in Figure 32 for comparison with 0.34\_15%CSA\_18%R; it can be seen that the moduli of these two specimens are very similar. The expansion results of these specimens are shown in Figure 33. Compared with the 0.34\_15%CSA\_0%LWA plain mixture, the 0.34\_15%CSA\_18%R mixture showed a 30% increase in expansion, based on the results at day 4. Moreover, considering only the shrinkage part of the plot (starting at day 4), 0.34\_15%CSA\_18%R showed 9% higher shrinkage compared with the 0.34\_15%CSA\_0%LWA plain mixture. It can be concluded that a change in dynamic modulus can indeed result in a change in deformation: a lower modulus can result in more expansion and more shrinkage.

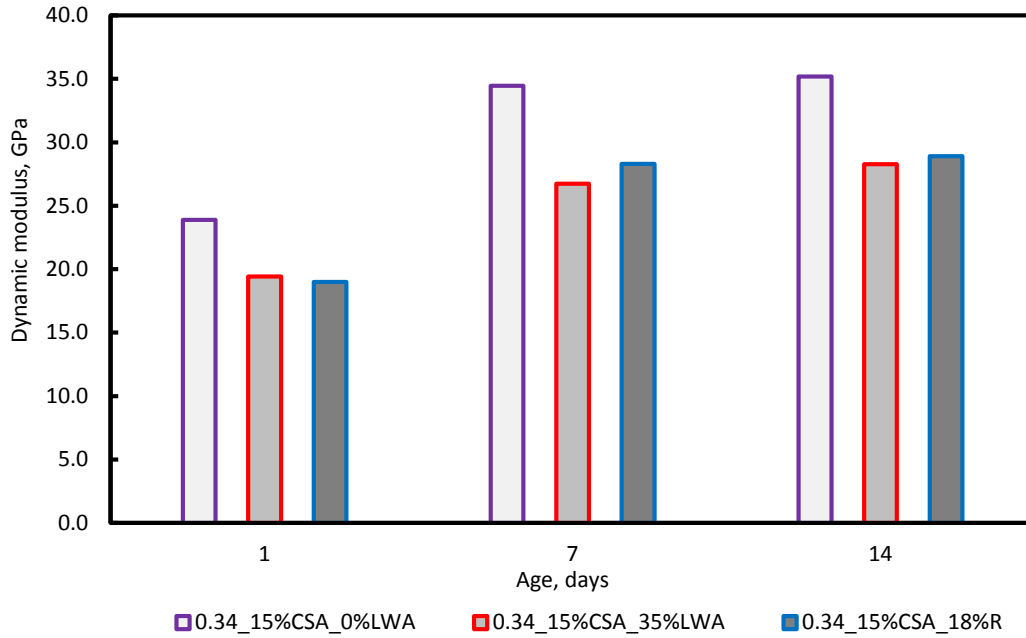


**Figure 32. Effect of addition of crumb rubber on dynamic modulus of OPC-CSA mortar samples (1 GPa = 145 ksi).**

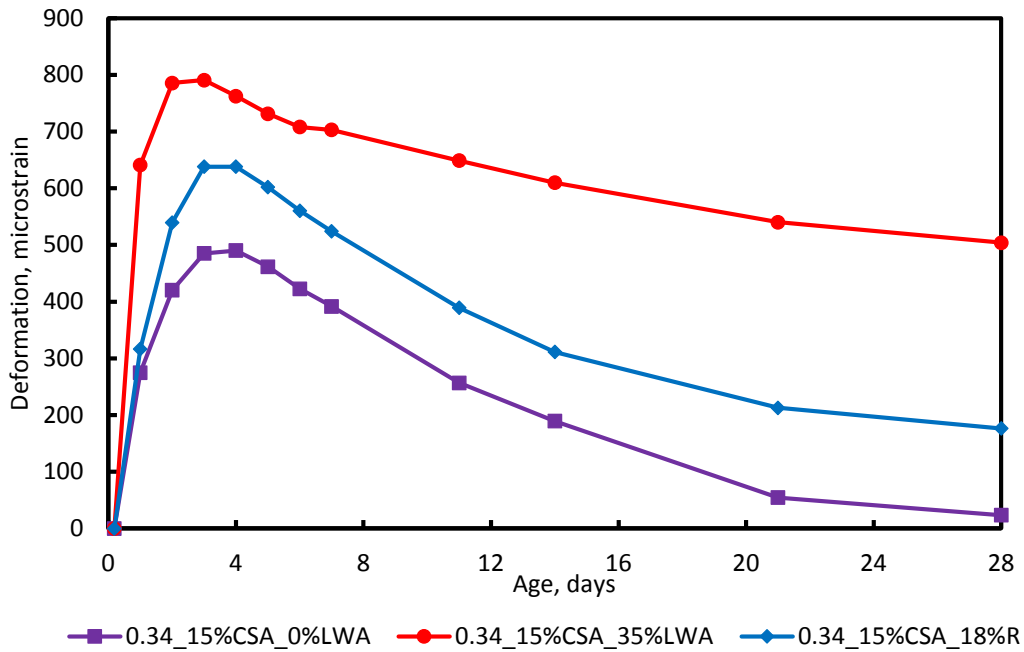


**Figure 33. Deformation results of OPC-CSA mortar specimens in a sealed curing condition.**

## 4.5 SUMMARY

This chapter summarized preliminary work on the combined effects on shrinking mitigation using expansive cements and LWA. Because CSA-based expansive additives such as Type K cements are known to require higher amounts of water for hydration, two different approaches for providing the same amount of extra water—increasing the effective (mixing) w/c ratio and incorporating internal curing using pre-soaked LWA—were studied.

It was observed that using LWA can increase the early-age expansion of mortar and concrete mixtures with Type K cements in a sealed condition, as compared with increasing the effective w/c ratio. Using an inert material (crumb rubber), it was shown that the bulk modulus of elasticity affects length deformation behavior: a lower modulus results in greater length deformation, whether shrinkage or expansion. However, it is clear that an LWA mix expands more than the equivalent crumb rubber mix with a similar modulus of elasticity. Therefore, it is also clear that the greater expansion in the LWA mixes are due not only to lower modulus but also to an increase in hydration of ye'elinite, which results in an increased formation of ettringite crystals.

Increasing the effective w/c ratio will result in a more porous microstructure, leading to absorption of a higher amount of moisture when the specimens are wet cured and therefore a greater early-age expansion compared with internally cured specimens with a lower effective w/c ratio. However, since an increase in the mixing w/c can result in an increase in permeability and affect durability of the mixture, using pre-soaked LWA as an alternative can be beneficial in terms of reducing shrinkage while avoiding the mentioned detrimental effects.

Moreover, it was observed that although the addition of LWA to Type K mixtures can decrease early-age compressive strength, it results in an increase in compressive strength at later ages (28 days). The preliminary results reported here are encouraging, and further detailed study related to durability is recommended before possible field application.

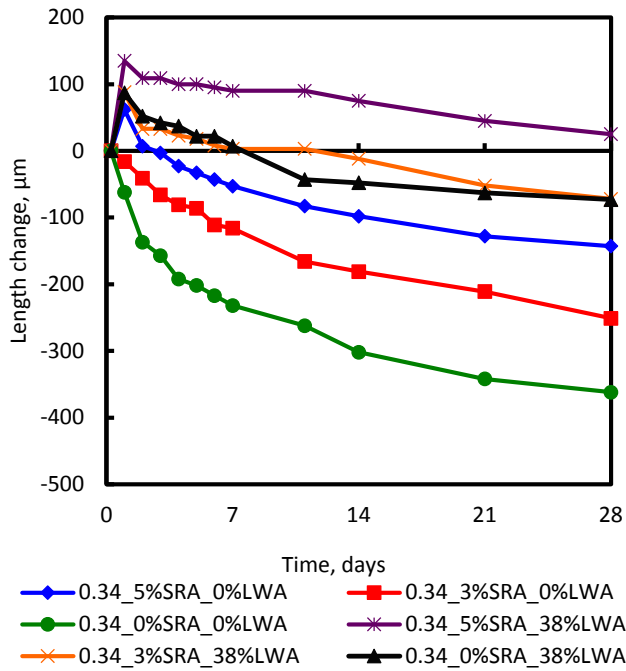
## **CHAPTER 5: EFFECTS OF COMBINING INTERNAL CURING WITH USE OF SHRINKAGE-REDUCING ADMIXTURES ON SHRINKAGE OF MORTAR AND CONCRETE**

In this chapter, the effects of combining LWA with shrinkage-reducing admixtures (SRA) on shrinkage of mortar and concrete are explored. As discussed previously, although LWA can be very effective in reducing autogenous shrinkage and counteracting self-desiccation, it could have an undesirable effect on drying shrinkage of mortar and concrete mixtures (for instance refer to Figure 6). Here, the results of a preliminary study on the interaction of SRA and LWA and their combined effects on autogenous and drying shrinkage of mortar and concrete mixtures are reported.

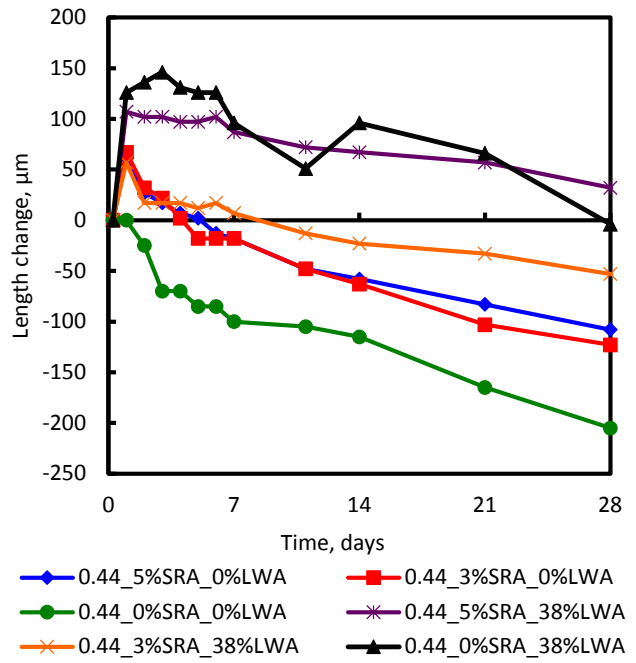
### **5.1 EFFECTS OF SRA ON AUTOGENOUS DEFORMATION OF MORTAR AND CONCRETE MIXTURES WITH INTERNAL CURING**

Figure 34 shows the autogenous deformation of mortar mixtures with SRA and LWA. Two dosages of SRA, 3% and 5% (based on weight of water), were chosen for this investigation. It should be noted that the manufacturer recommends a dosage in the range of 1% to 3%. A higher dosage of 5% was used in this study to pronounce the effect of addition of SRA in internally cured mixtures. Mixes with internal curing contained 38% LWA, in terms of replacement percentage of fine aggregate with LWA. It can be seen from Figure 34 that with an increase in the dosage of SRA, for either the control mixture or the mixture with LWA, autogenous shrinkage is reduced. It can also be observed that addition of LWA alone can be a better shrinkage compensating strategy as compared with addition of SRA alone. Although, it is evident from Figure 34 that the addition of SRA to mixes with internal curing can further reduce autogenous shrinkage. If sufficient SRA (5%) is added to the mixture, the mixture can remain somewhat volumetrically stable (shrinking only 110 microstrain in 27 days).

Figure 35 shows autogenous deformation for mortar mixtures with SRA and LWA and 0.44 w/c. The mixtures with only LWA alone, 0.44\_0%SRA\_38%LWA, showed a very low amount of shrinkage at 28 days. It is evident from Figure 35 that addition of 3% SRA to this mixture, 0.44\_3%SRA\_38%LWA, can actually increase the shrinkage considerably, whereas addition of 5% SRA to the mixture with LWA alone does not affect the net shrinkage at 28 days notably, 0.44\_0%SRA\_38%LWA as compared with 0.44\_5%SRA\_38%LWA. As shown in the figure, this increase in shrinkage can be a direct result of a reduction in early-age expansion. The highest early-age expansion occurs in the mixture with internal curing only. Therefore, at a relatively high w/c ratio, LWA alone can act better than SRA in reducing autogenous shrinkage, and the addition of SRA to mixtures with internal curing could increase the total shrinkage of mortar.



**Figure 34. Autogenous shrinkage of mortar mixtures with SRA and LWA at 0.34 w/c.**



**Figure 35. Autogenous shrinkage of mortar mixtures with SRA and LWA at 0.44 w/c.**

As before, a w/c ratio of 0.39 was selected for studying the effects of combining LWA with SRA in the autogenous shrinkage of concrete mixtures. The results for autogenous shrinkage of concrete mixtures with SRA and LWA are presented in Figure 36. The addition of LWA to a mixture without any SRA reduces the autogenous shrinkage considerably. The addition of SRA to the mix with LWA only further reduces autogenous shrinkage by a slight amount. Therefore, of the two methods (i.e., using LWA or SRA in reducing autogenous shrinkage of concrete mixtures), LWA performs considerably better.

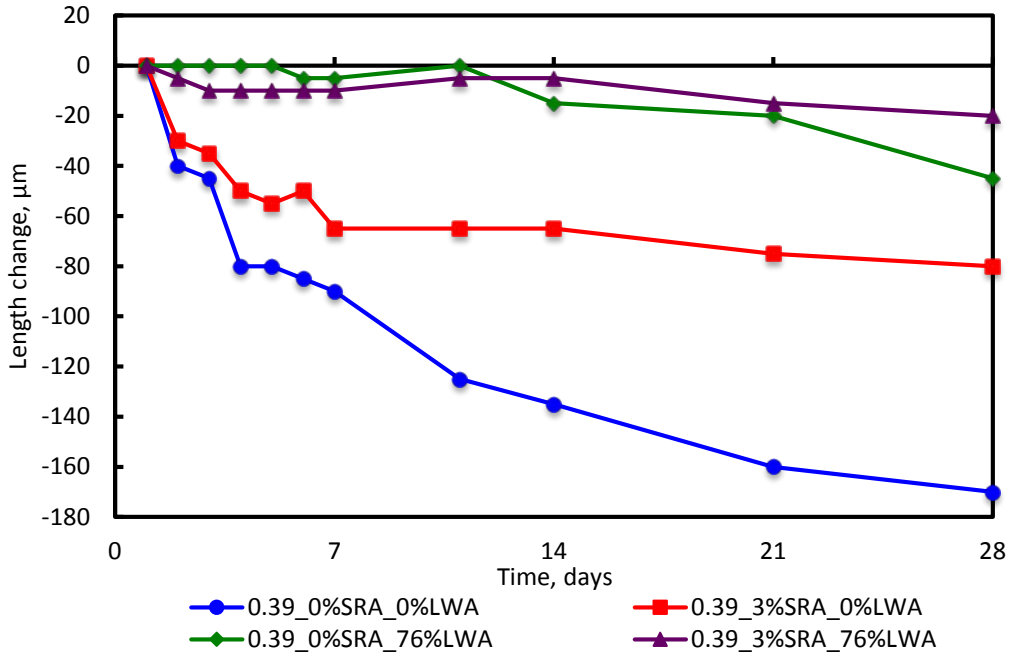
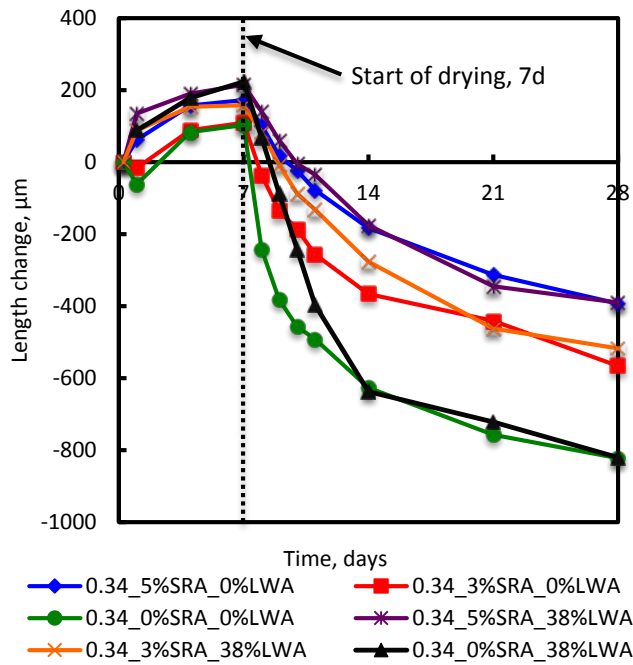


Figure 36. Autogenous shrinkage of concrete mixtures with SRA and LWA at 0.39 w/c.

## 5.2 EFFECTS OF SRA ON DRYING SHRINKAGE OF MORTAR AND CONCRETE MIXTURES WITH INTERNAL CURING

This section reports the results of a preliminary study on the effects of combining SRA and LWA on drying shrinkage of mortar and concrete mixtures. Figure 37 shows drying shrinkage of mortar mixtures with SRA and LWA at 0.34 w/c. At 28 days, total shrinkage of specimens depends merely on the dosage of SRA. The addition of LWA to the mixtures with SRA does not change the shrinkage behavior. A similar behavior was also observed for 0.44 w/c, as shown in Figure 38. As noted before, LWA is not beneficial in reducing the drying shrinkage of mortar.



**Figure 37. Drying shrinkage of mortar mixtures with SRA and LWA at 0.34 w/c.**

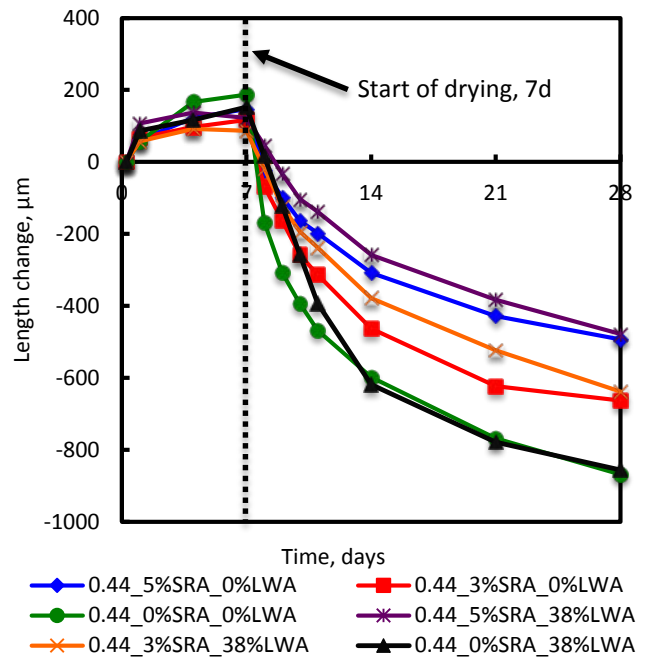


**Figure 38. Drying shrinkage of mortar mixtures with SRA and LWA at 0.44 w/c.**

Figure 39 shows the drying shrinkage of concrete mixtures with SRA and LWA at 0.39 w/c ratio. As was previously noted, the addition of LWA alone can increase the drying shrinkage of concrete. However, if SRA is added to the same mixture, the mixture can become more volumetrically stable and have a lower amount of drying shrinkage (Figure 39). Therefore, SRA alone can reduce drying shrinkage of concrete significantly, but the addition of LWA does not considerably change that behavior.

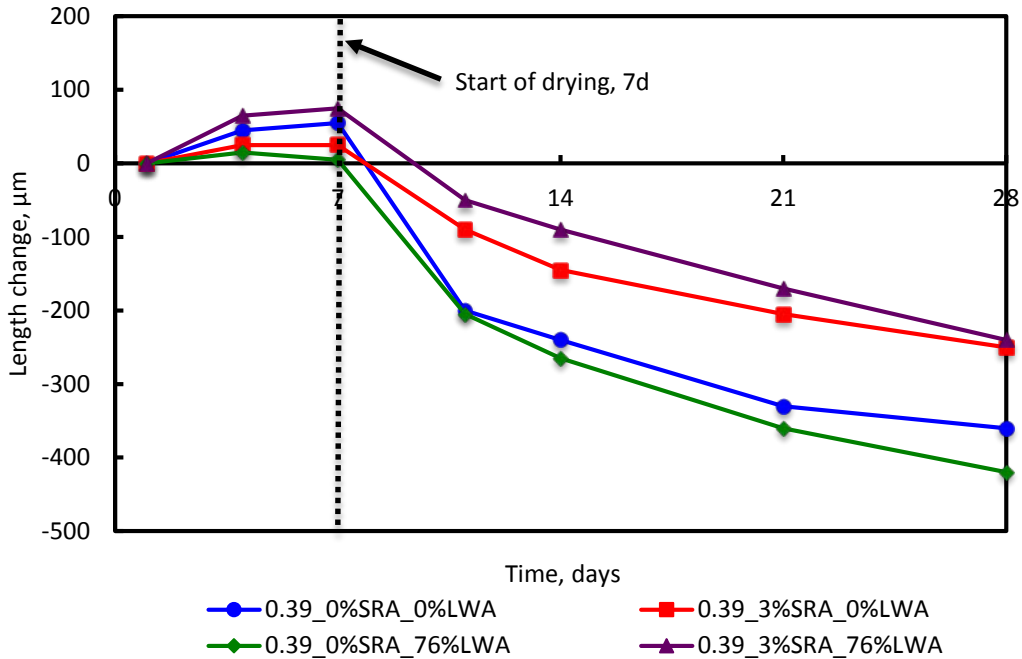


**Figure 39. Drying shrinkage of concrete mixtures with SRA and LWA at 0.39 w/c.**

### 5.3 SUMMARY

This chapter presented the combined effects of LWA and SRA on autogenous and drying shrinkage of mortar and concrete mixtures. Results with mortar mixtures showed that at a low w/c ratio of 0.34, the addition of SRA to internally cured mixtures can further reduce autogenous shrinkage. This behavior, however, was not observed at a high w/c ratio of 0.44. Moreover, for mortar mixtures with both a 0.34 and a 0.44 w/c ratio, drying shrinkage seems to be directly related to the amount of SRA in the mixture alone (i.e., incorporation of internal curing does not change the shrinkage behavior considerably).

In concrete mixtures, LWA alone can increase drying shrinkage. Therefore, the addition of SRA to mixes with LWA is highly recommended because it will make the mixture more volumetrically stable. Though this part of the study was preliminary, the results are encouraging and warrant further detailed study before possible field application.

## CHAPTER 6: BRIDGE DECK MODELS

The next step in the research was to use the small-scale laboratory concrete mixture designs developed by the University of Illinois at Urbana-Champaign in larger-scale prototypical bridge bays at Saint Louis University. These larger tests were conducted within a lab environment and provided additional insight into how different concrete mixes will behave when implemented in a full-scale bridge.

In Phase I of this research project, two such bridge bays were built and tested: 1) a control mix using a typical Illinois Department of Transportation (IDOT) concrete bridge deck mix design, and 2) a mix containing a partial replacement of portland cement with Type K cement. The results showed that the Type K cement has higher expansion than the control mix at early ages but the rate of the shrinkage is similar to the control mix (Chaunsali et al. 2013).

For Phase II of the project, two additional bays were studied using: 1) a mix design containing a partial replacement of sand with partially saturated lightweight fine aggregate, and 2) a mix design incorporating a shrinkage-reducing admixture (SRA). The results were compared with the control and Type K data from Phase I. In addition, a bridge deck near Peoria, Illinois, was constructed with concrete containing Type K cement and monitored and compared with the experimental results. Finite element models of all the experimental bridge bays, as well as the Peoria bridge, were created and compared with the measured strain data.

### 6.1 BRIDGE BAY DESIGN

The experimental bay for this study was designed based on IDOT recommendations, lab area restrictions, and to be consistent with the previous phase of the research project (Chaunsali et al. 2013).

Using typical bridge deck designs provided by IDOT, a 3 × 2 m (10 × 7 ft) representative bridge bay with a 20 cm (8 in.) deck thickness was designed. This experimental bridge deck is supported by two 3 m (10 ft) W12×79 steel girders at a spacing of 1.5 m (5 ft). The steel girders are connected to the reinforced concrete deck through shear studs spaced at 0.3 m (1 ft) longitudinally along the length of the girder. The girders are also constrained by two C6×8.2 steel channels to keep them free from twisting. The girders are raised off the ground at their ends with 0.3 m (1 ft) long W12 shapes. These 0.3 m long girders are used not only to simulate the bridge deck superstructure but also to raise the deck off the ground for better access to the underside of the slab.

Finally, four C10×15.3 steel channels were placed along the perimeter of the concrete deck. These channels were drilled to provide a location for reinforcement to be attached. These channels are intended to simulate the continuity of a real bridge superstructure. The grade-60 epoxy-coated reinforcement consists of top and bottom mats. The top reinforcement is located 5 cm (2 in.) from the top of the concrete, and the bottom reinforcement is located 4.5 cm (1.75 in.) from the bottom of the concrete. Ends of the reinforcement were threaded and attached to the channels using bolts. Caution was taken when bolting the reinforcement to the channels to avoid creating strain in the reinforcement. Figures 40 and 41 show the experimental deck before and after concrete placement.

The experimental deck design and construction were the same for all four concrete mixtures (control, Type K, internal curing LWA, and shrinkage-reducing admixture).



**Figure 40. Experimental deck before the pour.**



**Figure 41. Experimental deck after the pour.**

### **6.1.1 Strain and Temperature Gage Locations**

For consistency and easy comparison, the locations of the foil strain gages and temperature gages were the same for all four concrete decks. The deck containing a SRA had additional strain gages that will be explained in Section 6.4.2.1.

Multiple gages within the experimental deck recorded strain and temperature for a period of 6 months. Twenty strain gages were placed throughout the top and bottom reinforcement in both the longitudinal and transverse directions (see Figures 42 and 43 where strain gages are indicated by thick black lines). More gages were placed on the top layer of reinforcement because that is generally where a greater amount of cracking is found in actual concrete decks and was of greater interest for this study. Gages were also centrally located within the slab (as shown in Figures 42 and 43) to minimize any potential for local fluctuations caused by the channels and girders to affect the gages. Three strain gages were placed on each girder (Figure 44) to allow investigation of the effects of concrete shrinkage on the steel girders. Five additional gages were placed along the top surface of the concrete, as shown in Figure 45. The strain gages along the girders were the same type as those used for the reinforcement, but the strain gages along the top surface of the concrete were much larger, as recommended by the manufacturer. Thermocouples were placed on both the top and bottom reinforcement (Figures 42 and 43 and shown as stars T3 and T4), along the top and bottom surfaces of the concrete, and on the girders in a fashion similar to the strain gage locations (denoted by T in Figures 44 and 45). A Campbell Scientific CR3000 data acquisition system and the AM16/32B

multiplexer were used to collect strain and temperature data for the LWA and SRA concrete decks. Data for this phase were collected through the program LoggerNet and are comparable with the data collected from Phase I of the project.

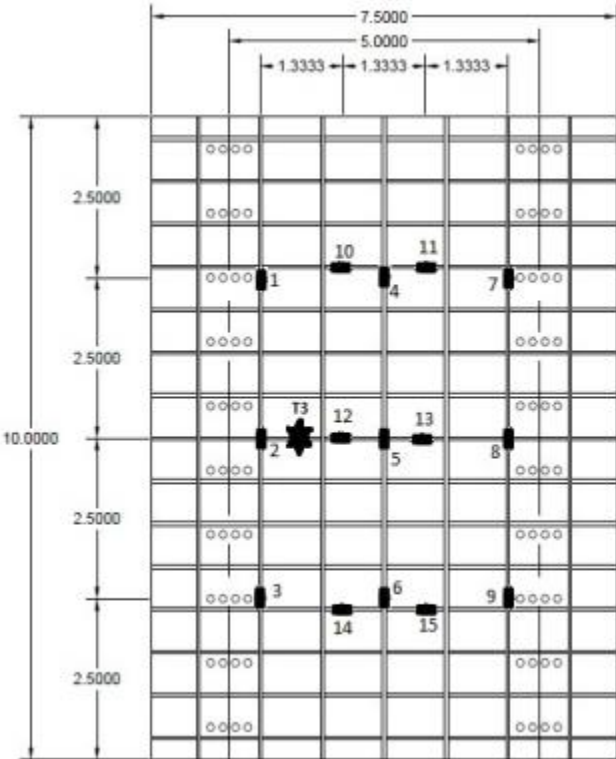


Figure 42. Top reinforcement strain gage and thermocouple (T) layout.

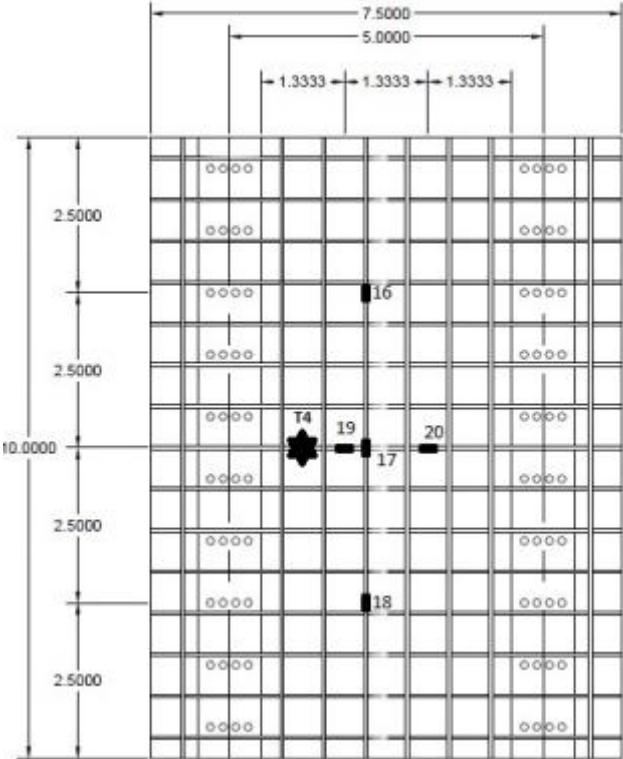


Figure 43. Bottom reinforcement strain gage and thermocouple (T) layout.

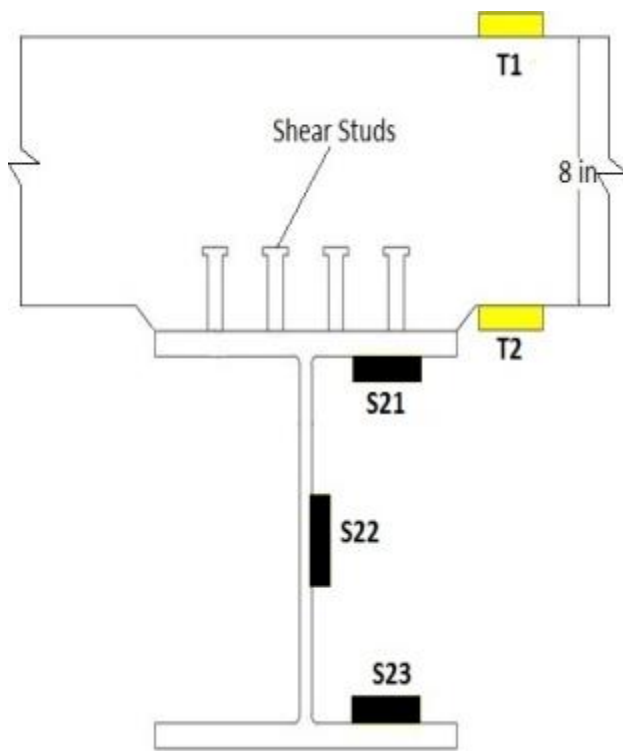


Figure 44. Girder strain gage and thermocouple (T) layout.

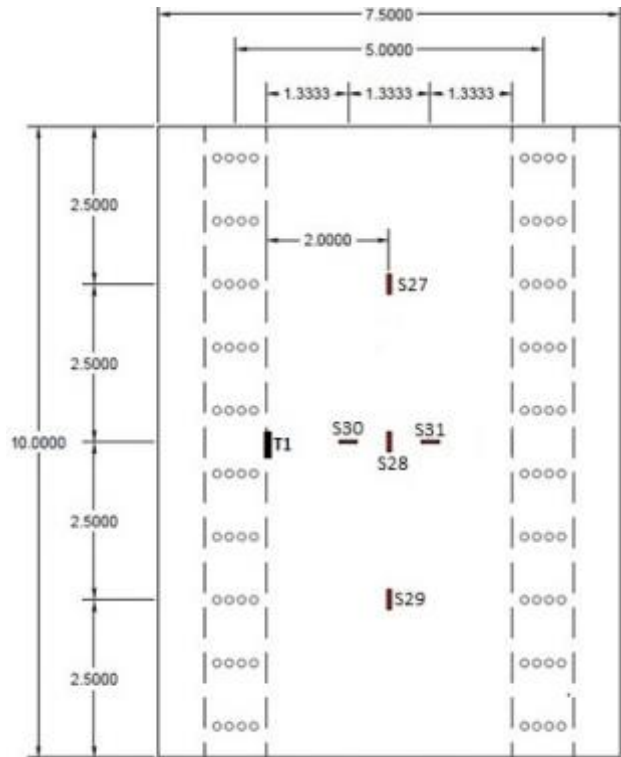


Figure 45. Concrete surface strain gage and thermocouple (T) layout.

## 6.2 MIX DESIGN

Mix designs for the control, Type K, LWA, and SRA concrete are shown in Table 3.

Table 3. Mix Designs, lb/yd<sup>3</sup>

	Control	Type K	LWA	SRA
Water	268	272	250	251
Cement	610	455	455	459
W/C	0.44	0.45	0.41	0.41
Fine aggregate	1130	1121	987	1184
Coarse aggregate	1826	1829	1827	1800
Class C fly ash	—	60	155	152
Komponent®	—	90	—	—
SRA-Eclipse®	—	—	—	1.4125

\*Units: lb/yd<sup>3</sup> (1 lb/yd<sup>3</sup> = 0.59 kg/m<sup>3</sup>)

### 6.3 CONCRETE TEST RESULTS

The concrete’s plastic properties were monitored during placement, and compressive strength was determined 7, 14, and 28 days following placement. Multiple slump and air content tests were conducted for all concrete placements. For Phase II, strength testing used 4 x 8 in. (10 x 20 cm) cylinders, while 6 x 12 in. (15 x 30 cm) cylinders were used for Phase I. The tests were conducted in accordance with ASTM standards.

For the control deck placement, an initial slump of 3.5 in. (9 cm) and a final slump of 2.5 in. (6 cm) were recorded over the 1-hour placement. Two air-content tests were conducted—one each at the beginning and end of the placement—with air contents of 5.8% and 6.0%, respectively. Cylinders were tested at 28 days, the compressive strength was 4560 psi (31.5 MPa).

For the experimental deck containing Type K cement, the initial and final slumps were the same (7.5 in. (19 cm)). The high slump can be attributed to the high w/c ratio specified for this mix due to the high water demand required by the Type K cement. The higher w/c ratio made the concrete more workable, and though the slump was at the high end of the specification, it was within the acceptable range. Air-content tests were also conducted, with values of 5.9% initially and 5.7% after the placement was completed. The 28-day compressive strength was 4340 psi (30.0 MPa).

For the deck containing a partial replacement of fine aggregate with pre-soaked lightweight fine aggregate, the initial slump was 4.5 in. (11 cm), increasing to a final slump of 7.0 in. (18 cm) at the conclusion of the 1-hour placement. Two air-content tests were conducted at the beginning and end of the placement: 9.3% and 7.5%, respectively. The 28-day compressive strength was 6990 psi (48.2 MPa). The higher strength could be attributed to the internal curing, and the strength can potentially be reduced by lowering the cementitious material within the mixture.

These concrete tests were repeated for the deck containing concrete with an SRA. The initial slump of the concrete was 7 in. (18 cm) with a final slump of 6.5 in. (16.5 cm) after approximately 1 hour. Meanwhile, two air-content tests were conducted at the beginning and the end of the placement, with a resulting air content of 2.0% for both tests. Low air content is a common problem for mixes containing SRAs, and while this concrete was placed in the laboratory, it would not be acceptable for use in the field. The 28-day compressive strength was 6220 psi (42.8 MPa), and this is common for SRA due to low air content.

The slump, air content, and compressive strength tests results are summarized in Tables 4, 5, and 6, respectively.

**Table 4. Slump Test Results**

	Control	Type K	LWA	SRA
Beginning of the pour*	3.5	7.5	4.5	7
End of the pour*	2.5	7.5	7.0	6.5

\*Units: in. (1 in. = 2.54 cm)

**Table 5. Air-Content Test Results**

	Control	Type K	LWA	SRA
Beginning of the pour*	5.8	5.9	9.3	2.0
End of the pour*	6.0	5.7	7.5	2.0

\*Units: %

**Table 6. Strength of Concretes**

	Control	Type K	LWA	SRA
7 Days	-	3030	5520	4610
14 Days	-	3690	6100	5460
28 Days*	4560	4340	6990	6220

\*Units: psi (1 psi = 6894 Pa)

## 6.4 STRAIN AND TEMPERATURE VARIATION IN THE BRIDGE DECKS

### 6.4.1 LWA Concrete Deck

The experimental deck containing a partial replacement of fine aggregate with pre-soaked lightweight fine aggregate was placed in September 2014. Unlike the control and Type K decks monitored in Phase I, all of the strain gages and thermocouples were connected to a Campbell Scientific CR3000 data acquisition system with data collection through the software LoggerNet. Strain and temperature readings were collected every 5 minutes from the beginning of the placement for a period of 6 months. After Phase I of the project, it was clear that an interval less than 5 minutes was unnecessary and tended to generate extra noise. MATLAB was used for post-processing of the data.

#### 6.4.1.1 Strain Gage Readings

Strain gage setup was the same as in Phase I of the project, and the same type of strain gage, thermocouple, and cable were used as well. Strain gages were zeroed 1.5 hours after concrete placement in order to eliminate initial strain from installation and vibration during concrete placement. The zero time was similar to that of the Type K deck (1 hour after the pour) and the same as the control deck. For the LWA concrete, the peak strain was between 0  $\mu\epsilon$  and 50  $\mu\epsilon$  for all gages, and the final strain at the end of the 6-month period was between -140  $\mu\epsilon$  and -250  $\mu\epsilon$  (individual strain time history plots can be found in Appendix B). Figures 46 through 50 plot the average strain versus time for the control, Type K, SRA, and LWA decks. Plots include average strains in the top and bottom longitudinal and average strains in the top and bottom transverse reinforcement, with exact locations presented in Figures 42 through 45.

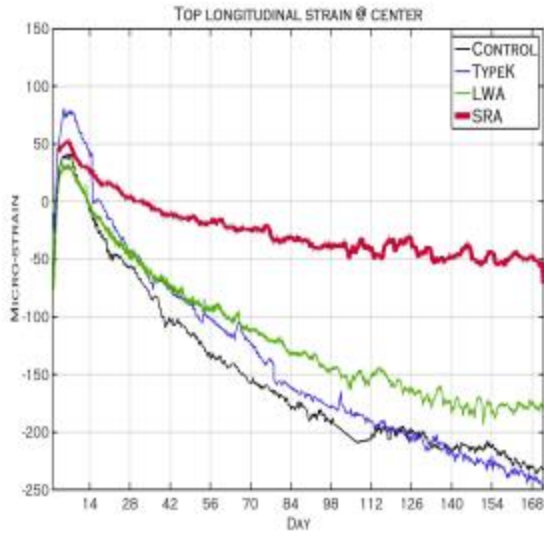


**Figure 46. Average top longitudinal reinforcement strain (strain gages 4 through 6).**

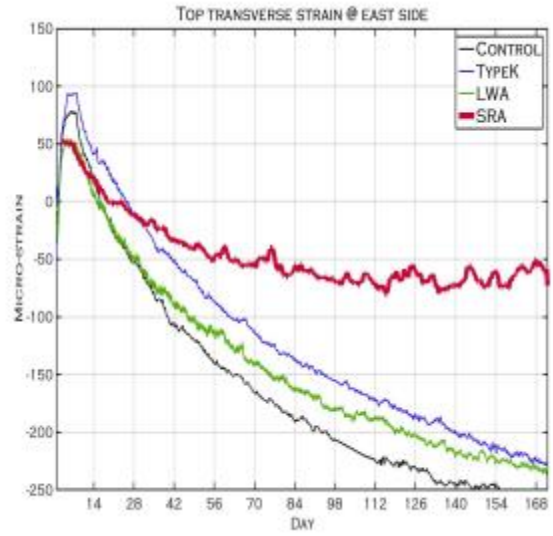


**Figure 47. Average top transverse reinforcement strain (strain gages 10 and 11).**

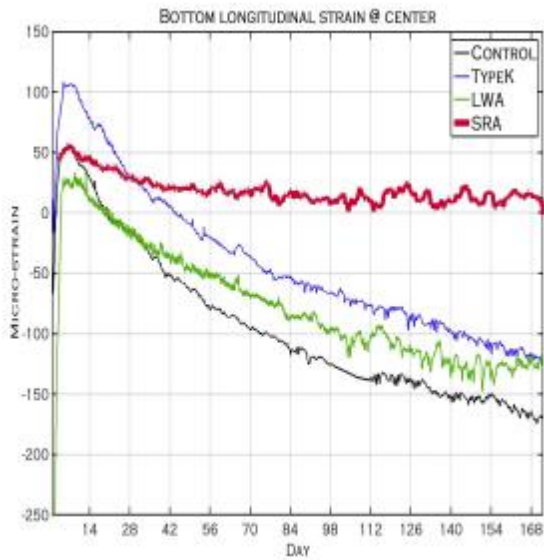


**Figure 48. Average bottom longitudinal reinforcement strain (strain gages 16 through 18).**

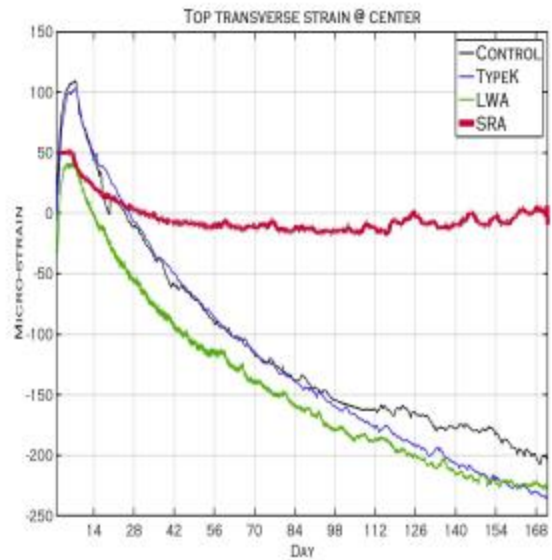


**Figure 49. Average bottom transverse reinforcement strain (strain gages 19 and 20).**

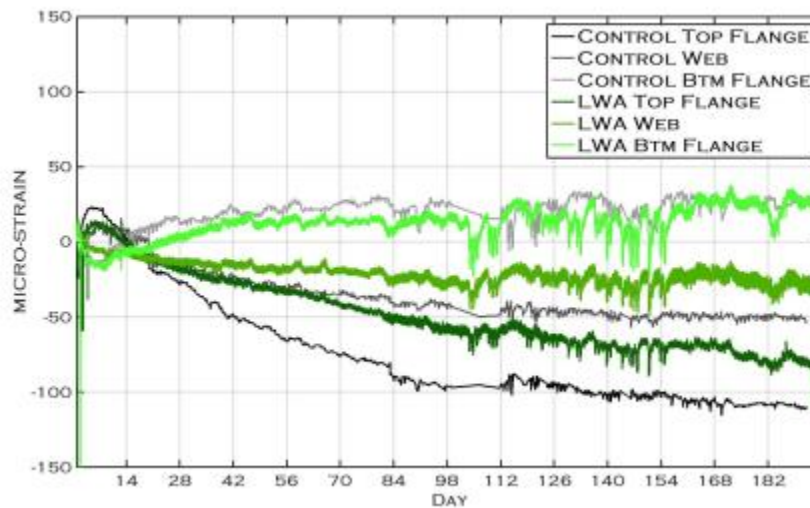


**Figure 50. Girder strain.**

As shown in Figures 46 through 50, the strain measured in the LWA deck is similar to the control deck, which demonstrated that, in this case, the addition of lightweight aggregate did not have a significant effect on the shrinkage behavior. Strain trends upward (strain increasing) during the first week following placement and reaches the peak strain around day 7. Strains begin to decrease at the conclusion of the curing period. Peak strain values for the LWA concrete were similar to or slightly smaller than the control and SRA decks but were still less than strains measured for the deck containing Type K cement. One major difference that makes LWA concrete deck different than both the control and Type K decks is that as the LWA concrete deck shrinks after the curing period, it shrinks at a slower rate. This can be observed in Figures 46 through 48, where it is shown that all of the LWA strains decreased at a slower rate compared with the control and Type K strain. The difference in the strain rate is a direct result of the slow release of water within the pre-soaked aggregate thereby slowing down moisture loss to the surrounding environment. A similar trend was also observed in the strain data collected from the girders (Figure 50), where strain recorded for the top flange of the girder also showed a slower shrinkage rate for the LWA deck compared with the control at the same location. Strain measurements and visual observations showed no cracks within or at the surfaces of the LWA concrete deck.

Figures 51 and 52 further illustrate average strain values for all four types of concrete deck. These figures show average longitudinal strains every 14 days. The bar charts show that the bottom layer of the concrete deck (Figure 52) shrank less than the top layer (Figure 51) for all four types of concrete. This can be observed from the strain at day 168, when the average strain from the bottom longitudinal reinforcement was less than the strain in the top longitudinal reinforcement at the same location. For instance, the average LWA bottom longitudinal reinforcement strain was  $-141 \mu\epsilon$ , while the LWA top longitudinal reinforcement strain was  $-173 \mu\epsilon$ . The main reason the bottom of the deck shrank less than the top is the fact that the top concrete was uncovered after 7 days of curing, while the bottom of the deck was covered by formwork for 14 days, resulting in less water loss from the

bottom of the deck. The bottom concrete also showed slightly higher peak strains at 7 days, which was most likely due to the longer curing provided at the bottom of the deck. Figures 51 and 52 also show, in general, that the LWA deck had a slightly smaller peak strain at 7 days compared with the control deck. Comparing the total shrinkage strain following the initial expansion, the control and Type K decks had the largest total shrinkage. The deck containing the SRA had the smallest total shrinkage over time (Figure 53).

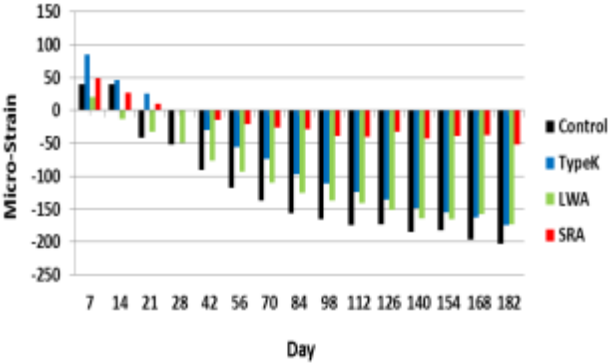


Figure 51. Average top longitudinal strain.

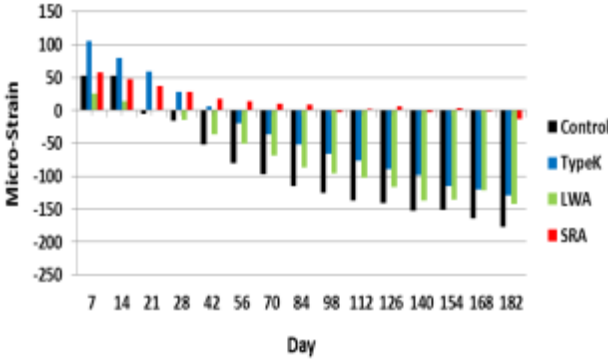


Figure 52. Average bottom longitudinal strain.

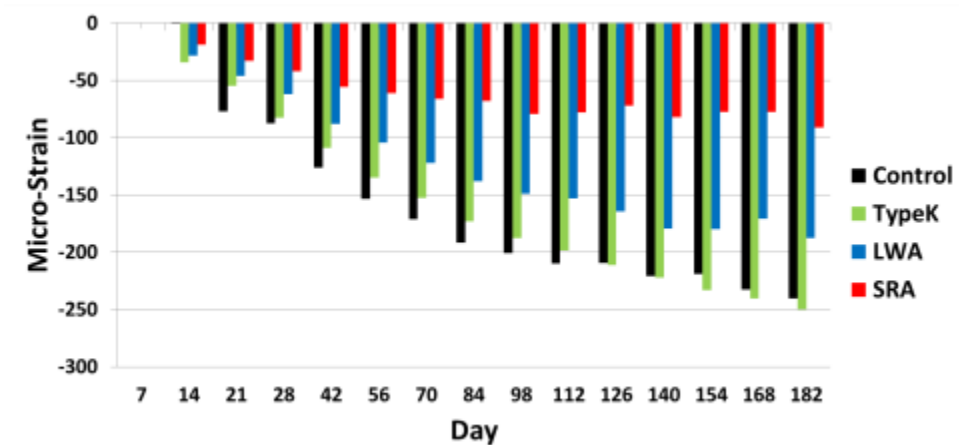
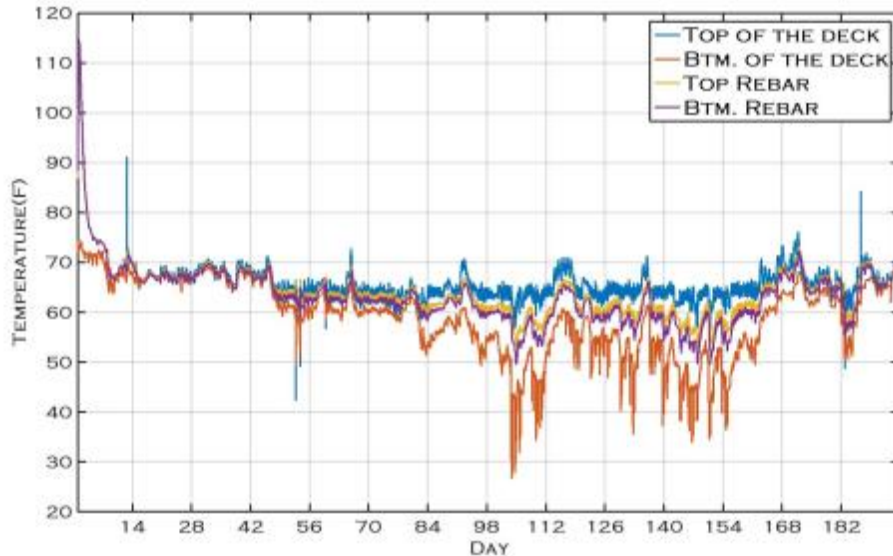


Figure 53. Average longitudinal total shrinkage.

6.4.1.2 Thermocouple Readings

The thermocouple readings did not need to be zeroed, and the thermocouples used for the LWA deck were the same as those used in Phase I. Four thermocouples were installed: one on the top concrete surface, one on the bottom concrete surface, and one each on the top and bottom reinforcement (see Figures 42 through 45 for the exact location of the thermocouples).

Figure 54 shows thermocouple readings for the LWA concrete deck. The temperature within the deck reached 115°F (46 °C) approximately 24 hours after placement (compared with a peak temperature of 108°F (42°C) for the Type K deck). Figure 54 also shows that the reinforcement within the deck and the top surface of the LWA deck stayed around room temperature, even when the underside of the deck was exposed to cold air.



**Figure 54. Temperature-time history of LWA concrete.**

## 6.4.2 SRA Concrete Deck

The SRA deck was placed in September 2015. The same type of gages, thermocouples, and data acquisition system were used as for the LWA deck. Readings were collected every 30 minutes throughout the recording time in order to eliminate noise and reduce the quantity of data collected. MATLAB was used for post-processing.

### 6.4.2.1 Strain Gage Readings

The strain gage setup for the SRA deck was slightly different than the other decks (control, Type K and LWA). In this case, 10 vibrating wire strain gages and 19 foil strain gages were added to the original 20 foil strain gages planned for the deck (and used in the other decks). Additional foil gages were added to gain a better understanding of the strain change within the deck and to provide more information for validating the finite element model. The intent was to instrument as much of the deck reinforcement as possible, but at the same time, not interfere with the bond between concrete and reinforcement (the waterproof coating of the strain gages and the wires that were tied to the reinforcement all affect bond). The final instrumentation layout focused on half of the deck because the deck was symmetric and the number of channels was limited by the data acquisition system and multiplexer. In addition to the foil strain gages, ten Geokon model 4200 vibrating wire strain gages (Figure 55) were added to measure the strain change within the concrete. In the past, concrete strain

and reinforcement strain were always assumed to be the same (i.e., it was assumed that concrete and reinforcement are fully bonded). However, that has not always been found to be the case . Therefore, the vibrating wire strain gages were added to allow investigation of the concrete strain and a comparison of the difference between the strain in the concrete and the reinforcement.

Figure 56 shows the additional strain gages that were added to the top mesh of the reinforcement. The red dots are the additional foil strain gages, and the blue triangles show the locations of the vibrating wire strain gages. Figure 57 shows the strain gages that were added to the bottom reinforcement. The strain gage and thermocouple setup for the girder and top surface of the concrete is the same as for the previous decks (shown in Figures 44 and 45).



**Figure 55. Vibrating wire strain gages (Geokon model 4200).**

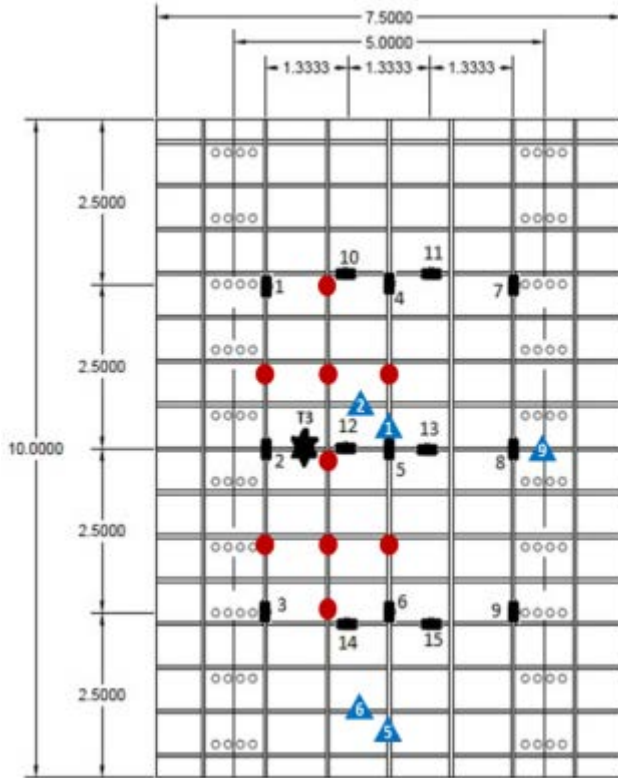


**Figure 56. Top reinforcement strain gage layout of SRA deck.**

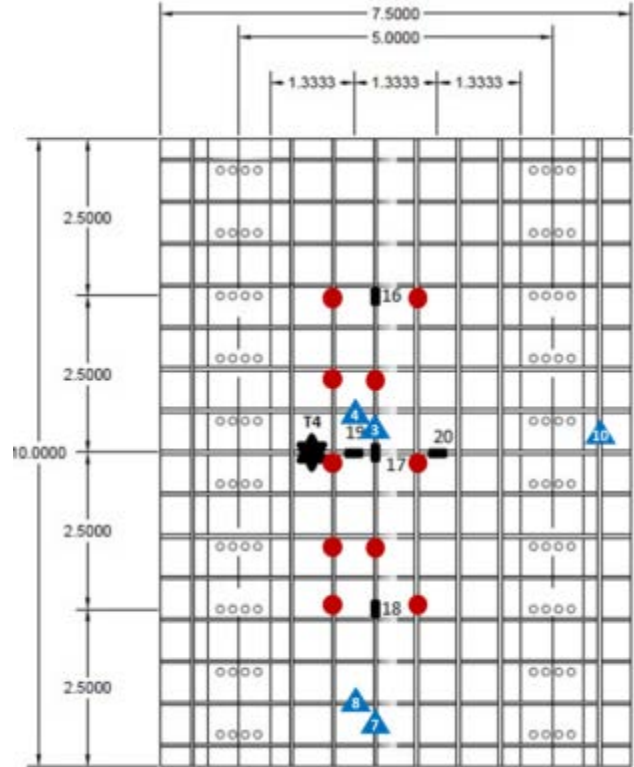


**Figure 57. Bottom reinforcement strain gage layout of SRA deck.**

#### 6.4.2.2 Foil Strain Gage Readings

For comparison, only the strain gages that also exist on the previous decks will be discussed in this section. The additional strain time histories are included in Appendix B. To simplify the comparison between each type of concrete, the figures include the average reading for each mixture from the same location. Individual plots of the complete strain data are included in Appendix B.

The peak strain (the highest strain reading occurring at the end of the curing period) for the SRA deck was nearly the same as the peak strain of the control concrete (Figures 58 through 61). As mentioned previously and as expected, the deck containing Type K cement experienced more expansion than the other three decks. Figures 58 through 61 also show the overall trend of the strain developed in the deck containing an SRA. Initially, strain expanded during the curing period (7 days) followed by shrinkage. The rate of shrinkage for the SRA deck, however, was much lower than for the other concrete mixtures. The shrinkage rate was particularly small after 84 days of drying. In fact, the strain remained almost unchanged from 84 to 168 days (Figures 58 through 60). After the first 7 to 28 days, the total strain measured in the SRA deck compared with the control, Type K, and LWA decks was less and the difference increased over time. After 168 days, the strain in the SRA deck was much lower than the other decks by at least  $50 \mu\epsilon$ . In addition, the overall strain change for the SRA deck was smaller than the others, which leads to smaller tensile forces within the concrete deck and therefore

less potential for cracking. Strain measurements and visual observations found no obvious cracking in the SRA experimental deck.

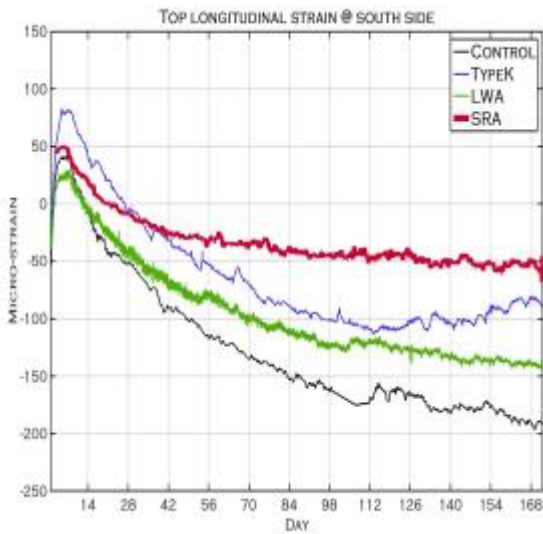


Figure 58. Average of gage 7 through 9.

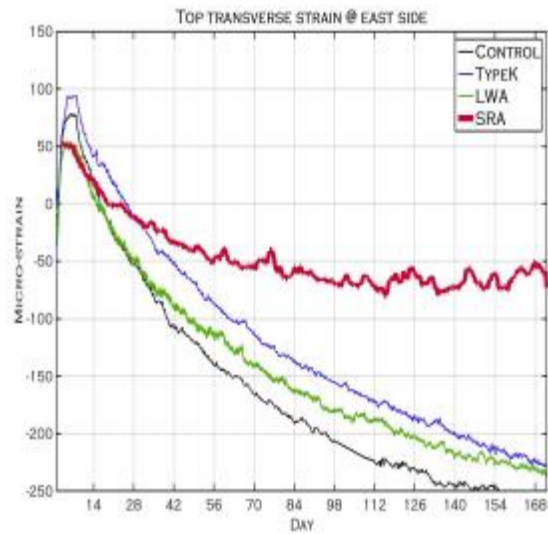


Figure 59. Average of gage 10 and 11.

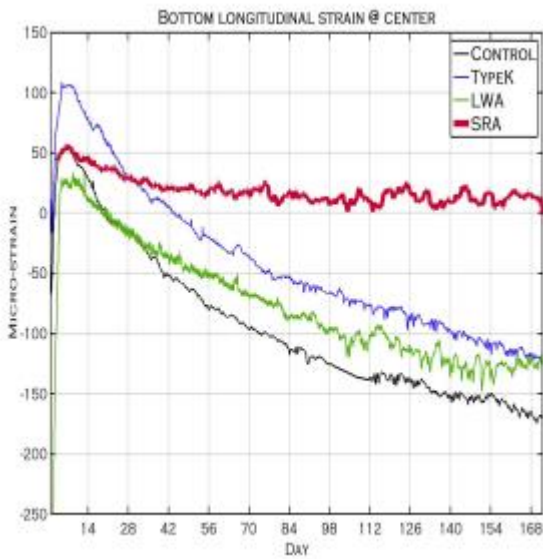


Figure 60. Average of gage 16 through 18

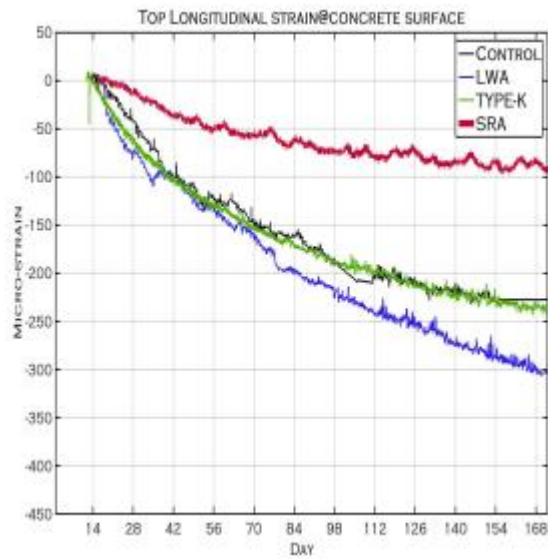


Figure 61. Average longitudinal concrete surface strain.

Overall, it is clear from these figures that the concrete containing an SRA shrank very slowly compared with the other decks. This was true for both the top and bottom layers of the deck, where the bottom strain layer strain was near  $0 \mu\epsilon$  at 168 days. The strain in the SRA deck increased between days 154 and 168, but this was due to an increase in temperature of the lab ( $10^\circ\text{F}$  increase, which can be seen in Figure 64). Comparing only the total shrinkage strain following initial expansion,

the deck containing Type K cement had the largest total shrinkage and was comparable to the shrinkage strain measured in the control deck. The SRA deck had the smallest total shrinkage at each age, which was about half the strain measured in the deck containing LWA.

### 6.4.2.3 Vibrating Wire Strain Gage Readings

Ten vibrating wire strain gages were installed at different locations on the top and bottom reinforcement in both the longitudinal and transverse directions (as shown in Figures 56 and 57). The gages were tied to the reinforcement using pipe ties, as shown in Figure 55, to make sure that the gages were secure while concrete was placed; however, the gages measured strain in the concrete rather than in the reinforcement. Installation of the vibrating wire gages was focused at the center of the deck, close to the edge of the deck, above the girder, and at the overhang region, as shown in Figures 56 and 57.

The strain measurements collected from the vibrating wire strain gages (concrete strain) were compared with the strain measurements collected from the foil strain gages (reinforcement strain). Figure 62 shows the vibrating wire gage 1 data, compared with the average foil strain gage reading from the same reinforcement (foil gages 4 and 6). Measured strain values were almost identical, indicating that the concrete and reinforcement were fully bonded. As a result, the strain measurements collected from the reinforcement can be assumed equal to the concrete strain at that location. The same trend was observed with vibrating wire gage 5 compared with the average foil strain gage readings (Figure 63). The exact locations of the strain gages are shown in Figures 56 and 57.

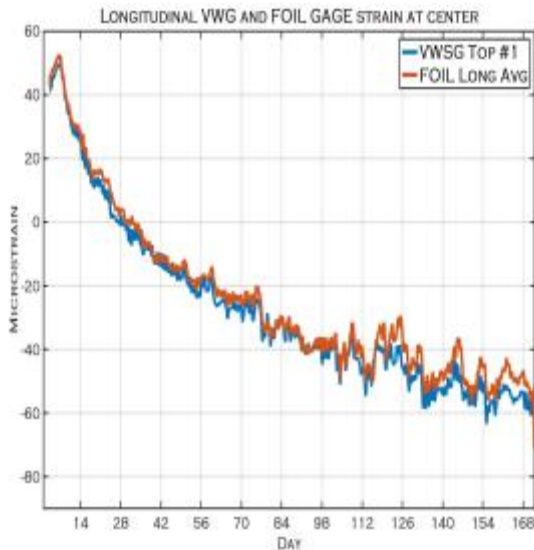


**Figure 62. Vibrating wire gage 1 compared with the average foil strain from the same location.**

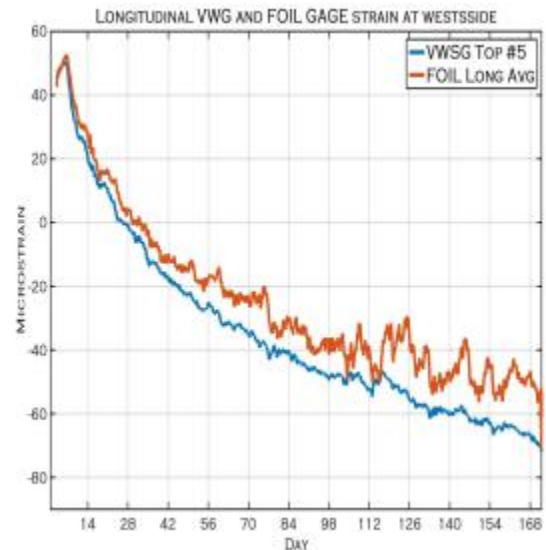


**Figure 63. Vibrating wire gage 5 compared with the average foil strain from the same location.**

#### 6.4.2.4 Thermocouple Readings

The vibrating wire strain gages also measured temperature. As a result, thermocouples were installed only on the top and bottom surfaces of the SRA concrete deck. The results indicated that the temperature within the deck (gages 1 through 10, shown in Figure 64) did not vary significantly when the bottom of the deck was exposed to cold air (when the temperature from the bottom surface starts to deviate from the other locations). This shows that the SRA concrete deck also had very low thermal conductivity as LWA, Type K, and control concrete decks.

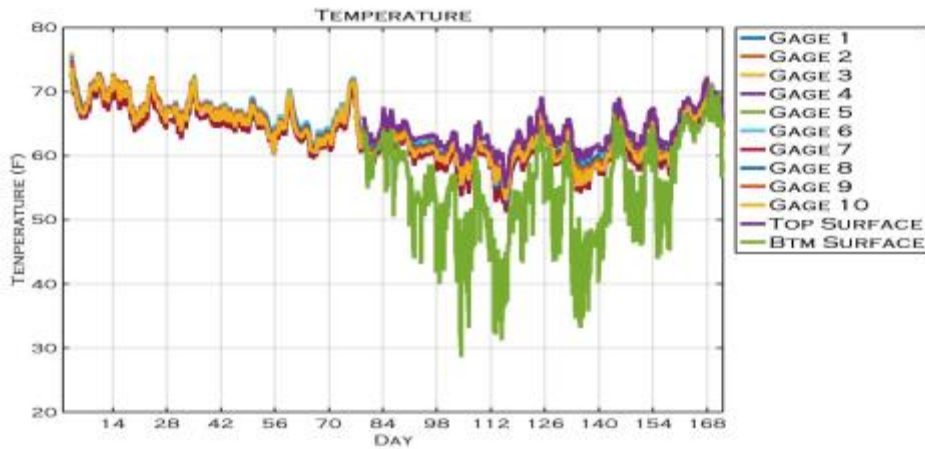


Figure 64. Temperature-time history of SRA concrete deck.

## 6.5 SUMMARY

In average, Type K cement exhibit the highest peak at seven days, however due to higher shrinkage rate it does not show major shrinkage reduction like the LWA and SRA deck. Whereas the LWA deck exhibit the smallest average peak strain at seven days but it shrink less than both control and Type K deck due to slower shrinkage rate. Overall, The rate of shrinkage for the SRA deck was much slower than that of the other three concrete mixtures. The shrinkage rate was especially small after 84 days. In fact, some strain remained almost unchanged from 84 to 168 days.

## CHAPTER 7: PEORIA TYPE K BRIDGE INSTRUMENTATION

The goal of instrumenting an actual bridge deck was to provide a better understanding of how strain changes under real service conditions and to compare and contrast the strain measured with the strain measured in the experimental decks. Eventually, the data collected will also help validate the full-bridge finite element model.

### 7.1 OVERVIEW OF THE BRIDGE

The bridge was selected by IDOT. Its structure is similar to the experimental decks constructed at Saint Louis University. The bridge (SN 072-0226) is located on IL-29 in Peoria County, Illinois, over

Boyd’s Hollow Creek (Figure 65). Stage 1 of the bridge was placed on June 3, 2015, and was instrumented by researchers from the University of Oklahoma. Stage 2 was placed on September 11, 2015, and was instrumented by Saint Louis University. This report includes data gathered in Stage 2 only. The mix design for the concrete bridge deck included 16% Type K cement by weight of total cementitious.

### 7.1.1 Structure of the Bridge

The Peoria Type K bridge is a single-span steel girder cast-in-place composite concrete bridge. The bridge is 18 m (60 ft) long, 20 cm (8 in.) thick and was placed in two separate stages (southbound and northbound). Each stage was 13 m (42 ft) wide (Figure 66) and consisted of seven steel plate girders spaced at 2 m (6.25 ft), as shown in Figure 67.



Figure 65. Location of the bridge.



Figure 66. Top view of bridge.

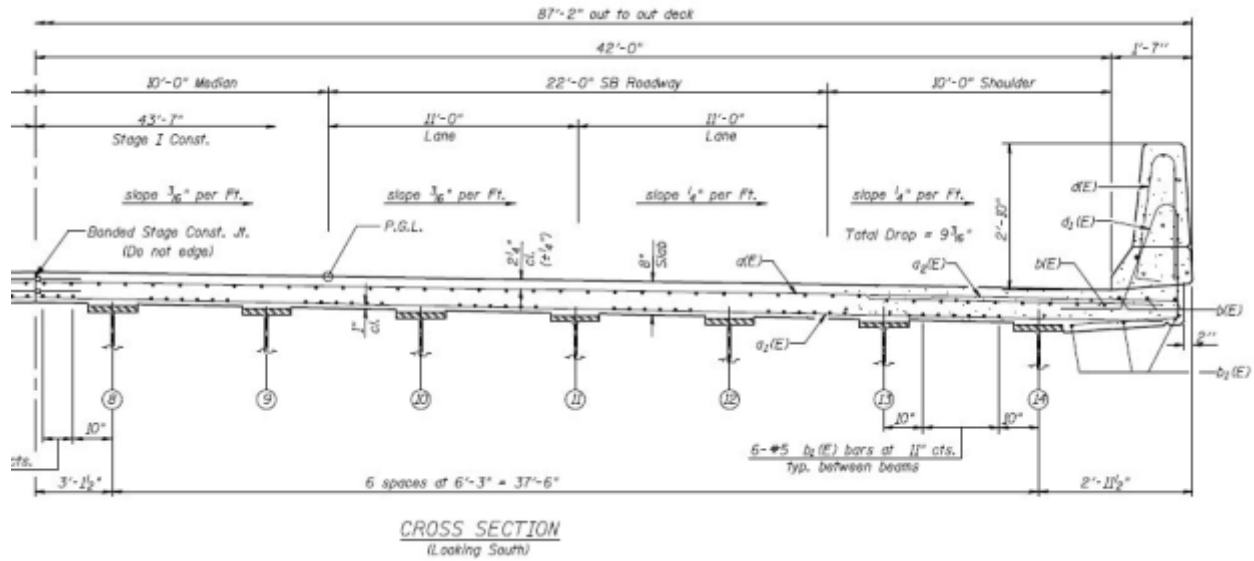


Figure 67. Cross section of the bridge.

### 7.1.2 Concrete Mix Design

The Type K concrete mixture design was supplied by CTS Cement utilizing their Komponent® material. The mix designs are shown in Table 7 for the IDOT Peoria bridge and the experimental deck cast at Saint Louis University.

Table 7. Mix Design, lb/yd<sup>3</sup>

	Type K, Peoria, IL	Type K, SLU
w/c	0.47	0.45
Water*	315	272
Cement*	455	455
Class C fly ash*	100	60
Fine aggregate*	909	1121
Coarse aggregate*	1884	1829
Cement Komponent®*	105	90

\*Unit: lb/yd<sup>3</sup> (1 lb/yd<sup>3</sup> = 0.59 kg/m<sup>3</sup>)

### 7.2 INSTRUMENTATION SETUP

The Type K bridge instrumentation plan was designed to be very similar to the experimental deck instrumentation setup in order to compare the data gathered. The bridge was monitored from the day of placement through 6 months—the same monitoring period as the experimental deck. The

monitoring period was from September 2015 to March 2016. Table 8 shows the equipment and gages used for instrumentation. Two kinds of strain gages were used to record the strain inside the concrete deck: foil strain gages (HBM K-LY4) were used to record the strain on the reinforcement, and vibrating wire strain gages (Geokon model 4200) were used to record the strain inside the concrete. All strain gages were attached to a data acquisition system (Campbell Scientific CR3000) through multiplexers (Campbell Scientific AM16/32B), and the system was connected to a wireless cellular modem (Sierra wireless Airlink Raven XTV) in order to monitor the system and collect data remotely. Owing to limited power available at the location of the bridge, two batteries (6V, 215AH in series) were also used. The batteries were recharged every 1.5 months to maintain the necessary voltage to power both the data acquisition system and the wireless cellular modem.

**Table 8. Equipment Used for Bridge Instrumentation**

<b>Brand and Model</b>	<b>Description</b>	<b>Quantity</b>
HBM K-LY4	Foil strain gage	45
Geokon model 4200	Vibrating wire strain gage	10
Campbell Scientific CR3000	Data acquisition	1
Campbell Scientific AM16/32B	Multiplexer	4
Sierra wireless Airlink Raven XTV	Wireless cellular modem	1
Duracell 6V; 215AH	Deep-cycle battery	2

### 7.2.1 Foil Strain Gage

Owing to limited time allowed in the field to instrument the bridge and a limited budget, the researchers at Saint Louis University suggested focusing on the foil strain gage installation at three locations, as shown in Figure 68. The foil strain gages (HBM K-LY4) were installed in three panels as shown in Figure 68: panel 1 located at the center of the deck between girder 3 and girder 4; panel 2 located close to the parapet at midspan between girder 1 and girder 2; and panel 3 located close to the north abutment between girder 3 and girder 4. Each panel has 15 strain gages installed on the top layer of reinforcement, nine strain gages on the longitudinal reinforcement, and six strain gages on the transverse reinforcement (shown in Figures 69 and 72). The original plan included instrumentation on the bottom reinforcement as well, but limited time and difficulty accessing the bottom reinforcement necessitated that gages on only the top reinforcement be installed. Forty-five foil strain gages were installed (15 per panel). The wires were tied to the reinforcement using zip ties and exited through a pre-cut slit between formwork (as shown in Figure 70) to the data acquisition setup beneath the bridge deck (Figure 71). The data acquisition system was installed inside two weatherproof enclosure boxes and fastened to the bottom flange of girder 2 closest to the north abutment (Figure 71). This location was selected to limit exposure to weather and to reduce inconvenience to construction crews during bridge construction.

All of the foil strain gages were protected by a waterproof coating (M-coat F suggested by Vishay Measurement Group), followed by self-fusing tape. Silicone was used as final layer of waterproofing (the orange and white shown in Figure 69).

Detailed strain gage locations and numbering for each panel are shown in Figure 72.

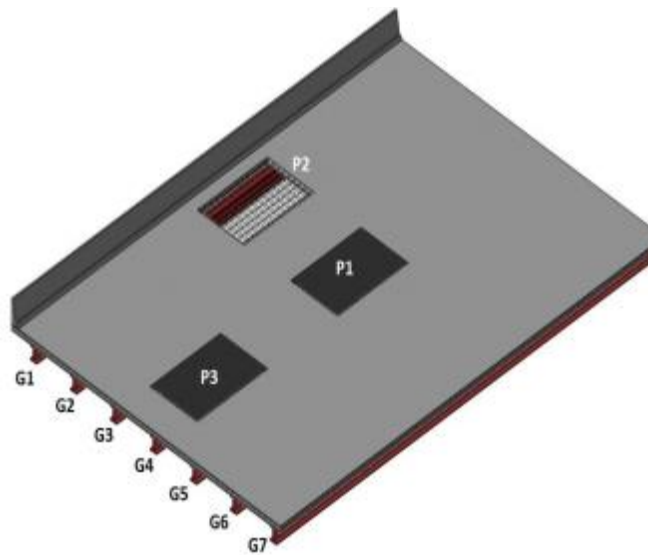


**Figure 68. Locations of foil strain gage panels.**



**Figure 69. Strain gage location (orange wrapped) at each panel.**



**Figure 70. Strain gage wire setup.**



**Figure 71. Data acquisition system installed on girder 2.**

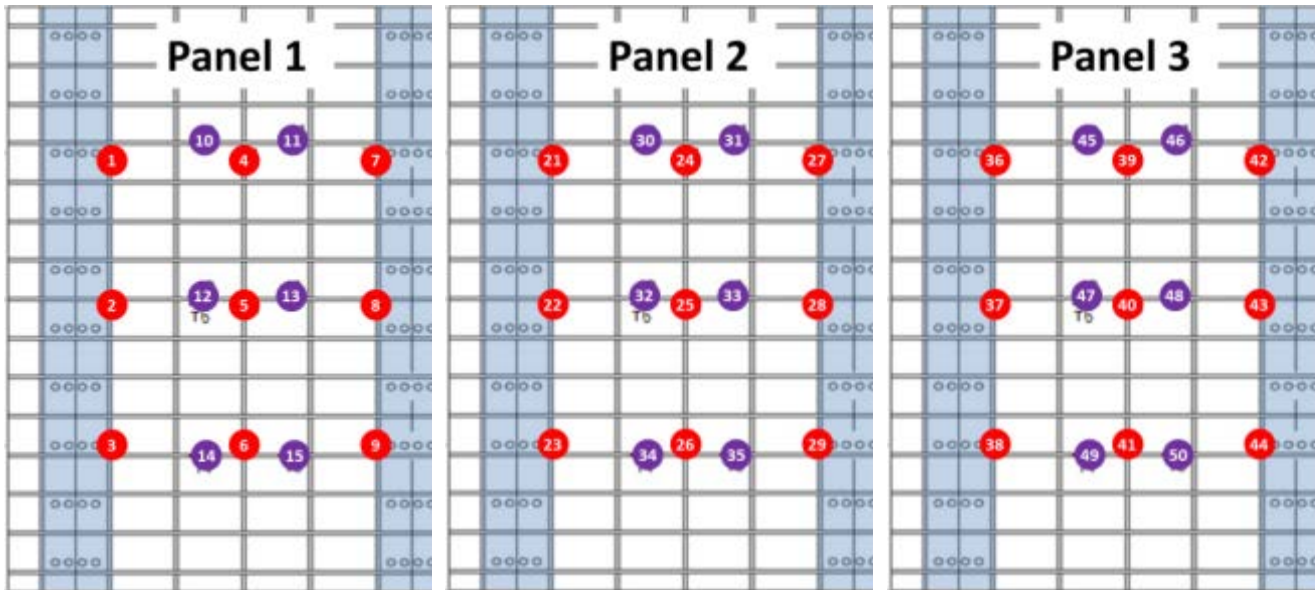


Figure 72. Foil strain gage numbering at each panel (the red dots are in the longitudinal direction, and the purple dots are in the transverse direction).

### 7.2.2 Vibrating Wire Strain Gage

The vibrating wire strain gages were used to measure the strain of the concrete near the reinforcement and to compare these strains with the strain of the reinforcement measured with the foil strain gages. Strains measured in the concrete and the reinforcement were nearly identical for the experimental decks; however, differences between the actual deck and the experimental deck, such as surface-to-volume ratio and reinforcement lengths, warranted additional examination. Geokon model 4200 concrete strain gages were installed on both the top and bottom mats at the locations shown in Figures 74 and 75. The combination of foil and vibrating wire strain gages covered three areas: the center portion of the deck where the deck connects to the abutment, the inside edge of the deck where it meets Stage I (southbound), and the outside edge where the portion between the exterior and interior girder contains a large amount of reinforcement for the parapet.



Figure 73. A close-up picture the vibrating wire strain gages.

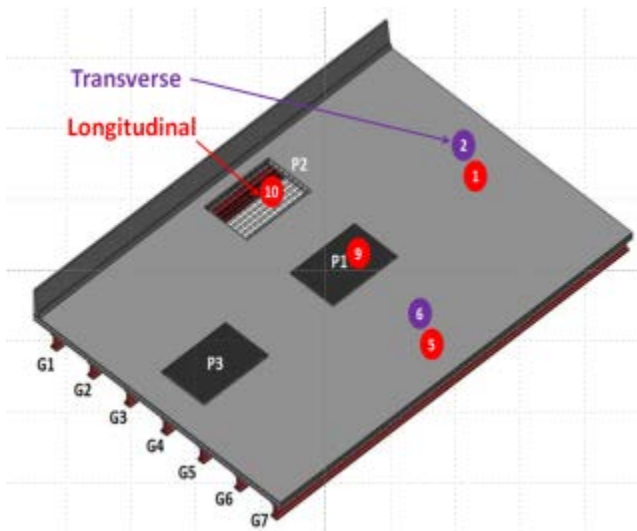


Figure 74. Vibrating wire strain gage numbering at the top layer of the concrete.

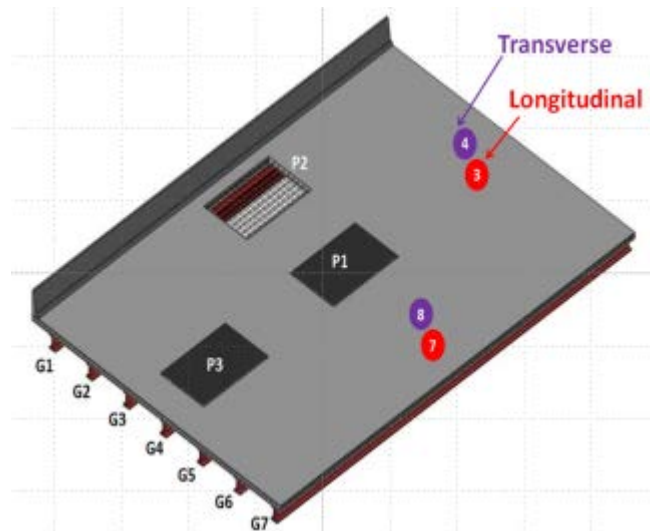


Figure 75. Vibrating wire strain gage numbering at the bottom layer of the concrete.

## **7.3 STRAIN AND TEMPERATURE VARIATION IN THE BRIDGE DECKS**

Unlike the experimental deck that was zeroed 1.5 hours after concrete placement, all of the gages in the Peoria bridge deck were zeroed 24 hours after the completion of the deck in order to eliminate any strain caused by construction activities that continued several hours after completion of concrete placement. This procedure also ensured that the strain did not include any strain resulting from the concrete self-weight. Data were collected every 6 hours in an effort to save power and not lose fidelity.

### **7.3.1 Foil Strain Gage Readings**

The foil strain gage readings from the Type K bridge deck in Peoria presented a very different trend (Figures 76 through 80) compared to the strain data collected from the experimental decks placed and measured in a laboratory. Unlike the strain readings from the experimental decks, which increased during the first 7 days and then began to decrease (rapidly at first) throughout the drying period, the majority of the Peoria strain readings followed a similar trend through day 21, but then began to increase again until day 42, after which the strain flattened out. A possible explanation presented in a technical report for the Indiana Department of Transportation (INDOT), Frosch et al. (2010) noted a similar trend, which was attributed to the formation of minor cracks. Figure 81 is from the INDOT technical report: foil strain gages 1 through 3 were located right at the crack location, while gage 4 was away from cracks. Gage 4 of the Indiana deck showed the same trend as the strain measured in the experimental deck at SLU, while gages 1 through 3 deviated from the SLU trend around day 10. According to the INDOT report, this effect is due to minor crack propagation. However, based on early bridge inspection (around 1 month after placement), there were no cracks found in the Peoria bridge deck. It is possible that the cracks were not visible at the time of the survey, or that the tensile strain on the reinforcement was the result of a slip between the concrete and reinforcement. Note that 21 days (approximately the time when most of the strain readings went from decreasing to increasing) is the time the pavement leading up to the approach slab was milled, so it is also possible that the vibration from the nearby milling machine caused slip between the concrete and reinforcement. Based on the strain collected, it is evident that some strain gages (Figures 78 and 79) followed the same trend as those observed in the experimental decks, which show a continuous decrease in strain.

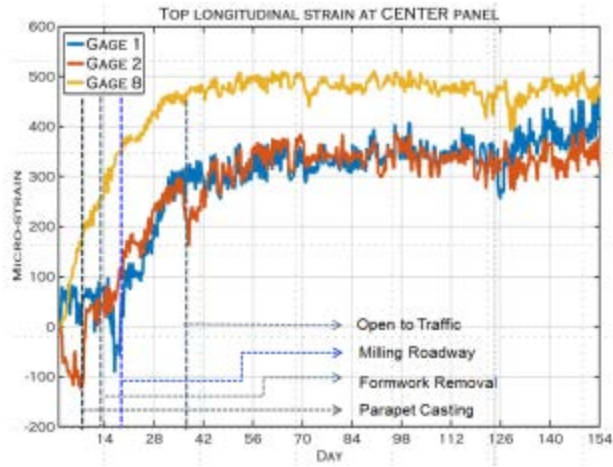


Figure 76. Longitudinal foil strain of panel 1.

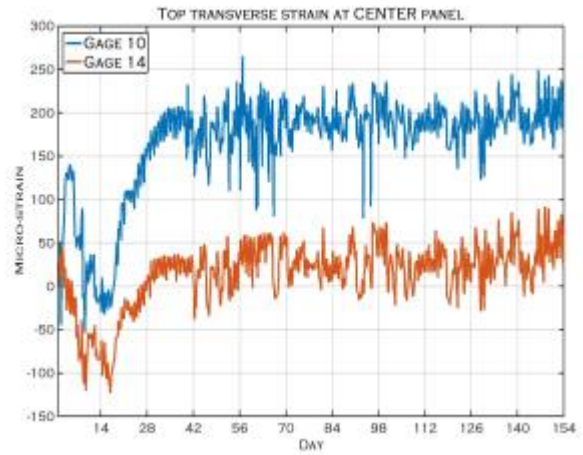


Figure 77. Transverse foil strain of panel 1.

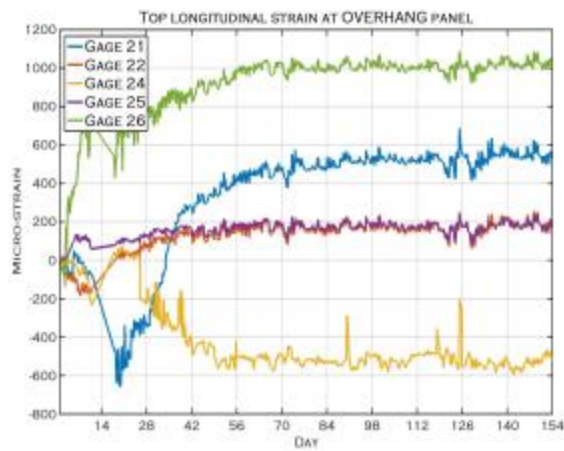


Figure 78. Longitudinal foil strain of panel 2.

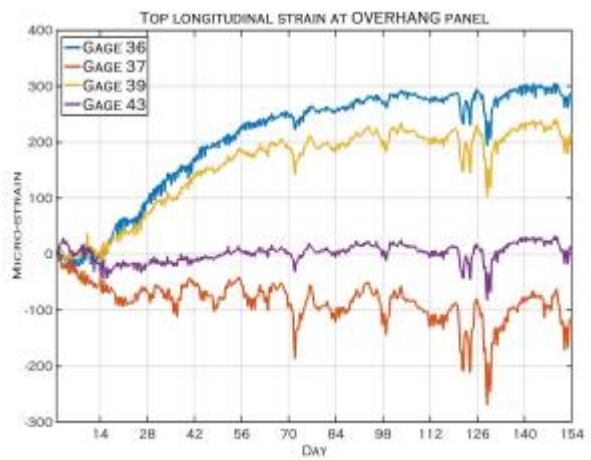
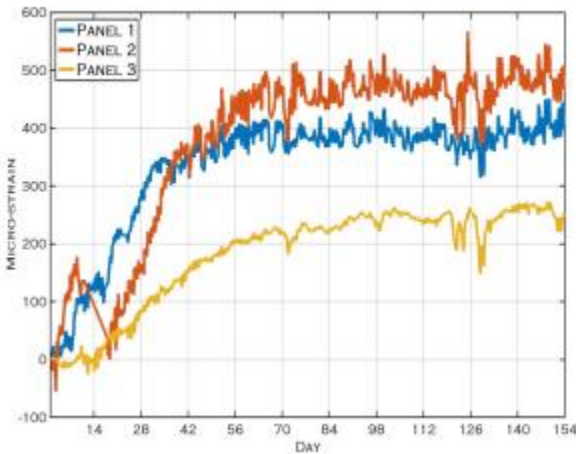
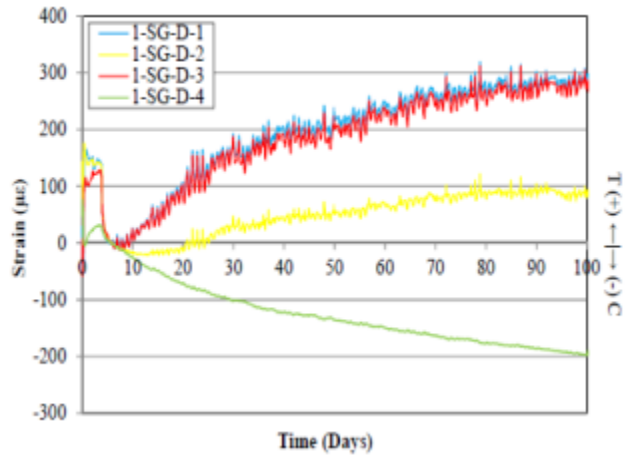


Figure 79. Longitudinal foil strain of panel 3.



**Figure 80. Average longitudinal foil strain from each panel.**



**Figure 81. Strain graph from INDOT technical report; cracks were present at gages 1 through 3 (Frosch et al. 2010).**

### 7.3.2 Vibrating Wire Strain Gage Readings

Vibrating wire strain gages were installed by the same technique that was used for the experimental deck. The vibrating gages were tied to the reinforcement using pipe ties (Figure 73) to ensure that the gages were immobilized during concrete placement. The vibrating wire strain gages were zeroed at the same time as the foil strain gages, 24 hours after the completing concrete placement.

Figures 82 through 85 show the strain measurements collected from the vibrating wire strain gages embedded in the deck (see Figures 74 and 75 for the location of the gages). All of the gages showed a reduction in strain throughout the time the data were collected; the strain at the end of the 6-month period was around  $-300 \mu\epsilon$ . Unlike the vibrating wire strain collected from the experimental deck, the Peoria deck strain showed a lot of variation from day to day. This variation was due to the temperature change from morning to night and from traffic.

Regarding the overall trend of the strain graph, it still shows the Type K concrete continuing to shrink over time; however, it does not have an obvious peak expansion at the conclusion of the curing period like the behavior observed for the experimental deck (see Figures 82 through 85). A comparison between average longitudinal strains between the Peoria Type K deck and the SLU Type K experimental deck is shown in Figure 86. (Note that the mix design for both Type K decks were also different, as shown in Table 7.)

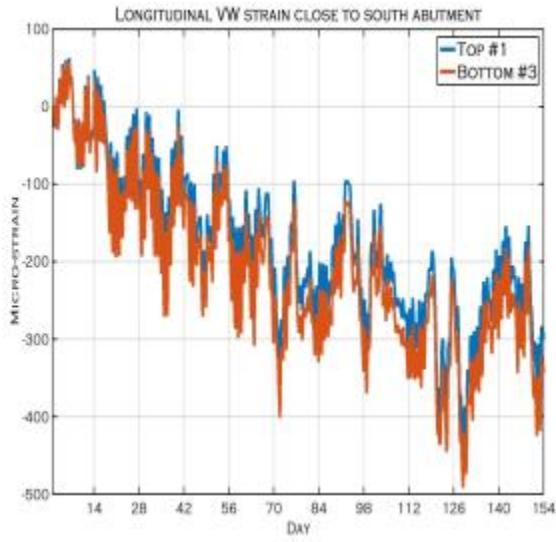


Figure 82. Longitudinal vibrating wire strain.

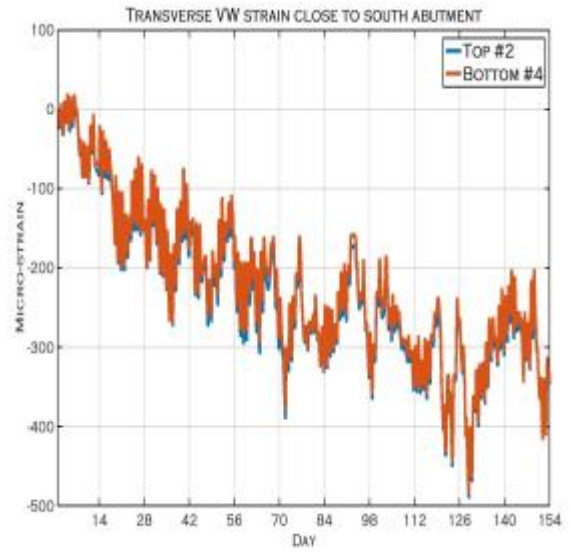


Figure 83. Transverse vibrating wire strain.

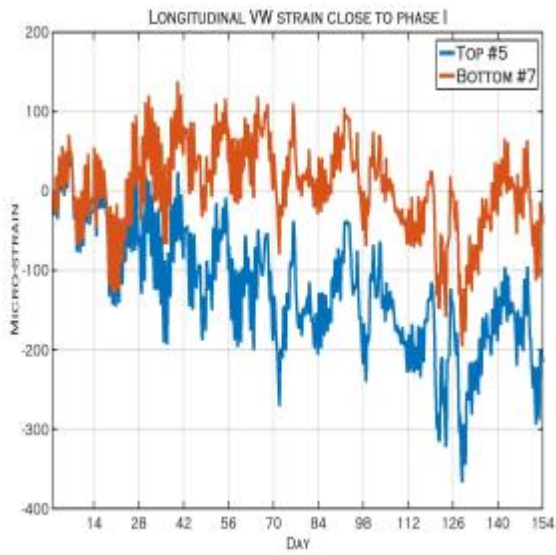


Figure 84. Longitudinal vibrating wire strain.

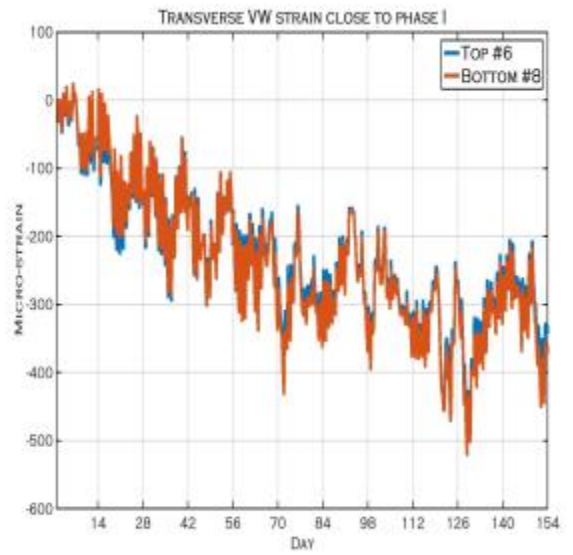


Figure 85. Transverse vibrating wire strain.

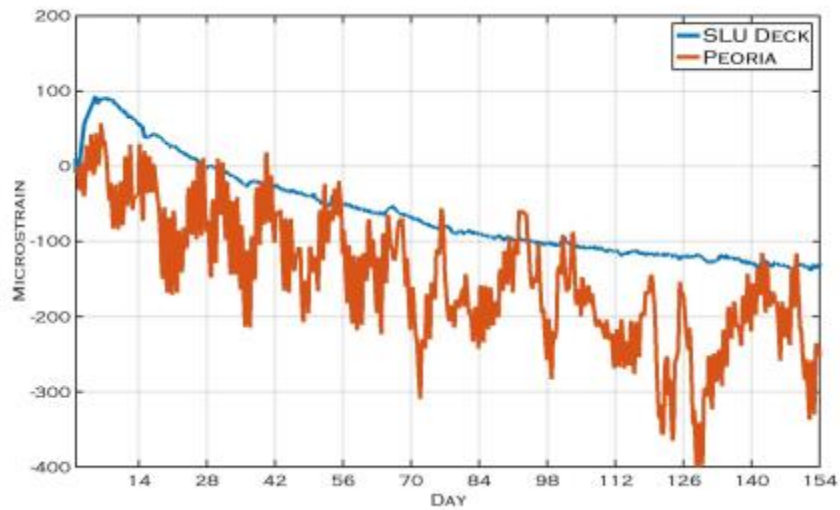


Figure 86. Average longitudinal strain comparison between SLU Type K and Peoria Type K.

### 7.3.3 Temperature Readings

The vibrating wire strain gages were also used to measure temperature at the same time the strain measurements were taken. The variation in temperature change within the Peoria Type K bridge deck is shown in Figure 87. The peak temperature of the deck right after concrete placement was 105°F (40°C), and the temperature at day 7 was 83°F (28°C).

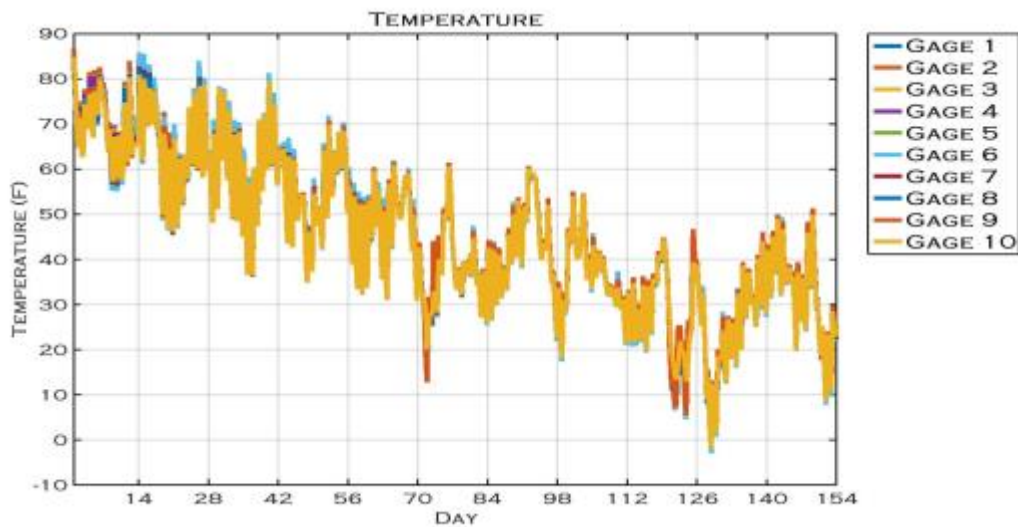


Figure 87. Temperature-time history of Peoria Type K deck.

## 7.4 SUMMARY

The majority of foil gage strain readings from the Peoria deck showed a very different trend from the strain of the experimental deck. For the Peoria deck, the strain measurements flipped, indicating expansion after 21 days of drying. This is possibly due to slip between concrete and reinforcement, minor cracks at the gage locations, or some other malfunction. The vibrating wire strain gage readings were similar to the trend that was observed with the experimental deck, which expanded during the first 7 days after placement followed by shrinkage beginning at 7 days and continuing throughout the recording period. One major difference is that the strain graph for the experimental deck was smooth as a result of constant temperature, while the Peoria bridge deck strain data shows significant daily variations resulting from daily temperature differences and traffic loading. When comparing the average longitudinal strain from the Type K Peoria deck with the Type K experimental deck, the trend was similar. However, the Peoria Type K had a smaller expansion during the first 7 days (even with more Type K cement in the Peoria bridge: 105 lb/yd<sup>3</sup> in Peoria, 90 lb/yd<sup>3</sup> in the experimental deck), which might be due to the actual bridge deck having more restraint than the experimental deck, greater degree of evaporation in the field, or the use of Class C fly ash.

More strain data from other bridge decks are needed in order to draw further conclusions about the effect of using Type K mixture in actual bridge decks.

## CHAPTER 8: FINITE ELEMENT ANALYSIS

Once the experimental results were collected for the experimental deck, the next step was to create a finite element model (or FE model) to mimic the measured strains within the deck. This is a complex process because of the non-homogenous nature of concrete. ABAQUS finite element software was chosen to create the model, rather than the SAP2000 that was used for the Phase I analysis. Experience shows that ABAQUS performs better when examining minor strain changes at specific locations.

The goal of the finite element modeling is to develop design and construction recommendations and to investigate how the measured strains changed based on the mixture design.

### 8.1 ABAQUS EXPERIMENTAL BAY MODEL

The ABAQUS model contains the entire structure of the experimental deck. This includes the concrete deck, two layers of reinforcement, girders, and the channels surrounding the deck (shown in Figures 88 and 89). The model was constructed using eight-node solid elements except for the reinforcement, which was modeled using truss elements that consider only axial strain along the reinforcement length. The concrete and steel properties used for modeling are listed in Table 9. A different Young's modulus and weight-per-unit volume were used for the different types of concrete according to the measured mixture properties. The thermal coefficient of expansion for each type of concrete was unknown; as a result, a general thermal coefficient of expansion of  $5.5 \mu\text{in}^{-\circ}\text{F}$  was used for all types of concrete.

All the FE model elements are bounded by applying tied constraints, except for the reinforcement that was embedded inside the concrete deck, which allowed the concrete and reinforcement to act together when the concrete is expanding or shrinking. The entire experimental deck was fixed in the gravity direction at the support located at the bottom of the girders, as shown in Figure 90. Mesh convergence was used to select the optimum mesh size of the deck, reinforcement, girders, and channels, as shown in Figure 91.

**Table 9. Material Properties Applied to the ABAQUS Model**

	Control concrete	SLU Type K concrete	LWA concrete	SRA concrete	Peoria Type K concrete	Steel
Weight per unit volume (lb/ft <sup>3</sup> )	142	141	136	142	139.5	490
Modulus of elasticity (ksi)	3770	3668	4380	4430	3218	29000
Poisson's ratio	0.2	0.2	0.2	0.2	0.2	0.3
Thermal coefficient of expansion ( $\mu\text{in}^{-\circ}\text{F}$ )	5.5	5.5	5.5	5.5	5.5	6.5

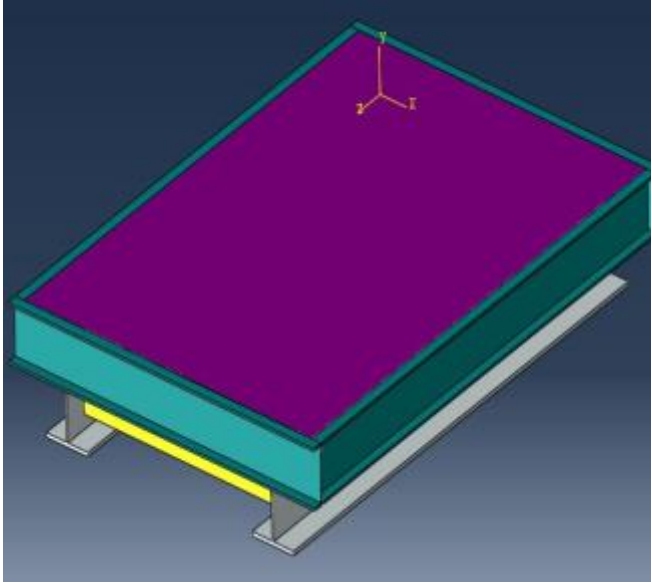


Figure 88. ABAQUS model of the experimental deck.

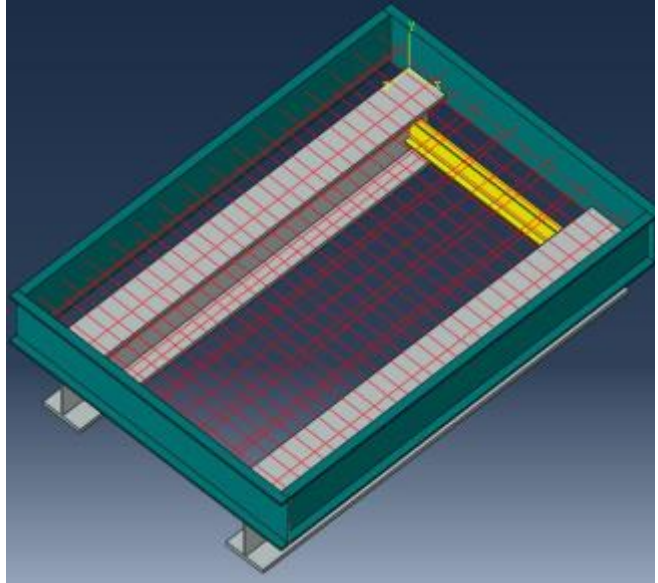


Figure 89. ABAQUS model of the experimental deck; the concrete deck was removed to show the reinforcement (in red).

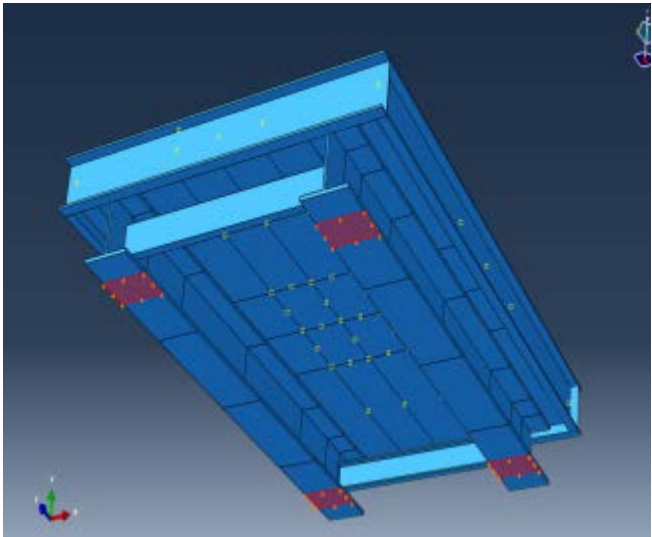


Figure 90. ABAQUS model; fixed in y direction (gravity direction) at the red marks.

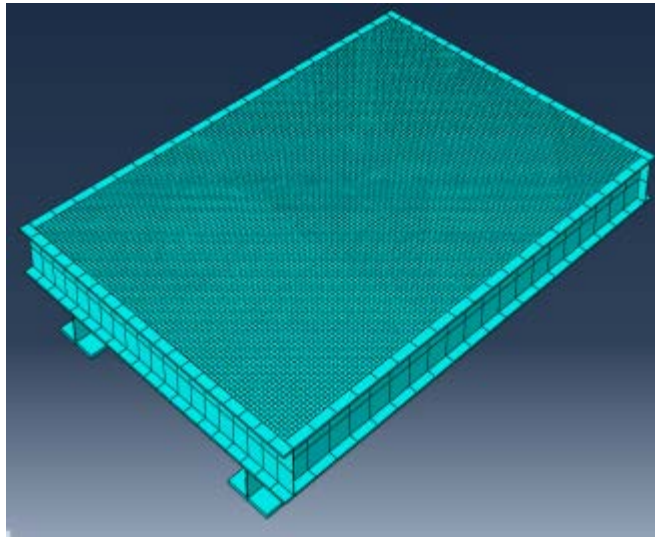


Figure 91. Meshed ABAQUS model.

## 8.2 RESULTS FOR ABAQUS EXPERIMENTAL BAY

Because applying the drying shrinkage strain directly to the model is not possible, a temperature load was used to model the shrinkage of the concrete. After comparing all data collected from both Phase I and Phase II, it was obvious that the strain measurements collected from different locations within the experimental deck showed no obvious trend; therefore, an average longitudinal total shrinkage (the strain value at that day minus the strain value at day 7) at each day was used to determine the temperature load. The temperature load applied to the deck was determined using the equation  $\epsilon = \alpha\Delta T$ . The strain ( $\epsilon$ , from the average longitudinal total shrinkage strain collected from the experiment deck) divided by the thermal coefficient of expansion ( $\alpha = 5.5 \mu\text{in}^{-\circ}\text{F}$ ) yields the temperature load applied to the concrete deck in the FE model. The temperature load applied to the model was constant throughout the deck for each individual day (rather than different temperature loads in different regions; see the [Phase I report](#) for detail). This avoids stress concentrations that do not exist in the actual structure and more accurately represents the uniform shrinkage expected with concrete. Figure 92 shows the temperature load applied to each type of concrete. These temperature loads permit shrinkage strains to be mimicked using ABAQUS. Results from the analysis are shown in Figures 93 through 96.

As shown in Figures 93 and 94, the strain results (ABAQUS compared with experimental) for the control and Type K deck were very similar until day 30, but by the end of 6 months, there was a deviation of about  $50 \mu\epsilon$ . However, the results for the LWA and SRA decks (Figures 95 and 96) were almost identical. Overall, the temperature load that was applied to the four types of experimental decks can result in a very similar average total shrinkage strain within the decks.

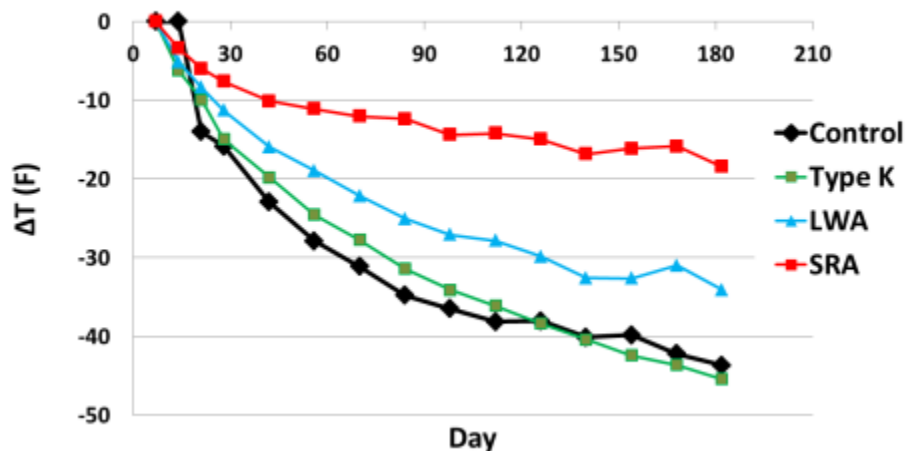


Figure 92. Temperature load applied to the FE model, in °F.

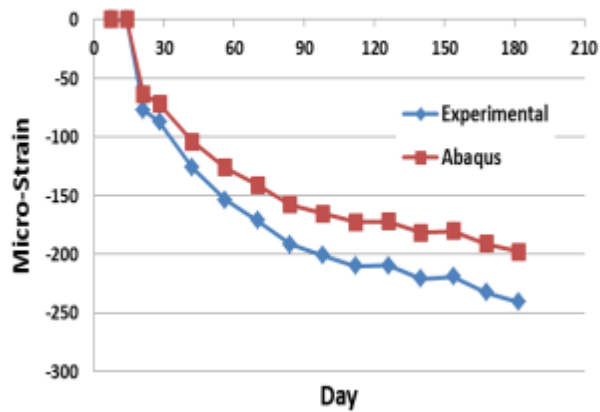


Figure 93. Control deck result.

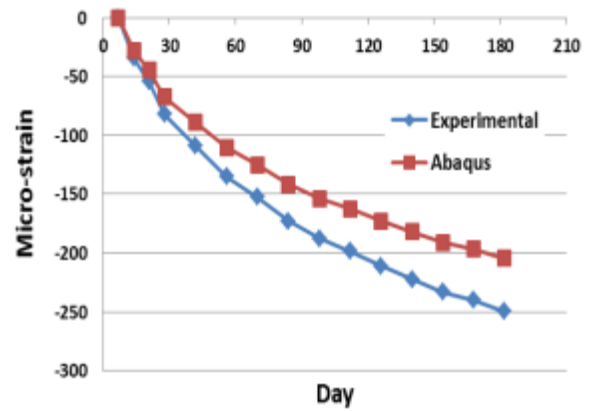


Figure 94. Type K deck result.

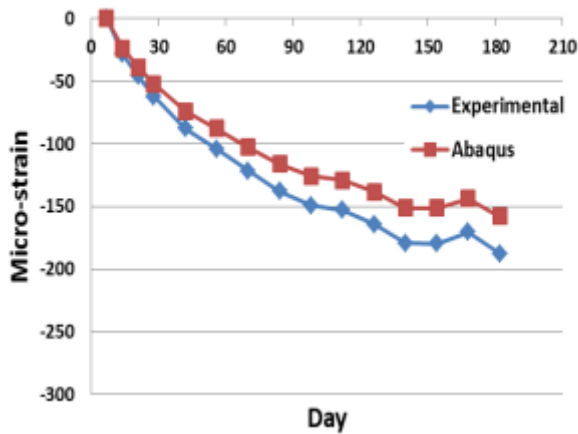


Figure 95. LWA deck result.

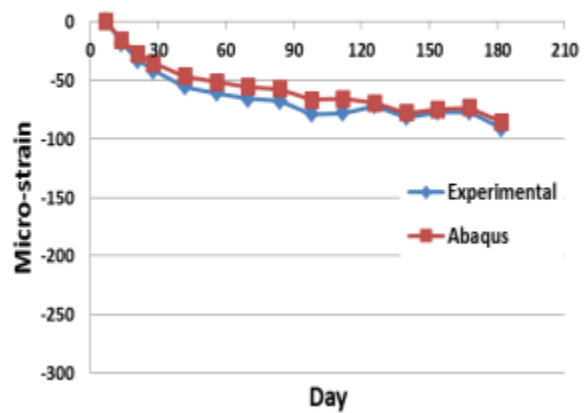


Figure 96. SRA deck result.

### 8.3 RESULTS FOR ABAQUS PEORIA TYPE K BRIDGE MODEL

The Peoria Type K bridge model was also constructed using the ABAQUS finite element modeling software, as shown in Figures 97 and 98, using the same modeling techniques described in Section 8.2. The bridge structure—including the deck, girders and two layers of reinforcement—were modeled, except the parapet was modeled as a uniformly distributed area load at the area covered by the parapet (the red area shown in Figure 97), and the load was applied at day 8 following placement (which was approximately the time the parapet placement was finished).

All the elements were modeled as fully composite by applying a tie constraint between the bottom of the concrete deck and girders. The mesh size for the deck and girders was 13 cm (5 in.), and the reinforcement was 2.54 cm (1 in.).

Because Stage 1 and Stage 2 of the bridge are symmetric and tied together along the deck using reinforcement, only Stage 2 of the bridge (northbound, which was monitored) was modeled. A symmetric constraint about the vertical plane was applied between the Stage 1 and Stage 2 portions of the deck (as shown in Figure 99). This method will help reduce the simulation process time and the size of the file. The entire bridge was modeled as simply supported at both abutment locations (as shown in Figure 99).

One of the biggest challenges of modeling the shrinkage in the Peoria Type K bridge was that the strain data collected from the foil gages were unusable because of minor crack formation, slip between concrete and steel, or errors in the measurements, which means that only the vibrating wire strain gage data could be used (the concrete strain) to develop the equivalent temperature loads. In this case, the vibrating wire strain gage data include not only the strain caused by shrinkage but also strain caused by traffic and temperature; therefore, only the general trend of these data was considered when modeling shrinkage.

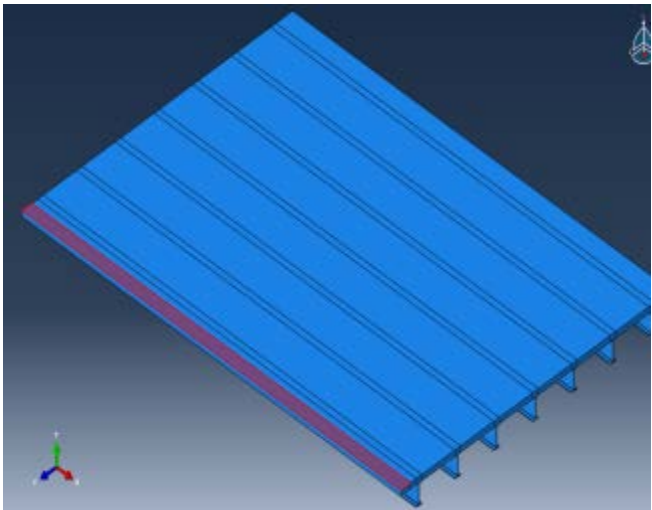


**Figure 97. Peoria full-bridge ABAQUS model; reinforcements are embedded inside the deck.**

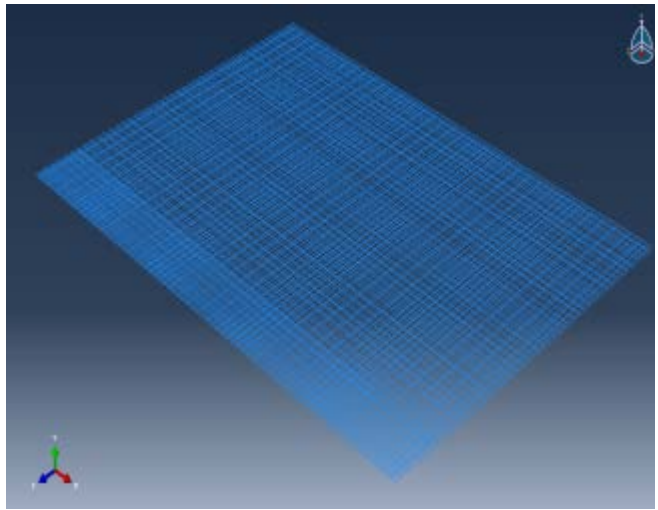


**Figure 98. Peoria full-bridge ABAQUS model; reinforcements only.**

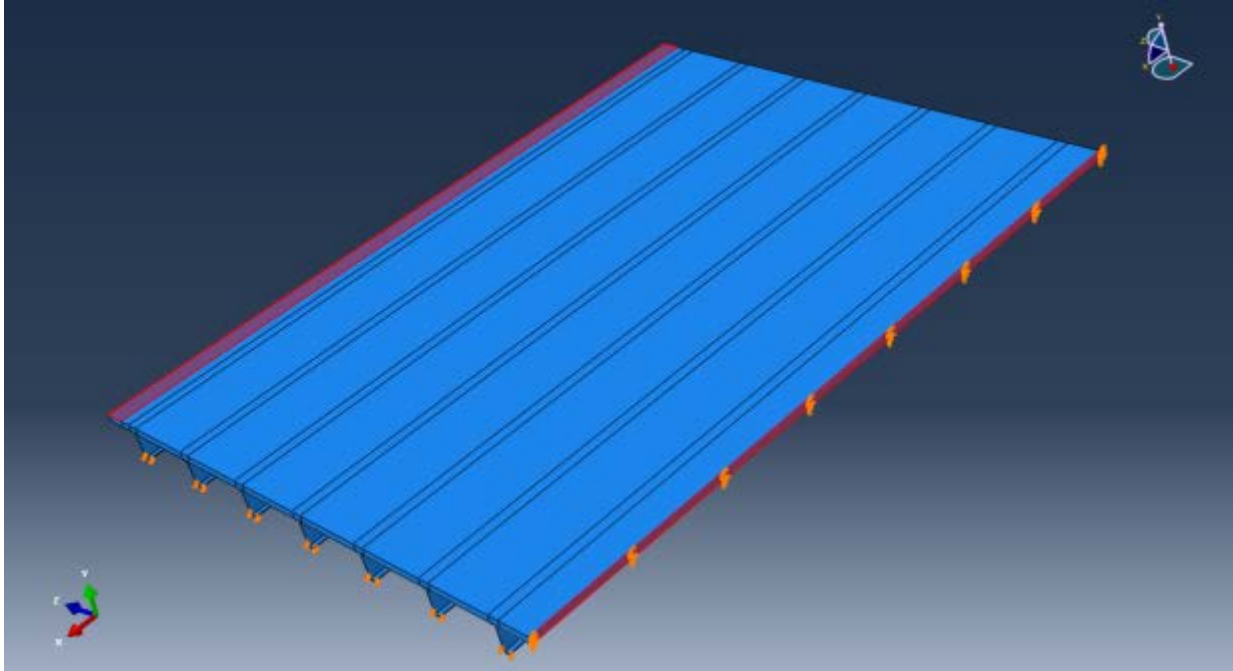


**Figure 99. Peoria full-bridge ABAQUS model showing boundary conditions.**

#### **8.4 ABAQUS PEORIA TYPE K BRIDGE RESULTS**

To determine the temperature load required to model shrinkage of the Peoria deck, the same “temperature loading” process ( $\epsilon = \alpha\Delta T$ ) was used as with the experimental decks. The strain ( $\epsilon$ , from the average longitudinal total shrinkage strain collected from the vibrating wire strain gage) divided by the thermal coefficient of expansion ( $\alpha = 5.5 \mu\text{in}^{-\circ}\text{F}$ ) yielded the temperature load being applied to the concrete deck in the FE model. However, the Peoria bridge deck was also exposed to actual temperature changes (as shown in Figure 87), and those temperature changes also affected the strain collected from the vibrating wire strain gages. As a result, the environmental temperature load was also applied to the model. Table 10 shows the temperature load that was applied at days 126, 140, and 154.

**Table 10. Temperature Load ( $^{\circ}\text{F}$ ) Applied to the Peoria FE Model**

<b>Temperature Load</b>	<b>Day 126</b>	<b>Day 140</b>	<b>Day 154</b>
$\Delta T$ to model the shrinkage	-43.3854	-49.5357	-57.8086
$\Delta T$ of the environment	-71.454	-37.3764	-49.7265
Total $\Delta T$ applied to the deck	-114.839	-86.9121	-107.535

\*Units:  $^{\circ}\text{F}$  ( $^{\circ}\text{C} = (^{\circ}\text{F} - 32) \times 5/9$ )

The results of the finite element analysis are shown in Figure 100, which include the average strain comparison between the average longitudinal total shrinkage strain observed from the ABAQUS model and the average longitudinal total shrinkage strain collected from the vibrating wire strain

gages. The results show that the average strain in the ABAQUS model is fairly close to the actual strain observed in the Peoria deck. A similar trend is shown in Figures 93 through 96 (the comparison between ABAQUS results with the SLU experimental deck results).

Figures 101 and 102 show the longitudinal strain contour for the concrete deck at the bottom and top layer of reinforcement, respectively. A close examination of the strain from the vibrating wire strain gage locations in the ABAQUS model shows less shrinkage strain in the area closer to Stage 1 of the deck. This is possibly due to the large amount of restraint in the area (the Stage 2 deck was tied to the Stage 1 deck). This strain difference was also presented in the strain data collected from the Peoria deck (Figure 84 compared with Figures 82, 83, and 85), which showed  $-209 \mu\epsilon$  at the location close to Stage 1, whereas the other locations showed strains around  $-300 \mu\epsilon$ .

This proved that applying uniform temperature load can closely simulate the shrinkage of concrete in both experimental and actual bridge decks, and in the future, the strain caused by shrinkage can be found by subtracting the strain caused by actual temperatures using the ABAQUS model. One major difference between the experimental deck and the Peoria bridge deck is that the strain inside the Peoria bridge deck was significantly influenced by the actual temperature change in the surrounding environment, whereas the experimental deck cast in a laboratory was not. This is because the experimental deck was exposed to temperature change only at the bottom of the deck rather than the entire deck, and the time that the bottom of the deck was exposed to the cooler temperature was not enough to allow the concrete to react (because of the low thermal conductivity of concrete).

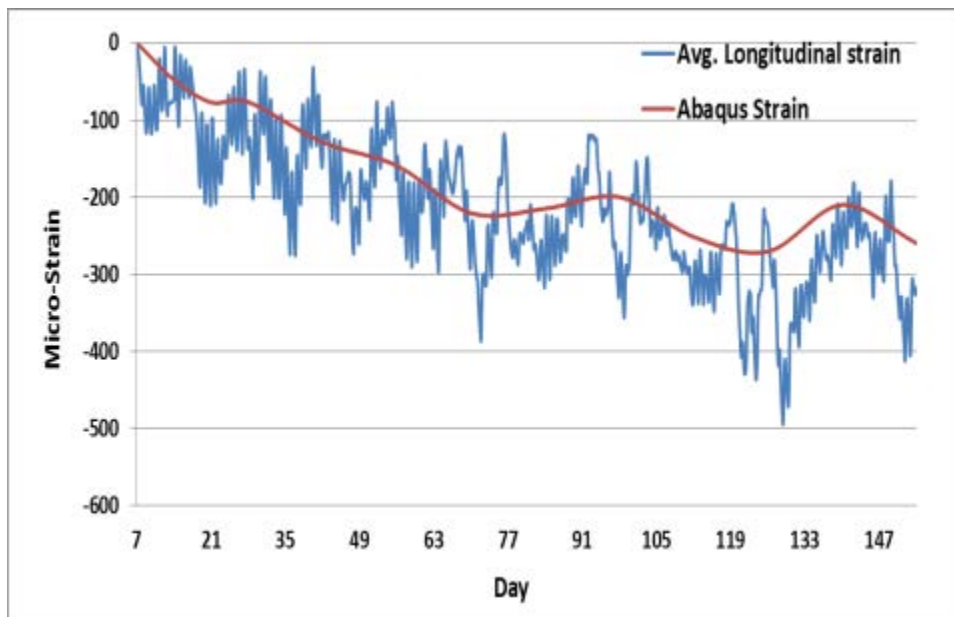


**Figure 100. Average longitudinal total shrinkage strain of ABAQUS and Peoria bridge deck.**

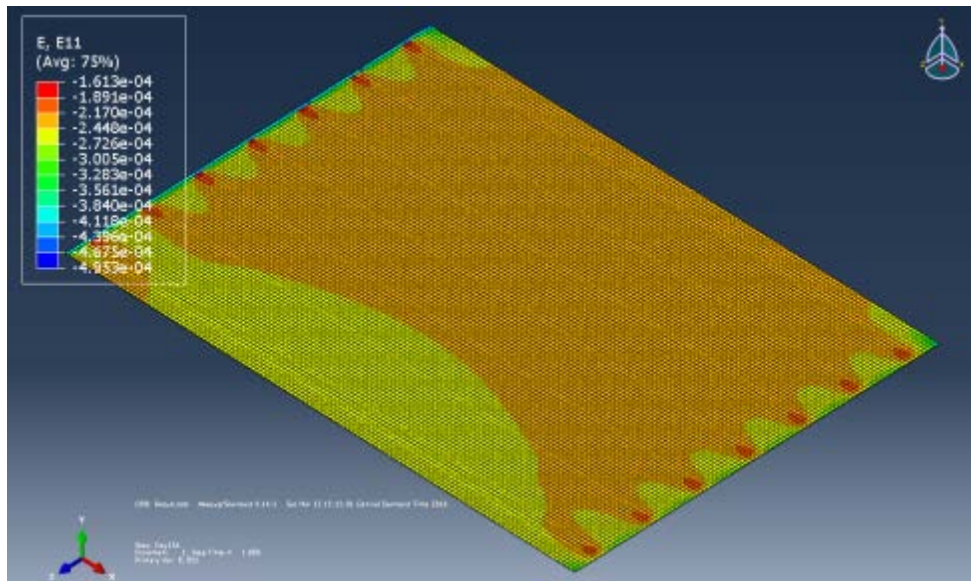


Figure 101. Bottom-layer longitudinal strain contour.

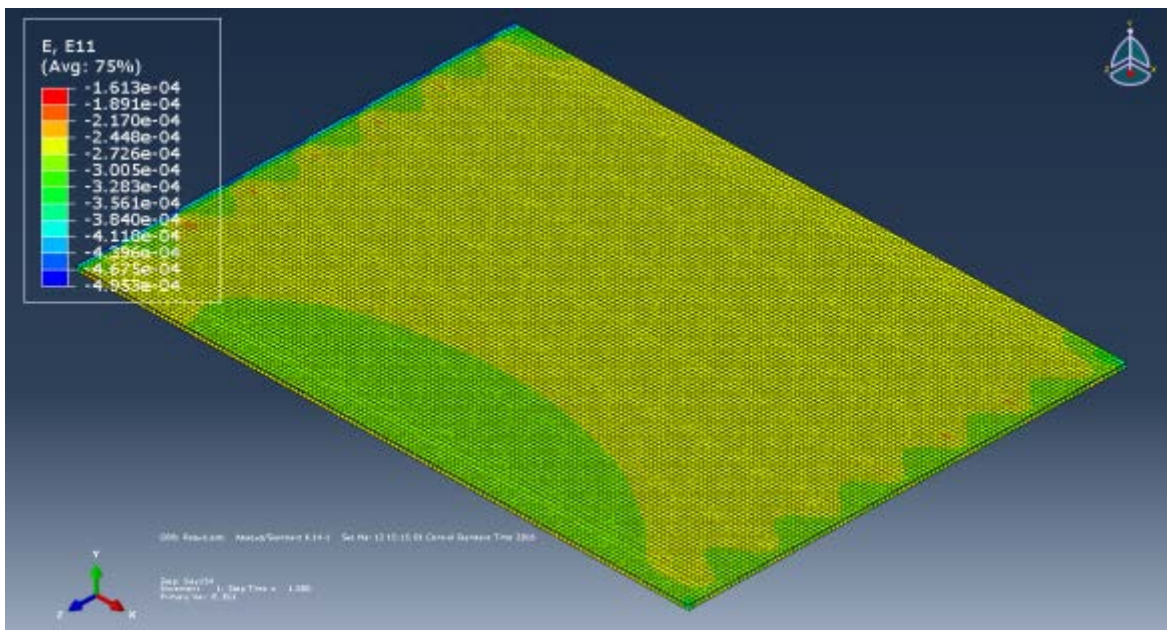


Figure 102. Top-layer longitudinal strain contour.

## **8.5 SUMMARY**

For finite element modeling, temperature loads applied to the four types of experimental decks can result in very similar average total shrinkage strain within the decks. Through application of a uniform temperature load, the shrinkage of concrete can be closely simulated in for both experimental and actual bridge deck models. In the future, the strain caused by shrinkage can be found by subtracting the strain caused by actual temperatures using the ABAQUS model.

## CHAPTER 9: CONCLUSIONS

The main conclusions of this study are as follows:

- Even when the same amount of internal curing water is provided, the type and source of LWA can cause a difference in autogenous and drying shrinkage of mortar mixtures, which is believed to be a result of different desorption characteristics, gradation, and modulus.
- In a sealed condition, the total shrinkage of mortar mixtures decreased as the dosage of the LWA increases.
- Longer soaking times for LWA could improve the effectiveness of LWA in reducing autogenous shrinkage in mortar mixtures. Generally, autogenous shrinkage is inversely proportional to the amount of internal curing water provided (i.e., increasing the amount of internal curing water, whether by increasing the dosage of LWA or by increasing the initial moisture content of LWA, results in a decrease in autogenous deformation).
- In a severe drying condition, when no curing method is applied, LWA was not beneficial in reducing drying shrinkage of mortar mixtures. However, in a milder drying condition, LWA could be beneficial in reducing drying shrinkage.
- Even in a severe drying condition, either curing method (wet or sealed) benefited the LWA mixture in reducing drying shrinkage. This finding shows the significance of conventional external curing, even in mixes for which internal curing is implemented.
- Wet curing was more beneficial than sealed curing in reducing drying shrinkage of mortar mixtures.
- In sealed conditions, addition of LWA could dramatically reduce the shrinkage of concrete.
- In unsealed conditions, addition of LWA did not change the drying shrinkage of concrete considerably. Therefore, addition of LWA should not be considered an effective way to mitigate drying shrinkage of concrete.
- Using LWA can increase the early-age expansion of OPC-Type K cement blends in a sealed condition. This behavior is attributed to an increase in hydration of ye'elimite, which results in an increase in formation of ettringite crystals.
- It was observed that although addition of LWA to OPC-Type K systems can decrease early-age compressive strength, it resulted in an increase in compressive strength at later ages (28 days).
- Using an inert material (crumb rubber), it was shown that the bulk modulus of elasticity affected length deformation behavior: a lower modulus resulted in higher length deformation, whether by shrinkage or expansion. However, the increase in expansion of the OPC-Type K mixes with LWA was due not only to the reduction in the elastic modulus but also to the increase in the Type K hydration. This outcome is promising because LWA can promote hydration of Type K, resulting in early-age expansion and shrinkage mitigation without the detrimental effects of increasing the w/c ratio. Though this part of the study was preliminary,

the results are encouraging and warrant further detailed study before possible field application.

- Results from mortar mixtures showed that at a low w/c ratio of 0.34, addition of SRA to internally cured mixtures can further reduce autogenous shrinkage. This behavior, however, was not observed at a high w/c ratio of 0.44.
- In mortar mixtures with and without LWA, for both 0.34 and 0.44 w/c ratios, drying shrinkage appeared to be directly related to the amount of SRA in the mixture (i.e., incorporation of internal curing does not change the shrinkage behavior considerably).
- Addition of SRA to mixes with LWA reduced the drying shrinkage considerably and made the mixture more volumetrically stable. The results of the combined SRA and LWA mixtures are encouraging and warrant further detailed study before possible field application.
- Peak strain values (the highest strain reading occurring at the end of the curing period) for the LWA experimental deck were similar to or slightly less than those for the control and SRA experimental decks but were still less than strains measured for the deck containing Type K cement.
- As the LWA experimental deck shrank after the curing period, it did so at a slower rate compared with the control and Type K experimental decks. The difference in the strain rate is a direct result of the slow release of water within the partially saturated aggregate—thereby slowing down moisture loss to the surrounding environment.
- No cracks formed within or at the surface of the LWA and SRA experimental decks.
- The bottom layer of the experimental deck shrank less than the top layer for all four types of concrete. The main reason was the fact that the top concrete was uncovered after 7 days of curing, while the bottom of the deck was covered by formwork for 14 days. As a result, less water was lost for the bottom layer of the concrete during that time period. The bottom concrete also showed slightly higher peak strains at 7 days, which was most likely due to longer curing provided at the bottom of the deck.
- In comparing the total shrinkage strain following the initial expansion, the experimental deck containing Type K cement had the largest total shrinkage and is comparable to the control. The experimental deck containing SRA had the least total shrinkage over time.
- The peak strain (the highest strain reading occurring at the end of the curing period) of the SRA experimental deck was nearly the same as the peak strain of the control concrete.
- The rate of shrinkage for the SRA deck was much slower than that of the other three concrete mixtures. The shrinkage rate was especially small after 84 days. In fact, some strain remained almost unchanged from 84 to 168 days.
- In addition, the overall strain change of the SRA experimental deck (from day 1 to 6 months) was smaller than the others, which led to smaller tensile forces within the concrete deck and therefore less potential for cracking.

- Measured strain values of the concrete were almost identical with the strain values of reinforcement, which indicates that the concrete and reinforcement were fully bonded.
- For the Peoria deck, the strain measurements of the reinforcement went from negative to positive, indicating expansion after 21 days of drying. This is possibly due to slip between concrete and reinforcement, minor cracks at the gage locations, or some other malfunction.
- The strain plots for the experimental decks were smooth because of the constant temperature, while the Peoria bridge deck strain data showed significant daily variations resulting from temperature differences and traffic loading.
- In comparing the average longitudinal strain from the Type K Peoria deck with the Type K experimental deck, the trend was similar; however, the Peoria Type K had a smaller expansion during the first 7 days, even with more Type K material in its mix (105 lb/yd<sup>3</sup> in Peoria, 90 lb/yd<sup>3</sup> in the experimental deck). This finding might be due to more restraint in the actual bridge deck compared with the experimental deck or the use of Class C fly ash, which can inhibit Type K's expansion.
- For finite element modeling, temperature loads applied to the four types of experimental decks resulted in very similar average shrinkage strain within the decks.
- Through application of a uniform temperature load, the shrinkage of concrete can be closely simulated for both experimental and actual bridge deck models. In the future, the strain caused by shrinkage can be found by subtracting the strain caused by actual temperatures using the ABAQUS model.

## REFERENCES

- Aitcin, P.C., 2003. The durability characteristics of high-performance concrete: a review. *Cement and Concrete Composites*, 25(4), pp. 409-420.
- Bentz, D.P., 2002. Influence of curing conditions on water loss and hydration in cement pastes with and without fly ash substitution. *NISTIR*, 6886, p. 15.
- Bentz, D.P., 2007. Internal curing of high-performance blended cement mortars. *ACI Materials Journal*, 104(4), p. 408.
- Bentz, D.P., Hansen, K.K., Madsen, H.D., Vallee, F. and Griesel, E.J., 2001. Drying/hydration in cement pastes during curing. *Materials and Structures*, 34(9), pp. 557-565.
- Bentz, D.P., Halleck, P.M., Grader, A.S. and Roberts, J.W., 2006, August. Four-dimensional X-ray microtomography study of water movement during internal curing. In *Volume changes of hardening concrete: testing and mitigation*. Proceedings of the international RILEM conference, Denmark (pp. 11-20).
- Bentz, D.P., Lura, P. and Roberts, J.W., 2005. Mixture proportioning for internal curing. *Concrete International*, 27(2), pp. 35-40.
- Bentz, D.P. and Snyder, K.A., 1999. Protected paste volume in concrete: extension to internal curing using saturated lightweight fine aggregate. *Cement and concrete research*, 29(11), pp. 1863-1867.
- Bentz, D.P. and Weiss, W.J., 2011. Internal curing: a 2010 state-of-the-art review. US Department of Commerce, National Institute of Standards and Technology.
- Brooks, J., 2014. *Concrete and masonry movements*. Butterworth-Heinemann.
- Browning, J., Darwin, D., Reynolds, D. and Pendergrass, B., 2011. Lightweight aggregate as internal curing agent to limit concrete shrinkage. *ACI Materials Journal*, 108(6), pp. 638-644.
- Castro, J., Keiser, L., Golias, M. and Weiss, J., 2011. Absorption and desorption properties of fine lightweight aggregate for application to internally cured concrete mixtures. *Cement and Concrete Composites*, 33(10), pp. 1001-1008.
- Chaunsali, P., Lim, S., Mondal, P., Foutch, D.A., Richardson, D., Tung, Y. and Hindi, R., 2013. *Bridge Decks: Mitigation of Cracking and Increased Durability*. Illinois Center for Transportation (ICT).
- Eldin, N.N. and Senouci, A.B., 1993. Rubber-tire particles as concrete aggregate. *Journal of materials in civil engineering*, 5(4), pp. 478-496.
- Espinoza-Hijazin, G. and Lopez, M., 2011. Extending internal curing to concrete mixtures with W/C higher than 0.42. *Construction and Building Materials*, 25(3), pp. 1236-1242.
- Golias, M., Castro, J. and Weiss, J., 2012. The influence of the initial moisture content of lightweight aggregate on internal curing. *Construction and Building Materials*, 35, pp. 52-62.
- Golias, M., Bentz, D.P. and Weiss, J., 2013. Influence of exposure conditions on the efficiency of internal curing. *Advances in Civil Engineering Materials*, 2(1), 12 pp.

- Henkensiefken, R., Briatka, P., Bentz, D., Nantung, T. and Weiss, J., 2010. Plastic shrinkage cracking in internally cured mixtures made with pre-wetted lightweight aggregate. *Concrete international*, 32(2), pp. 49-54.
- Henkensiefken, R., Nantung, T. and Weiss, W., 2009a, June. Internal Curing-From the Laboratory to Implementation. In *International Bridge Conference*.
- Henkensiefken, R., Bentz, D., Nantung, T. and Weiss, J., 2009b. Volume change and cracking in internally cured mixtures made with saturated lightweight aggregate under sealed and unsealed conditions. *Cement and Concrete Composites*, 31(7), pp. 427-437.
- Henkensiefken, R., Castro, J., Kim, H., Bentz, D. and Weiss, J., 2009c. Internal curing improves concrete performance throughout its life. *Concrete in Focus*, 8(5), pp. 22-30.
- Henkensiefken, R., Nantung, T. and Weiss, J., 2011. Saturated Lightweight Aggregate for Internal Curing in Low w/c Mixtures: Monitoring Water Movement Using X-ray Absorption. *Strain*, 47(s1).
- Hopper, T., Manafpour, A., Radlińska, A., Warn, G., Rajabipour, F., Morian, D. and Jahangirnejad, S., 2015. *Bridge Deck Cracking: Effects on In-Service Performance, Prevention, and Remediation* (No. FHWA-PA-2015-006-120103). Report FHWA-PA-2015-006-120103. FHWA, US Department of Transportation.
- Krauss, P.D. and Rogalla, E.A., 1996. Transverse cracking in newly constructed bridge decks (No. Project 12-37 FY'92).
- Moreno, D., Martinez, P. and Lopez, M., 2014. Practical Approach for Assessing Lightweight Aggregate Potential for Concrete Performance. *ACI Materials Journal*, 111(2).
- Powers, T., 1935. Absorption of water by portland cement paste during the hardening process. *Industrial & Engineering Chemistry*, 27(7), pp. 790-794.
- Radlinska, A., Rajabipour, F., Bucher, B., Henkensiefken, R., Sant, G. and Weiss, J., 2008. Shrinkage mitigation strategies in cementitious systems: A closer look at differences in sealed and unsealed behavior. *Transportation Research Record: Journal of the Transportation Research Board*, (2070), pp. 59-67.
- Shin, K.J., Bucher, B. and Weiss, J., 2010. Role of lightweight synthetic particles on the restrained shrinkage cracking behavior of mortar. *Journal of Materials in Civil Engineering*, 23(5), pp. 597-605.
- Trtik, P., Münch, B., Weiss, W.J., Kaestner, A., Jerjen, I., Josic, L., Lehmann, E. and Lura, P., 2011. Release of internal curing water from lightweight aggregates in cement paste investigated by neutron and X-ray tomography. *Nuclear Instruments and Methods in Physics Research Section A: Accelerators, Spectrometers, Detectors and Associated Equipment*, 651(1), pp. 244-249.
- Videla, C. and Lo, M., 2000. Mixture proportioning methodology for structural sand-lightweight concrete. *Materials Journal*, 97(3), pp. 281-289.
- Villarreal, V.H., 2008. Internal curing—Real world ready mix production and applications: A practical approach to lightweight modified concrete. *Special Publication*, 256, pp. 45-56.
- Wasserman, R. and Bentur, A., 1996. Interfacial interactions in lightweight aggregate concretes and

- their influence on the concrete strength. *Cement and Concrete Composites*, 18(1), pp. 67-76.
- Zhutovsky, S. and Kovler, K., 2012. Effect of internal curing on durability-related properties of high performance concrete. *Cement and concrete research*, 42(1), pp. 20-26.
- Zhutovsky, S., Kovler, K. and Bentur, A., 2004. Influence of cement paste matrix properties on the autogenous curing of high-performance concrete. *Cement and Concrete Composites*, 26(5), pp. 499-507.
- Frosch, R., Gutierrez, S., and Hoffman, J., 2010. Control and Repair of Bridge Deck Cracking. Indiana Department of Transportation (INDOT).

# APPENDIX A: MATERIALS AND METHODS

## A.1 MATERIALS

### A.1.1 Raw Materials

Type I portland cement (from Essroc Co.) and a commercially available CSA cement (sold as KSC Komponent by CTS Cement) were used in this study. Quantitative X-ray diffraction (QXRD) analysis was performed to determine the mineralogical composition of OPC and CSA cement and the results are presented in Table A.1. Natural sand (fine aggregate FA 1 based on IDOT specification) with a specific gravity of 2.6, a fineness modulus of 2.7, and absorption of 1.7% was used. Pre-soaked LWA was therefore prepared by adding 15.5% water to oven-dried, air-cooled LWA at least 24 hours before mixing. Coarse aggregates (CA7) confirming to IDOT specification were utilized in concrete proportioning. Tetraguard (BASF) was also utilized as a shrinkage-reducing admixture.

**Table A.1. Mineralogical Composition  
(Mass Fraction) of OPC and CSA Cement**

Mineral	CSA cement	OPC
$C_4A_3\bar{S}$	19.3	—
$C\bar{S}H_2$	15.0	—
$C\bar{S}$	16.1	—
$C\bar{S}H_{0.5}$	9.4	—
$C_2\bar{S}$	34.8	14.1
$C_4AF$	—	5.4
$C_3\bar{S}$	—	62.2
$C_3A$	—	9.9

Coarse aggregate used in this study was limestone with a nominal maximum size of 19 mm. The SSD specific gravity and absorption for the coarse aggregate were measured to be 2.69 % and 2.0%, respectively. The coarse aggregate was sieved into four ranges of particle sizes, 4.75 to 9.5 mm, 9.5 to 12.5 mm, 12.5 to 19 mm, and 19 to 25 mm and then mixed with specific proportions to meet the CA7 gradation specified by Illinois Department of Transportation.

### A.1.2 Mixture Proportions

Tables A.2 through A.7 show the proportions of various concrete mixtures used in this study. The mix design procedure followed by IDOT was used to design the concrete mixtures. The base concrete mix was finalized as the one with cement factor of 610, mortar factor of 0.86, and w/cm ratio of 0.44. The cement factor of 610 lb/yd<sup>3</sup> is higher than the minimum requirement for Class BS concrete according to IDOT specification. For mixture with LWA, a percentage of fine aggregate (sand) was replaced with LWA. Therefore, the dosage of LWA is reported as the replacement dosage of fine aggregate with LWA.

**Table A.2. Mixture Proportions of Mortar Mixtures with Three Types of LWA**

Materials	0.34 w/c				0.44 w/c			
	0% LWA	38% LWA-A	54% LWA-B	35% LWA-C	0% LWA	38% LWA-A	54% LWA-B	35% LWA-C
OPC (lb/yd <sup>3</sup> )	1154	1154	1154	1154	1002	1002	1002	1002
Water (lb/yd <sup>3</sup> )	433	417	411	419	481	466	459	467
OD Sand (lb/yd <sup>3</sup> )	2371	1466	1090	1539	2371	1466	1090	1539
SSD LWA (lb/yd <sup>3</sup> )	0	666	1077	550	0	666	1077	550

(1 lb/yd<sup>3</sup> = 0.59 kg/m<sup>3</sup>)**Table A.3. Mixture Proportions of Mortar Mixtures with Different LWA Dosages**

Materials	0.34 w/c				0.44 w/c			
	0% LWA	13% LWA	26% LWA	38% LWA	0% LWA	13% LWA	26% LWA	38% LWA
OPC (lb/yd <sup>3</sup> )	1154	1154	1154	1154	1002	1002	1002	1002
Water (lb/yd <sup>3</sup> )	433	428	422	417	481	476	471	466
OD sand (lb/yd <sup>3</sup> )	2371	2069	1767	1466	2371	2069	1767	1466
SSD LWA (lb/yd <sup>3</sup> )	0	222	444	666	0	222	444	666

(1 lb/yd<sup>3</sup> = 0.59 kg/m<sup>3</sup>)**Table A.4. Mixture Proportions for Mortar Specimens**

Materials	I: 0.34_0%LWA	II: 0.34_38%LWA	III: 0.43_0%LWA
OPC (lb/yd <sup>3</sup> )	1154	1154	1020
OD sand (lb/yd <sup>3</sup> )	2371	1466	2371
Water (lb/yd <sup>3</sup> )	393	393	435
SD LWA (lb/yd <sup>3</sup> )	0	666	0
Extra water to bring sand to SSD (lb/yd <sup>3</sup> )	40	25	40
Water provided by internal curing (lb/yd <sup>3</sup> )	0	100	0
Effective w/c	0.34	0.34	0.43
Total w/c	0.34	0.43	0.43

(1 lb/yd<sup>3</sup> = 0.59 kg/m<sup>3</sup>)**Table A.5. Mixture Proportions for Concrete Specimens**

Materials		0.39_0%LWA	0.39_76%LWA	0.55_0%LWA
OPC (lb/yd <sup>3</sup> )		610	610	610
OD Coarse Aggregate (lb/yd <sup>3</sup> )	19–25 mm	358	358	358
	12.5–19 mm	537	537	537
	9.5–12.5 mm	358	358	358
	4.75–9.5 mm	537	537	537
OD Sand (lb/yd <sup>3</sup> )		1188	282	934
SSD LWA (lb/yd <sup>3</sup> )		0	599	0
Mixing water (lb/yd <sup>3</sup> )		294	279	388

(1 lb/yd<sup>3</sup> = 0.59 kg/m<sup>3</sup>)

**Table A.6. Mixture Proportions for Mortar Specimens for CSA-OPC Mixtures**

Mixture	0.34_0%CSA _0%LWA	0.34_15%CSA _0%LWA	0.34_15%CSA _12%LWA	0.34_15%CSA _24%LWA	0.34_15%CSA _35%LWA	0.412_15%CSA _0%LWA
OPC (lb/yd <sup>3</sup> )	1154	981	981	981	981	885
CSA (lb/yd <sup>3</sup> )	0	173	173	173	173	156
OD sand (lb/yd <sup>3</sup> )	2371	2371	2095	1815	1539	2371
SD LWA (lb/yd <sup>3</sup> )	0	0	182	368	550	0
Mixing water (lb/yd <sup>3</sup> )	433	433	428	423	419	469
Effective w/c ratio	0.340	0.340	0.340	0.340	0.340	0.412
Total w/c ratio	0.340	0.340	0.364	0.388	0.412	0.412

(1 lb/yd<sup>3</sup> = 0.59 kg/m<sup>3</sup>)**Table A.7. Mixture Proportions for Concrete Specimens for CSA-OPC Mixtures**

Materials		0.34_0%CSA _0%LWA	0.34_15%CSA _0%LWA	0.34_15%CSA _71%LWA	0.49_15%CSA _0%LWA
OPC (lb/yd <sup>3</sup> )		610	518	518	518
CSA (lb/yd <sup>3</sup> )		0	92	92	92
OD Coarse Aggregate (lb/yd <sup>3</sup> )	19–25 mm	356	356	356	356
	12.5–19 mm	535	535	535	535
	9.5–12.5 mm	356	356	356	356
	4.75–9.5 mm	535	535	535	535
OD Sand (lb/yd <sup>3</sup> )		1264	1264	362	1037
SSD LWA (lb/yd <sup>3</sup> )		0	0	599	0
Mixing water (lb/yd <sup>3</sup> )		265	265	248	351
Effective w/c ratio		0.34	0.34	0.34	0.49
Total w/c ratio		0.34	0.34	0.49	0.49

(1 lb/yd<sup>3</sup> = 0.59 kg/m<sup>3</sup>)

## A.2 TEST METHODS

### A.2.1 Mixing Procedure

Mortar samples were prepared in accordance with ASTM C305 in a Hobart mixture. The mixing procedure for concrete complied with ASTM C192. The coarse and fine aggregate were initially dried in an oven and subsequently cooled before using in concrete. The amount of water to reach the saturated surface dry condition for aggregates was added separately to the mixing water. The oven-dried condition of aggregates was adopted to reduce the variation due to subjectivity of SSD test.

### A.2.2 Restrained Expansion of Type k Concrete

Restrained expansion of expansive concrete was monitored in accordance with ASTM C878. The concrete samples of size 3 × 3 × 10 in. (75 × 75 × 254 mm) were prepared in a mold shown in Figure A.1. The steel rod placed at the center with attached end plates provides a restraint for the concrete.

The samples were demolded after 6 hours, and were sealed immediately. Length measurements were performed after 6 hours (demolding time) and 28 days. Intermediate length measurements were also taken to get more information regarding the rate of expansion. The 7-day expansion value provides useful information as it can be related to the maximum expansion experienced by a structural member in the field [ACI 223-R 2010].



**Figure A.1. A typical mold for restrained expansion in accordance with ASTM C878.**

### **A.2.3 Unrestrained (Free) Deformation of Mortar Mixtures**

Deformation of mortar mixtures at early ages (within 24 hours) was measured using ASTM C1698. The mortar mixtures were encapsulated in corrugated polyethylene tube in accordance with ASTM C1698 (Figure A.2). This test method allows monitoring the linear deformation by providing increased restraint against lateral deformation and minimizing the restraint of the fresh paste in the linear direction only. The length measurements were started after final set (as determined by the Vicat needle test in accordance with ASTM C191).



**Figure A.2. A dilatometer for monitoring the unrestrained deformation of cement pastes in accordance with ASTM C1698.**

#### A.2.4 Compressive Strength

Compressive strength of  $2 \times 2 \times 2$  in. ( $50 \times 50 \times 50$  mm) cubes was determined right after demolding at 24 hours and also after 7 and 28 days of moist curing in accordance with ASTM C39.

#### A.2.5 Drying Shrinkage of Mortar and Plain Concrete

The drying shrinkage of mortars containing portland cement and graded sand were monitored using ASTM C596 (Figure A.3). For this test,  $1 \times 1 \times 11.25$  in. ( $25 \times 25 \times 285$  mm) mortar prisms were prepared. The specimens were either cured in lime-saturated water or sealed to measure autogenous deformation. Free shrinkage was measured at constant temperature ( $22^\circ\text{C} \pm 2^\circ\text{C}$ ), and constant relative humidity ( $50\% \pm 4\%$ ).

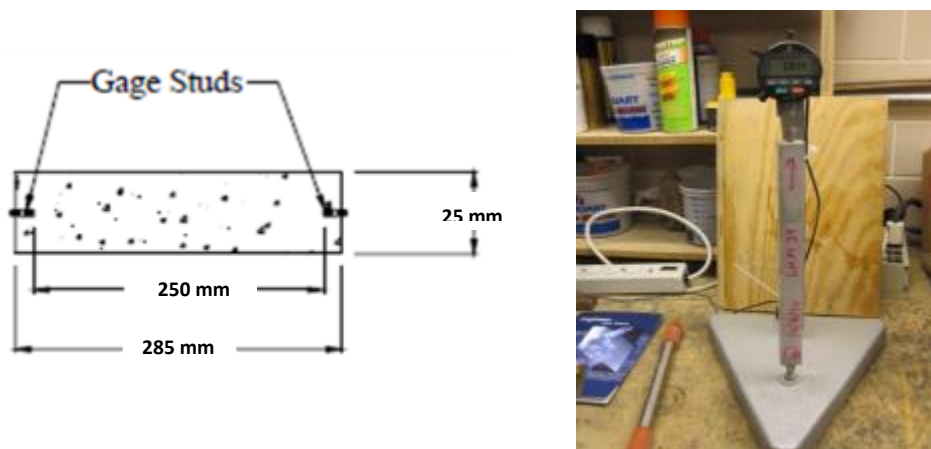


**Figure A.3. Typical mortar sample and digital length comparator for free shrinkage measurement.**

The free drying shrinkage of plain concrete (without any expansive component) was determined using ASTM C157. Samples of size  $3 \times 3 \times 11.25$  in. ( $75 \times 75 \times 285$  mm) were prepared, and cured in sealed environment for 24 hours. Afterwards the samples were demolded and cured in saturated limewater for 7 days before exposing them to constant temperature ( $22^\circ\text{C} \pm 2^\circ\text{C}$ ) and relative humidity ( $50\% \pm 4\%$ ). The length measurements were carried out intermittently over the period of time.

#### A.2.6 Measurement of Capillary Porosity and Evaporable Water Content

Total capillary porosity of the mortar samples was determined using the solvent exchange method. Cylindrical samples of 1 in. (25 mm) diameter were prepared and then samples of 1 to 2 mm height were cut using a low speed saw. The samples were then immersed in isopropanol alcohol for 24 hours. Afterward, the samples were dried under vacuum in a desiccator. The difference in weight of the sample before and after drying in the vacuum was used to calculate the volume of capillary water. The total volume of the sample was determined by buoyancy method using isopropanol

alcohol as the medium. Therefore, capillary porosity was determined as the volumetric ratio of capillary porosity and total sample volume.

Evaporable water was measured using prisms with dimensions of 1 × 1 × 11.25 in. (25 x 25 x 285 mm) (same dimensions as to shrinkage prisms in order to maintain a constant surface area to volume ratio). After demolding at age of one day, the specimens were kept in an oven of 105°C until constant weight (less than 0.1% weight loss in a few hours) was reached. For these specimens it generally took less than a day for a constant weight to be achieved. The difference between the weights before and after oven drying is generally referred to as evaporable water. To be able to compare the amount of evaporable water between different mixes, here, the ratio of evaporable water weight to the original weight of unhydrated cement in the specimen is reported. Original weight of cement was determined using sample's original weight (before oven drying) and the mix design information.

# APPENDIX B: LARGE-SCALE TESTING RESULTS

## B.1 LARGE-SCALE TESTING RESULT: LWA

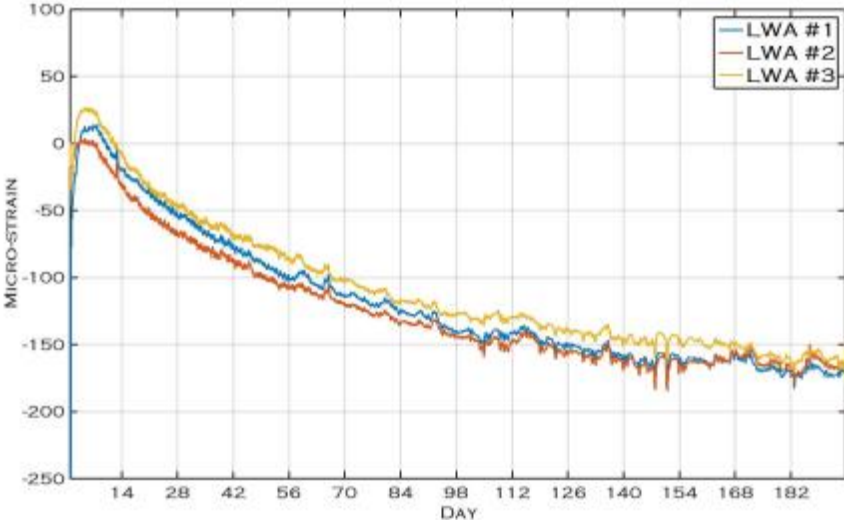


Figure B.1 Top longitudinal strain.

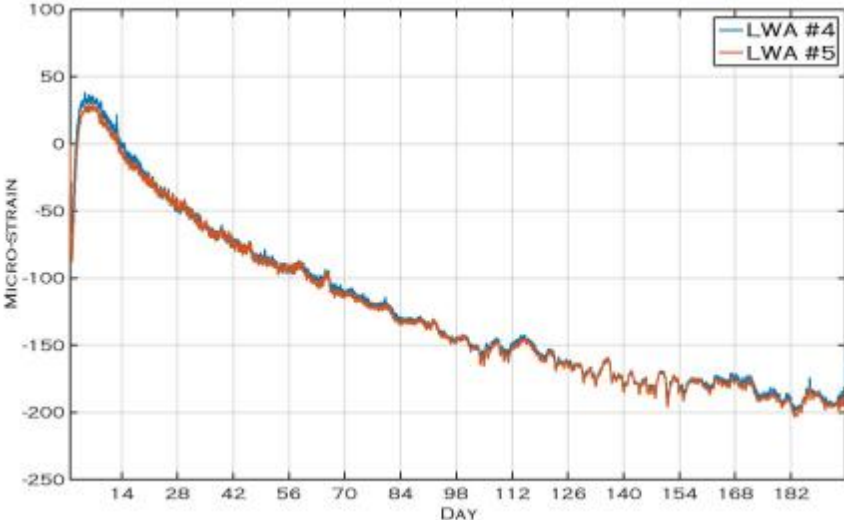
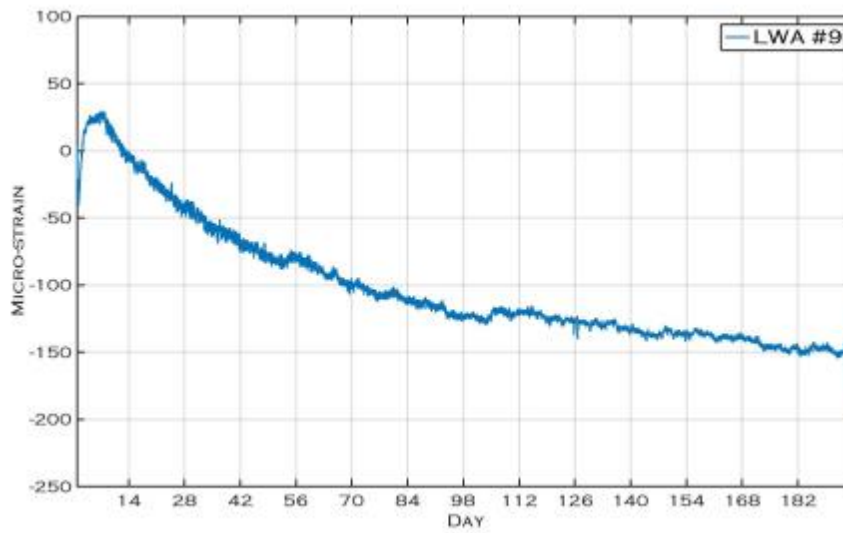
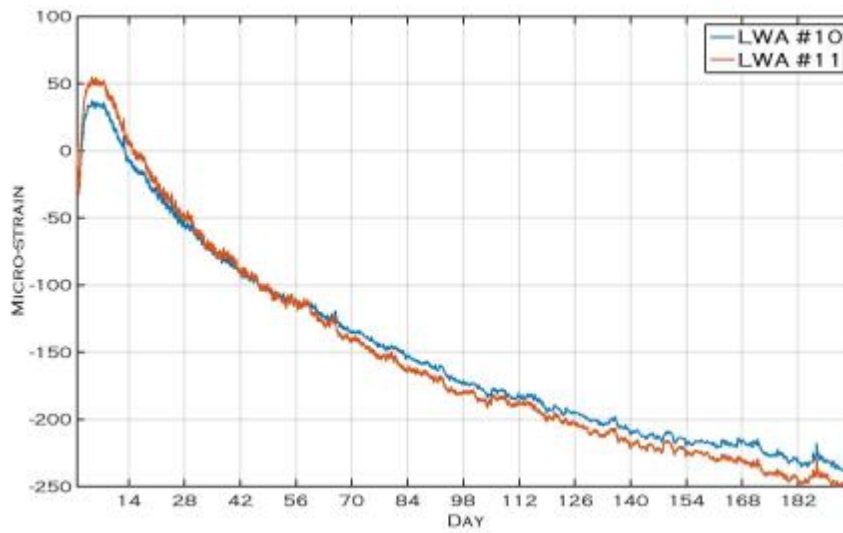


Figure B.2 Top longitudinal strain.



**Figure B.3 Top longitudinal strain.**



**Figure B. 4 Top transverse strain.**

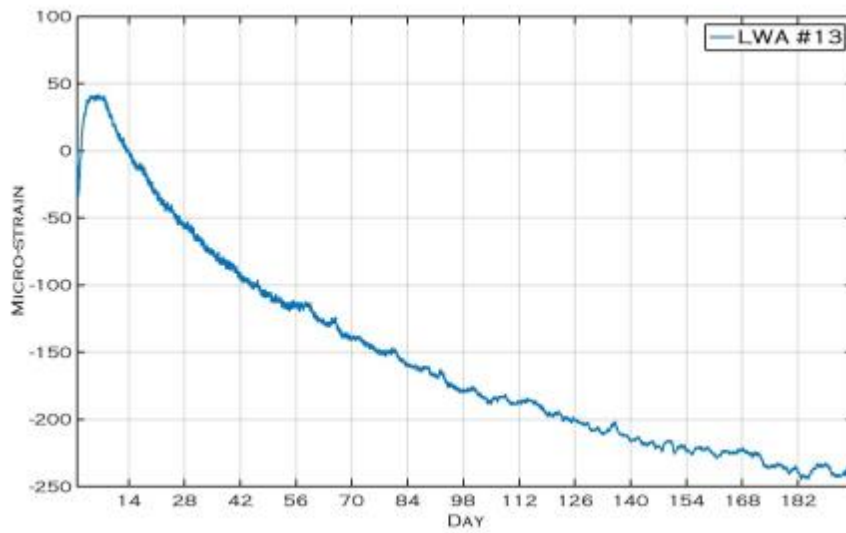


Figure B.5 Top transverse strain.

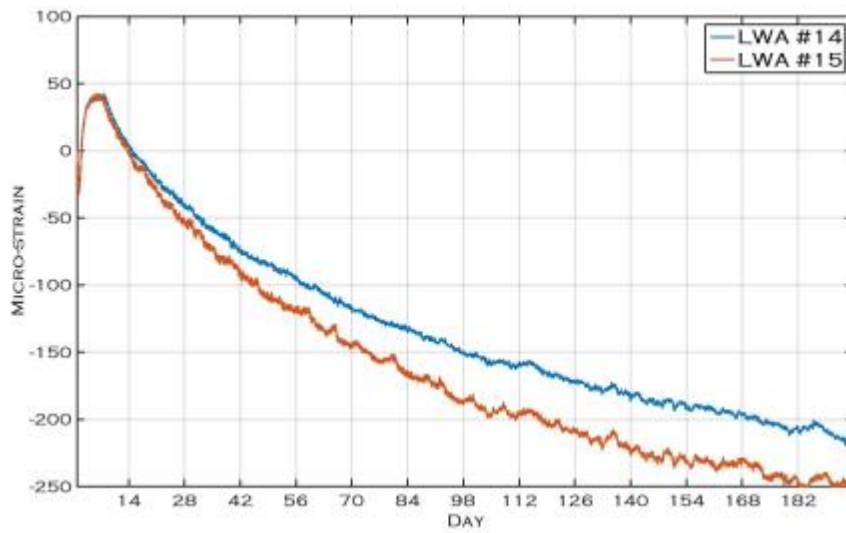
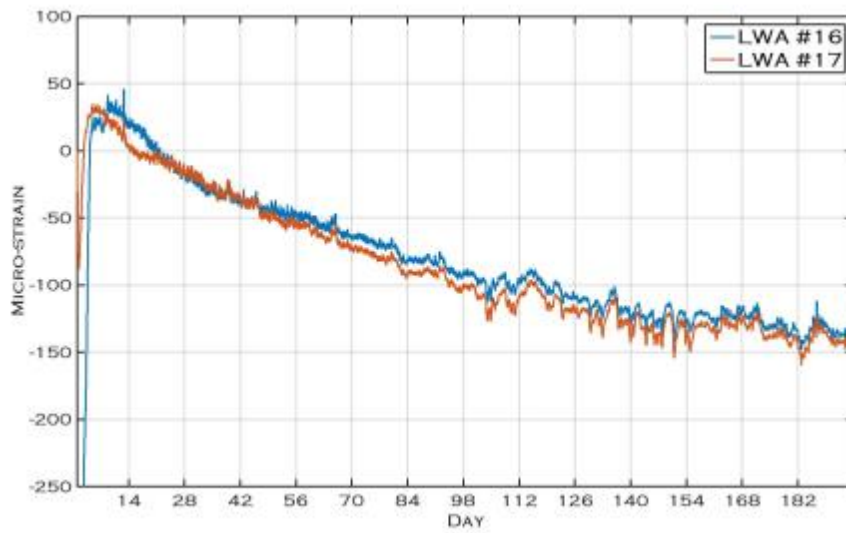
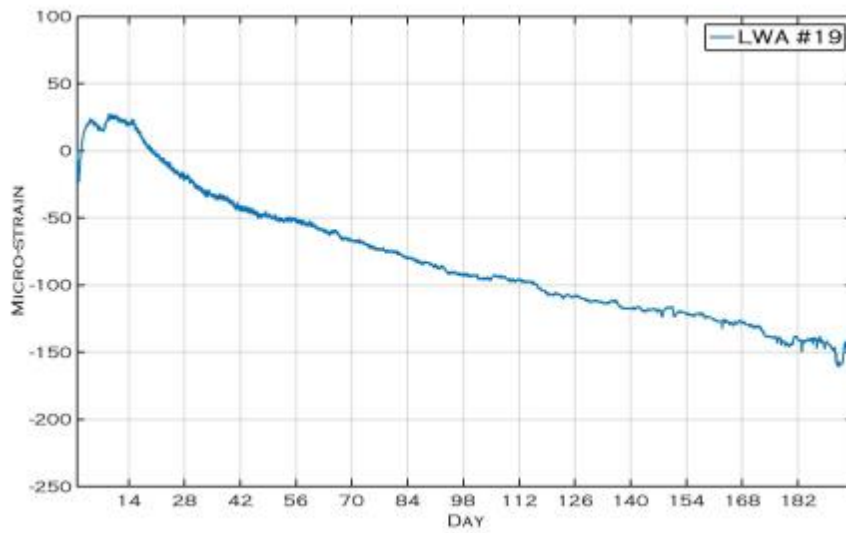


Figure B.6 Top transverse strain.



**Figure B.7 Bottom longitudinal strain.**



**Figure B.8 Bottom transverse strain.**

**B.2 LARGE-SCALE TESTING RESULT: SRA**

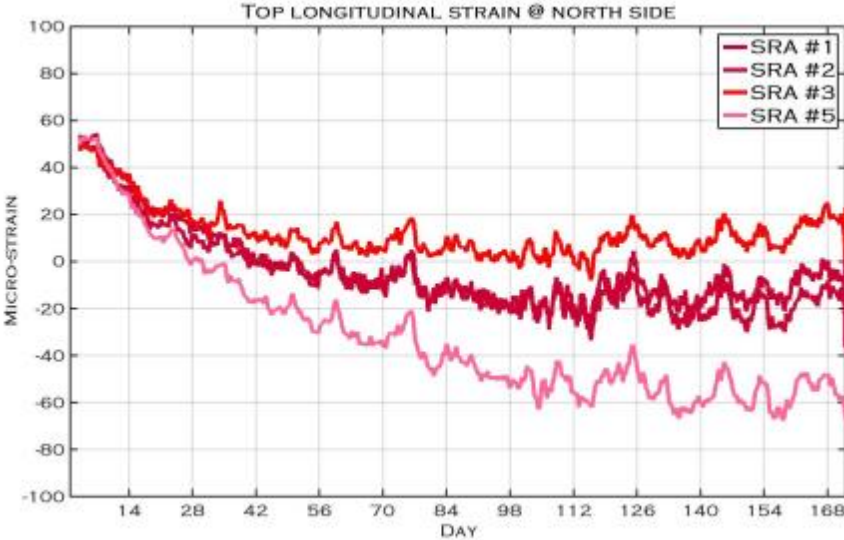


**Figure B.9 Top longitudinal strain.**

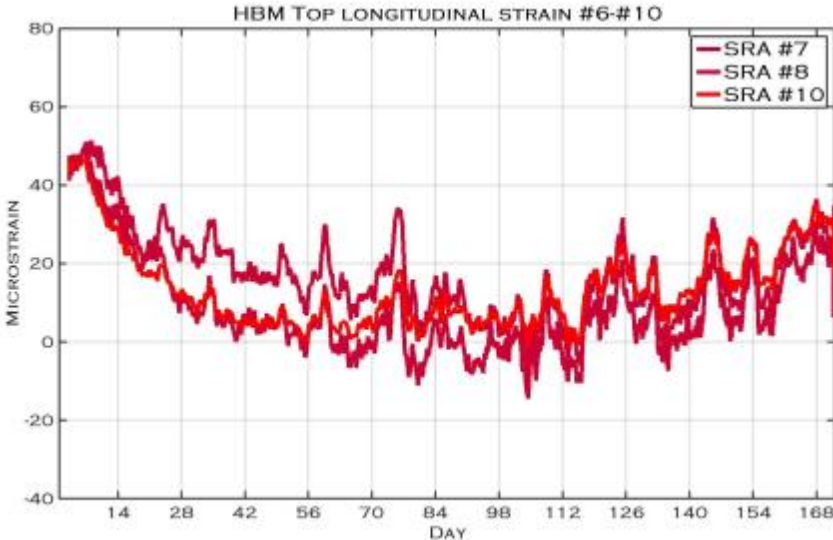


**Figure B.10 Top longitudinal strain.**

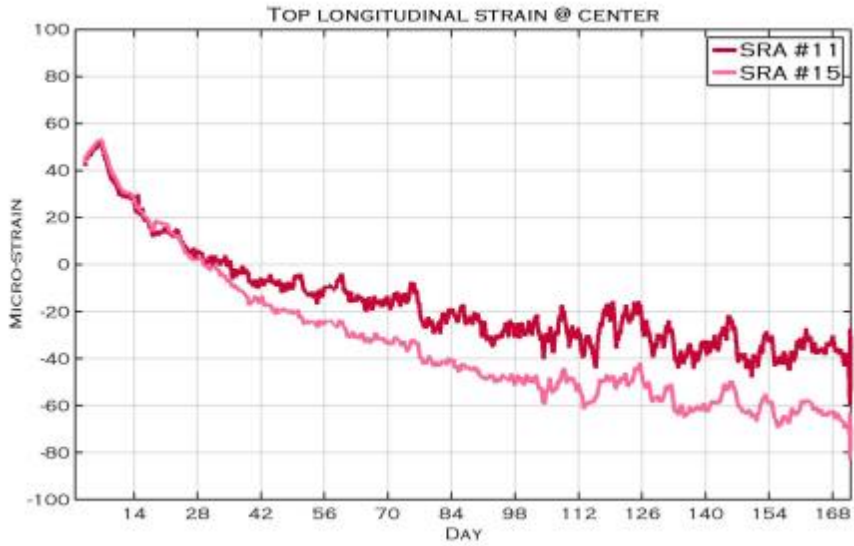


Figure B.11 Top longitudinal strain.

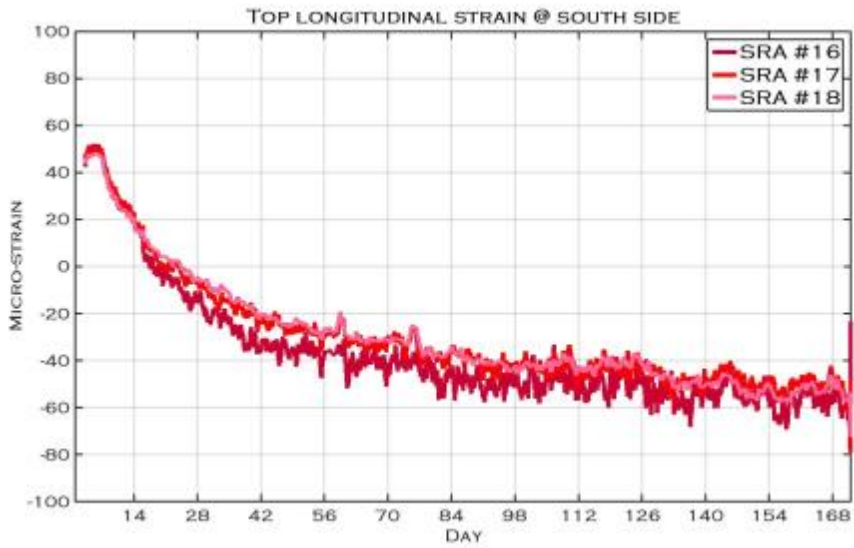


Figure B.12 Top longitudinal strain.

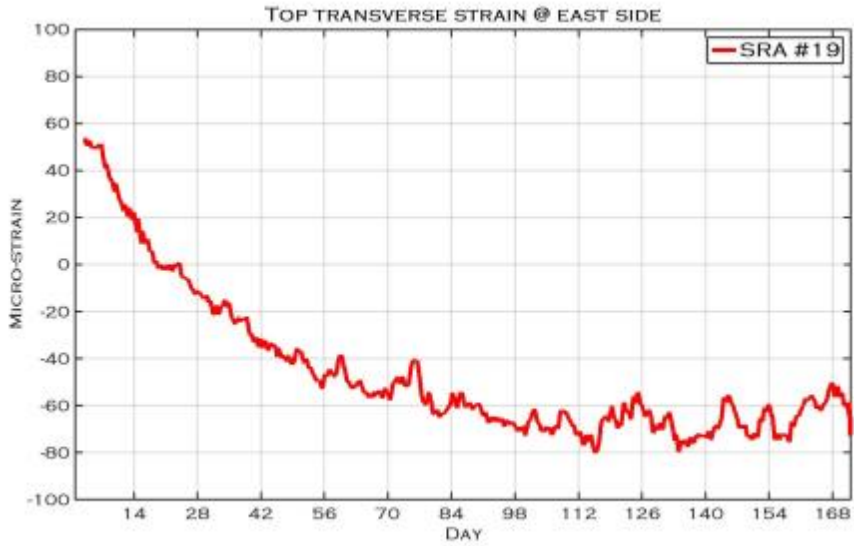


Figure B.13 Top transverse strain.

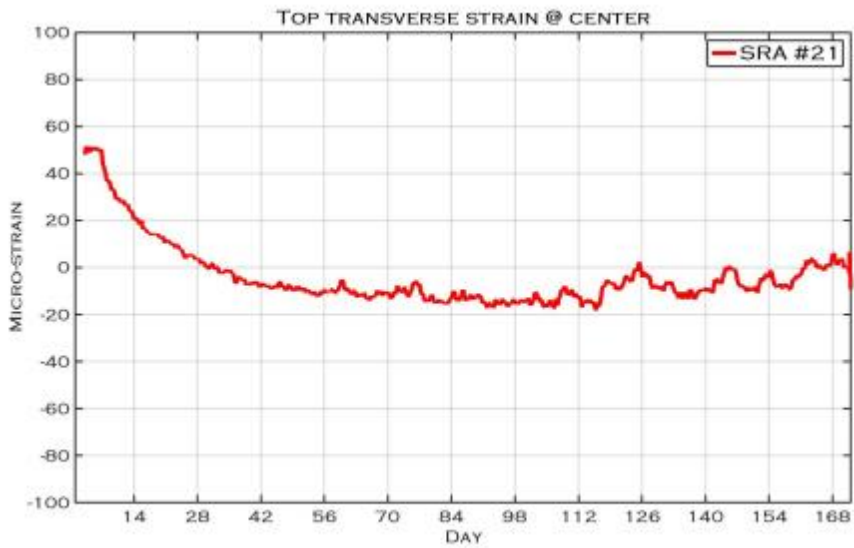


Figure B.14 Top transverse strain.

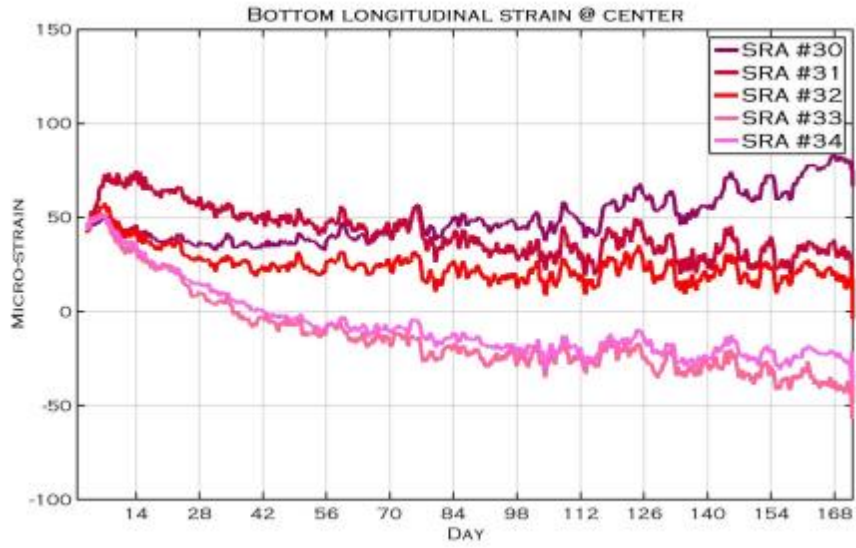


Figure B.15 Bottom longitudinal strain.



